Cosmic Ray Factories

Andrei M. Bykov
Ioffe Institute, St Petersburg

Co-author D.C.Ellison

Cosmic Rays in the Galaxy

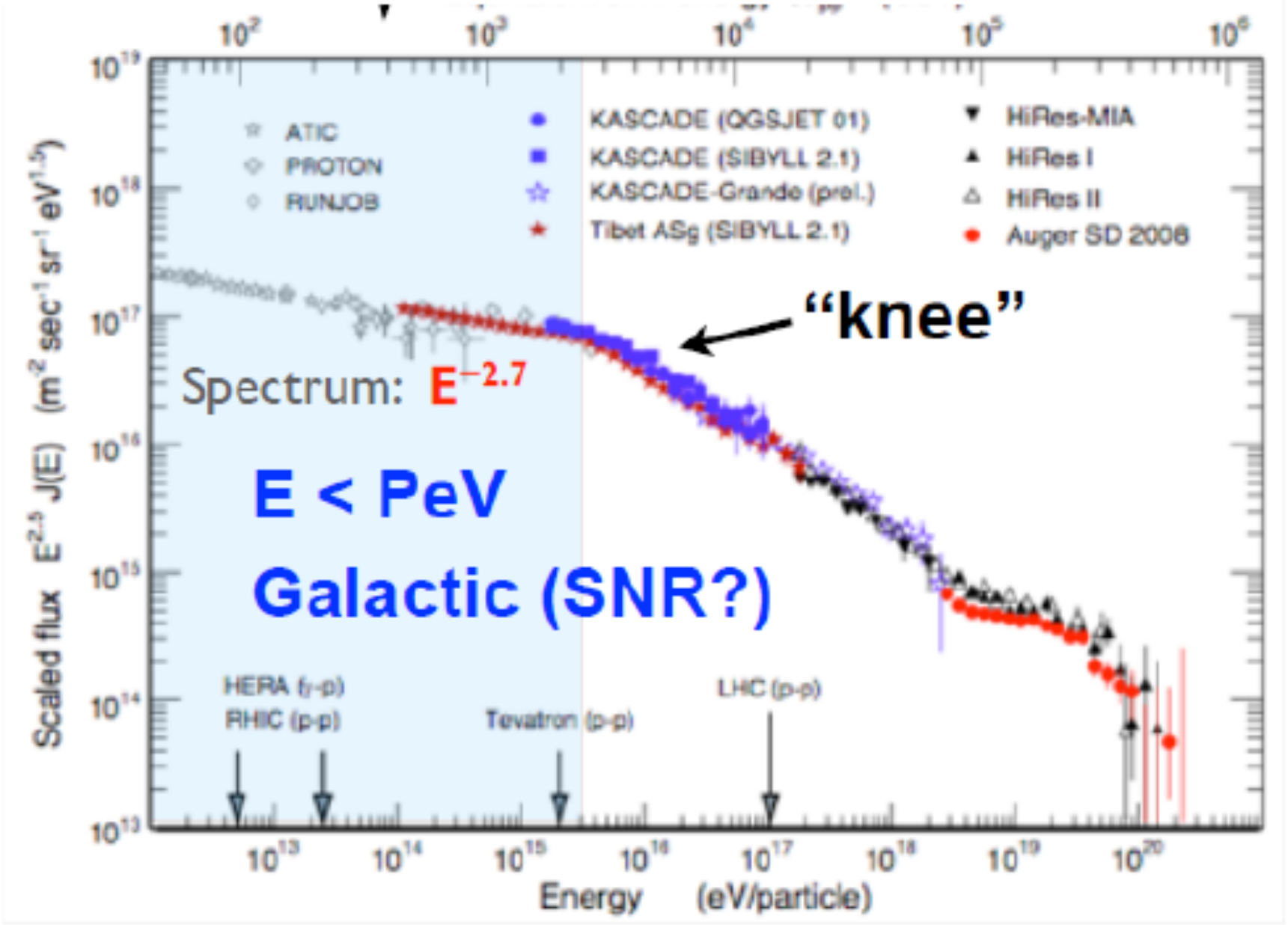

Hillas diagram for Emax

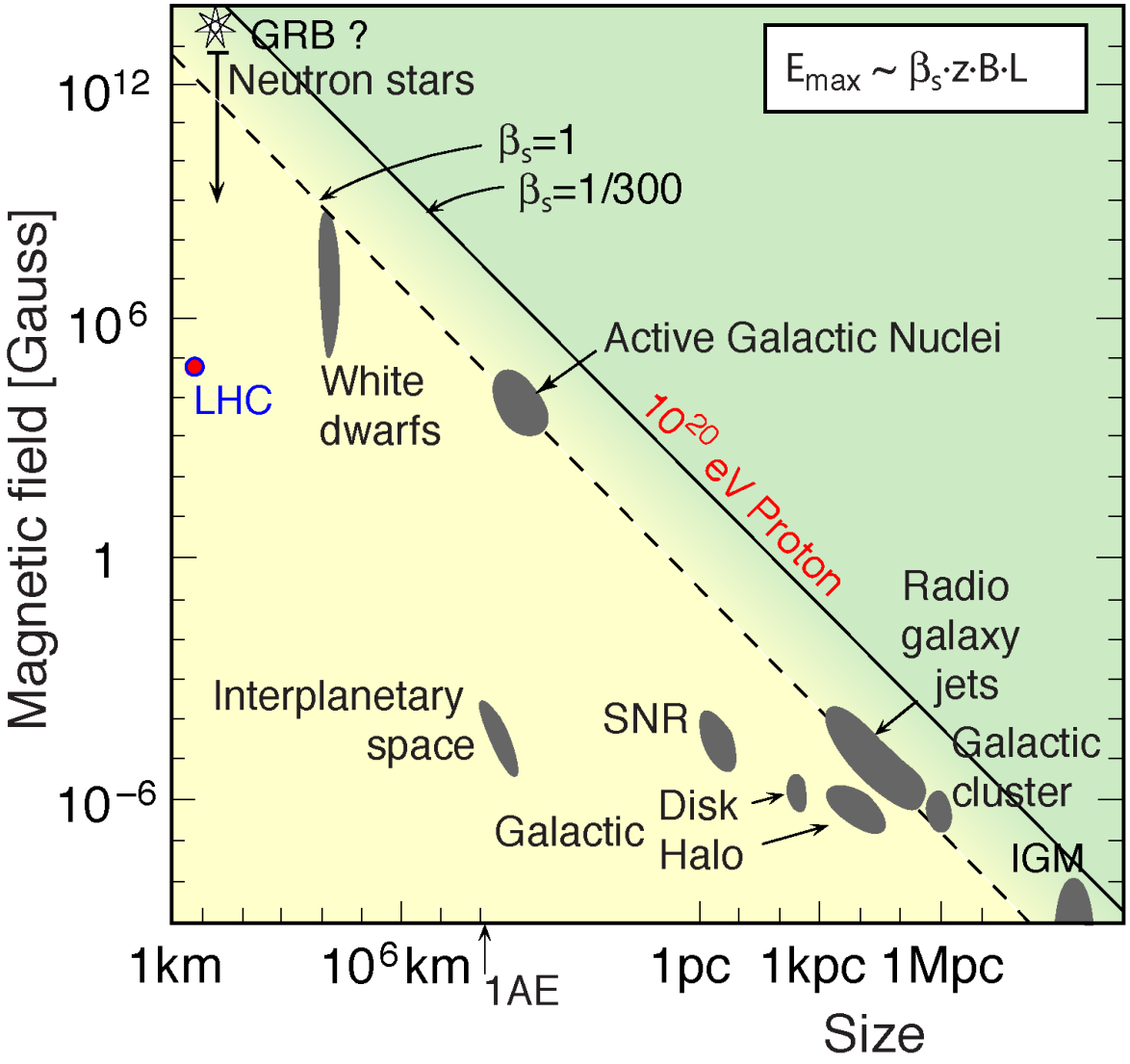

General constrain on the maximal CR particle energy achievable in MHD (out)flows

$$t_a^{-1} = \eta \omega_g, \quad \omega_g = \frac{ecB}{\varepsilon}$$

$$comoving\ frame: \frac{t_{dyn}}{t_a} = \eta \omega_g t_{dyn} > 1$$

$$\text{total luminosity}: \quad L_{tot} > 6 \times 10^{44}\, \theta^2 \beta^3 \Gamma^2 \eta^{-2} Z^{-2} E_{20}^2 \ \text{erg s}^{-1}$$

See M.Lemoine lecture

Lovelace 76; Waxman 94; Anaronian 06; Lemoine 09

Supernovae

SN Ia 1994D in NGC 4526
Hubble Space Telescope

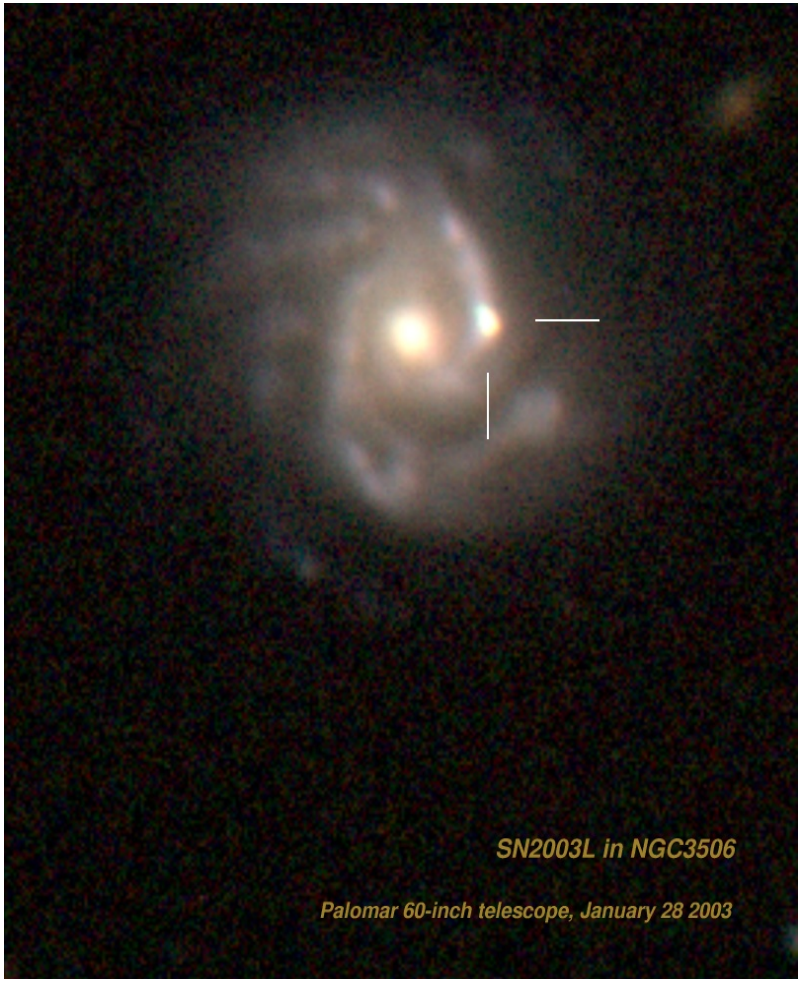

http://www.eso.org/public/images/ann11014a/

Supernova optical light curves (luminosities) vary….

Superluminous SNe
L(t) dt ≈$10^{50\text{-}51}$erg

"Standard" SNe
L(t) dt ≈10^{49}erg

Giant star eruptions
e.g. η Car

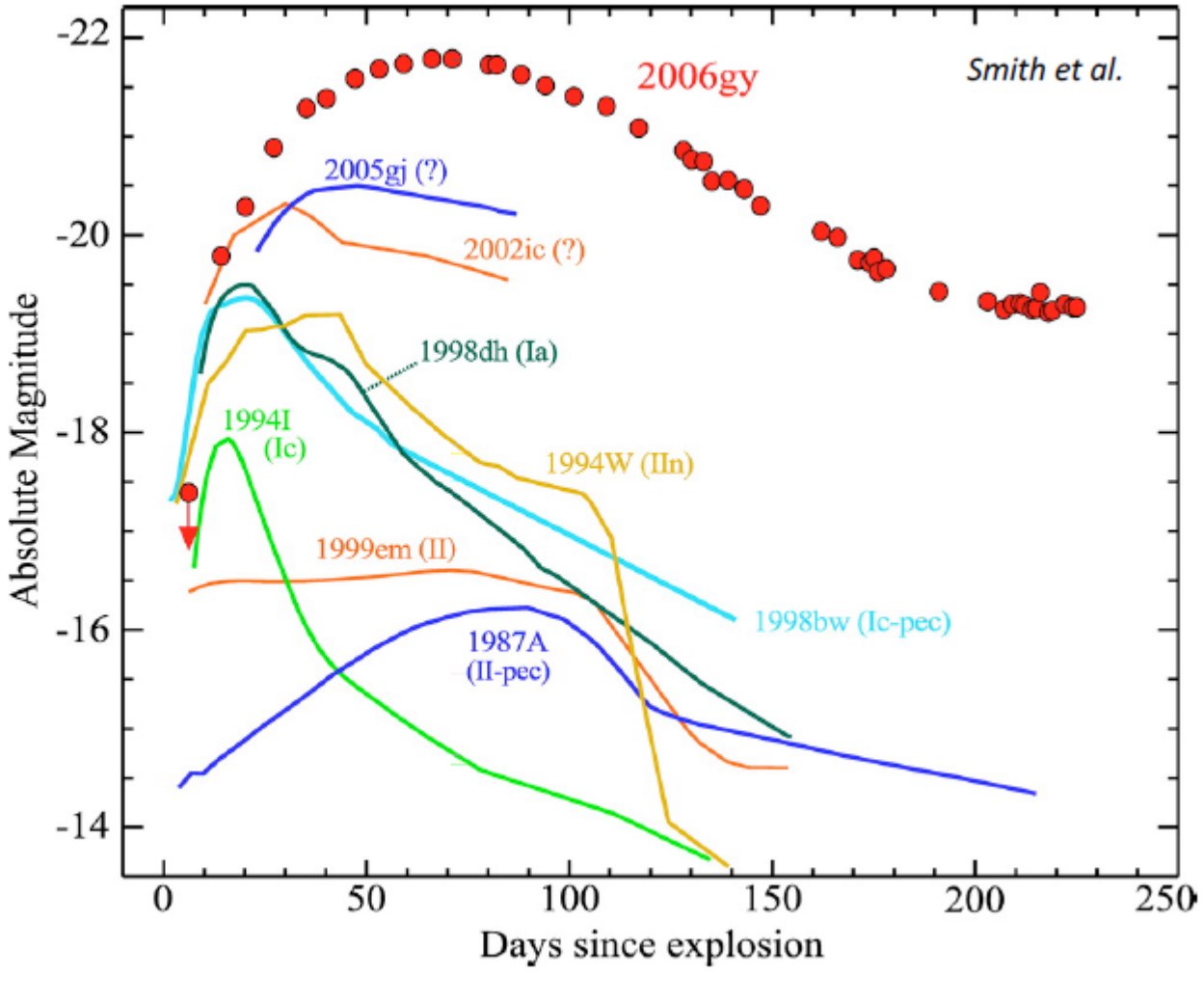

Supernovae

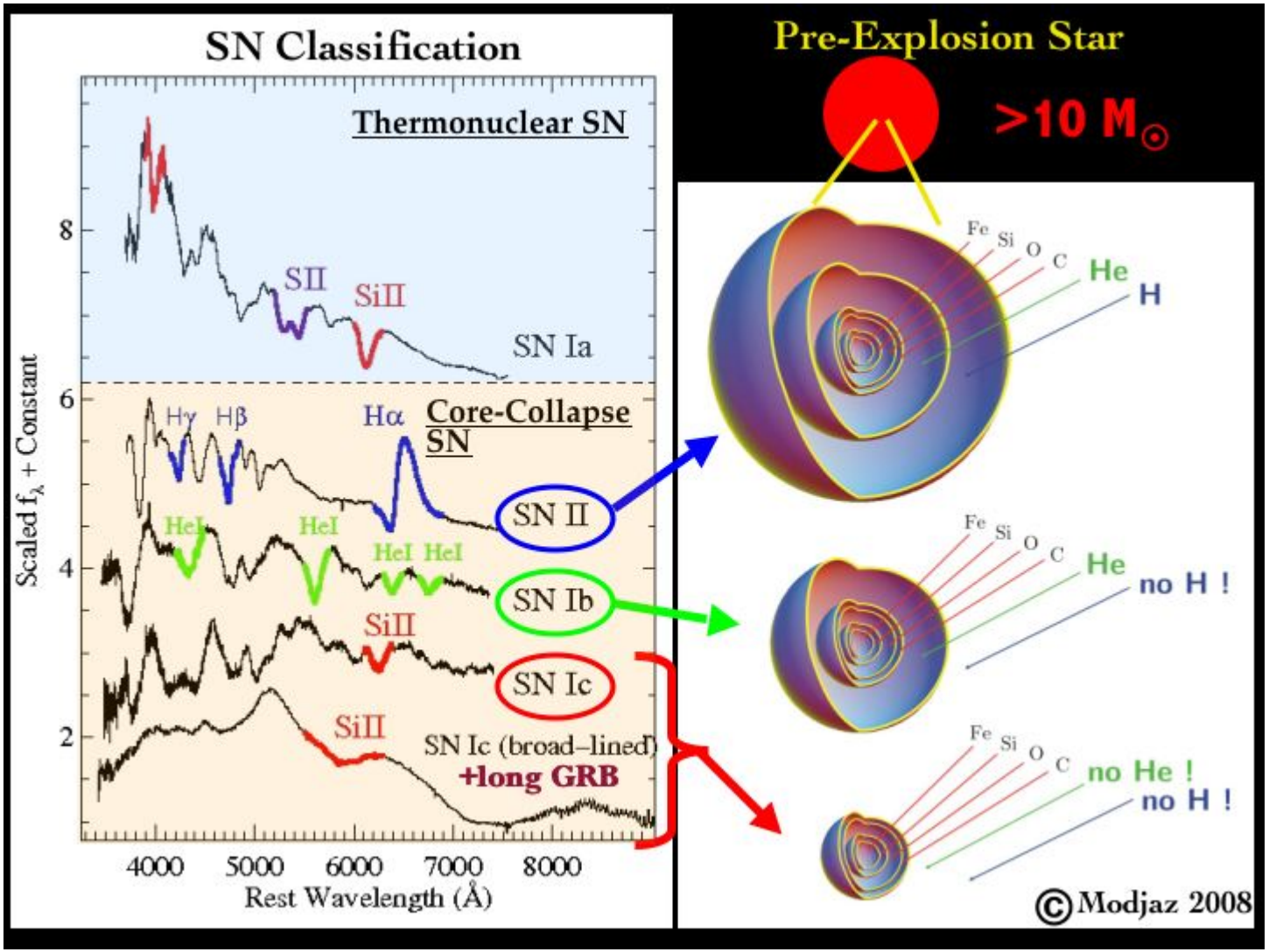
SN Classification
Thermonuclear SN
SII
SiII
SN Ia
Hγ
Hβ
Hα
Core-Collapse SN
HeI
HeI
HeI
HeI
SN II
SN Ib
SiII
SN Ic
SiII
SN Ic (broad–lined)
+long GRB
Scaled f_λ + Constant
8
6
4
2
4000
5000
6000
7000
8000
Rest Wavelength (Å)
Pre-Explosion Star
>10 $M_\odot$
Fe
Si
O
C
He
H
Fe
Si
O
C
He
no H !
Fe
Si
O
C
no He !
no H !
© Modjaz 2008

Supernovae type Ia, IIb, IIn

Relativistic SNe type Ib/c

Gamma-ray bursts

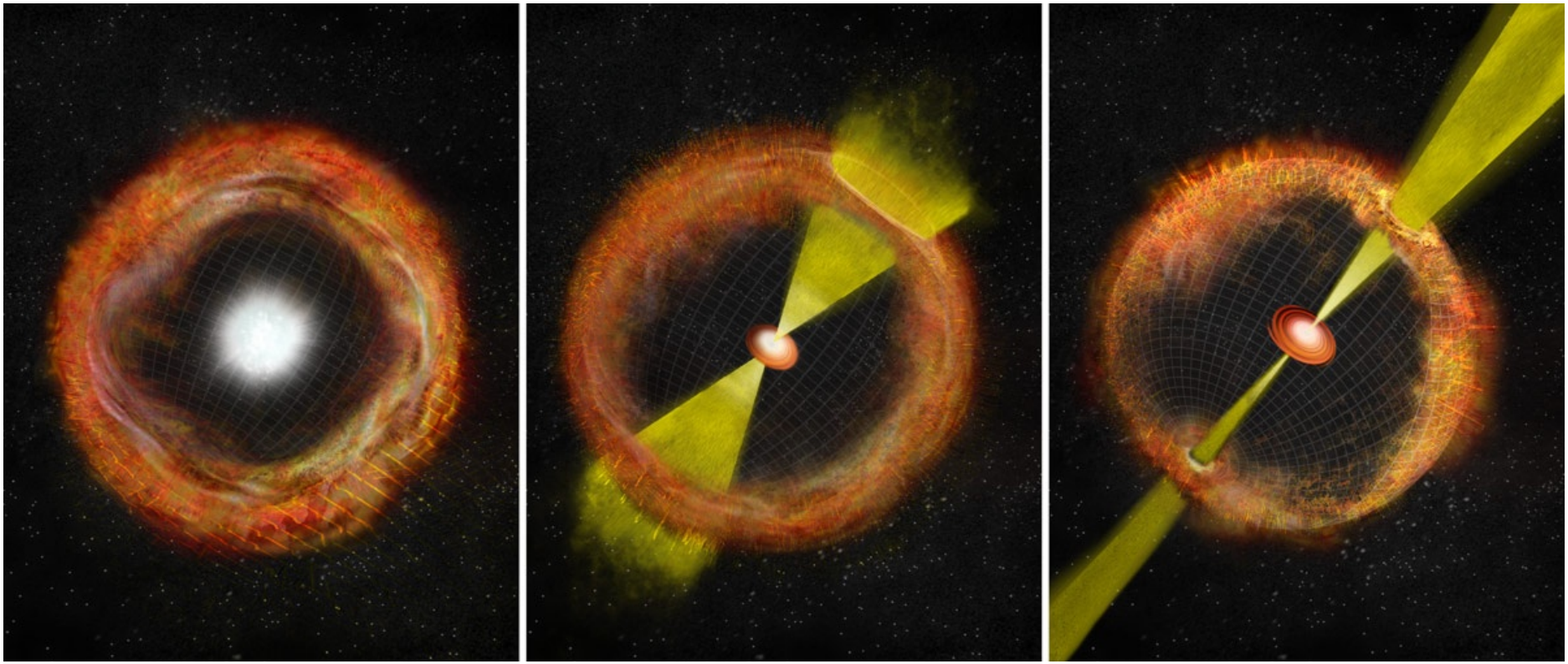

Radio observations
SN 2009bb 2012ap

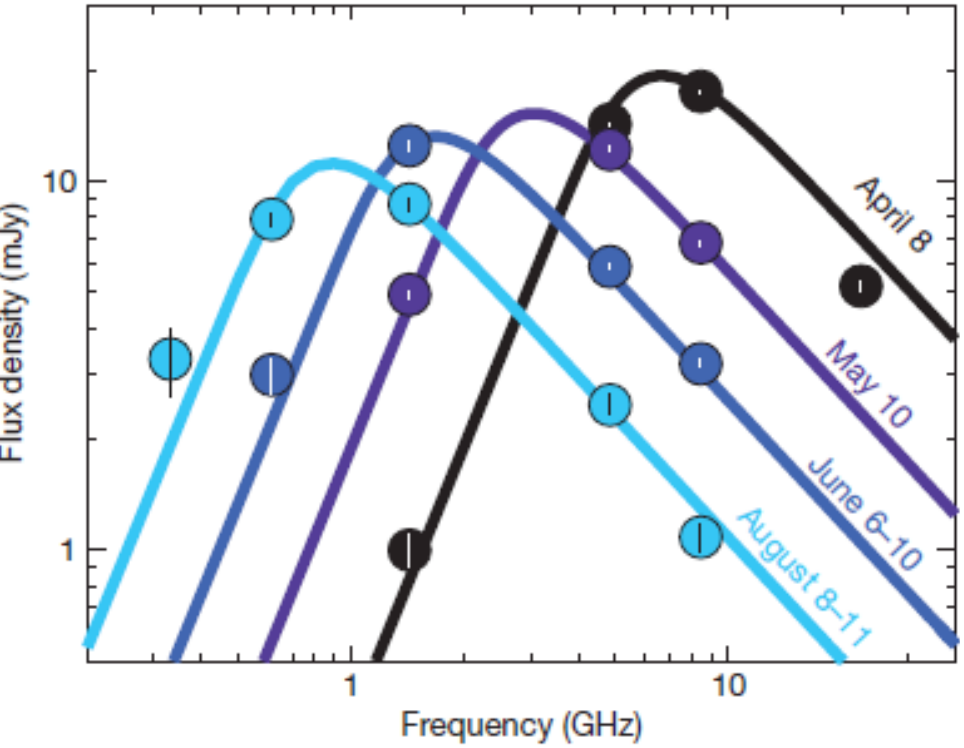

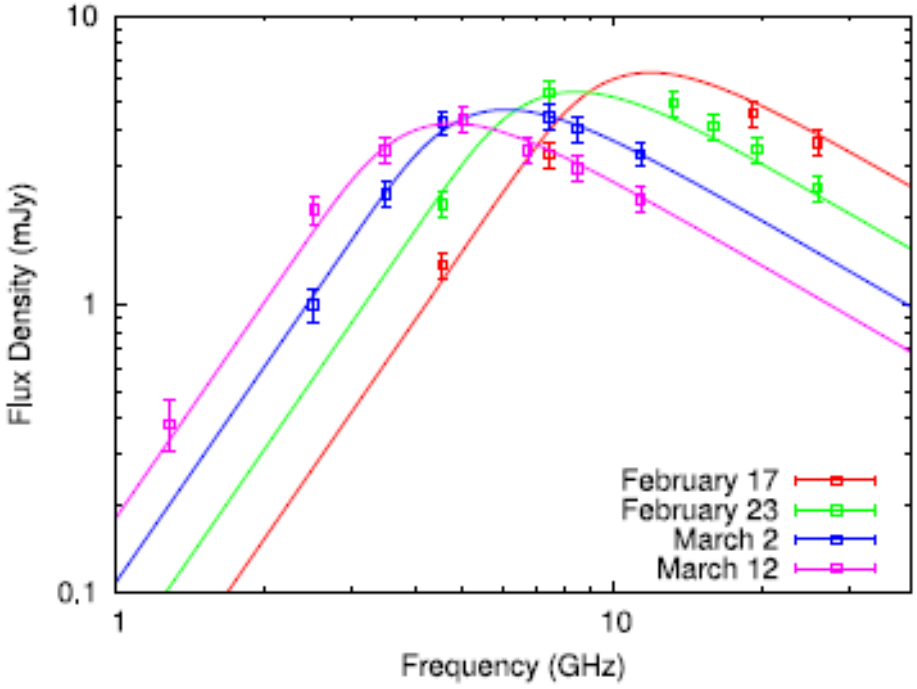

A.Soderberg + 2010; S.Chakraborti+ 2015

Relativistic supernovae

SN 2009bb 2012ap

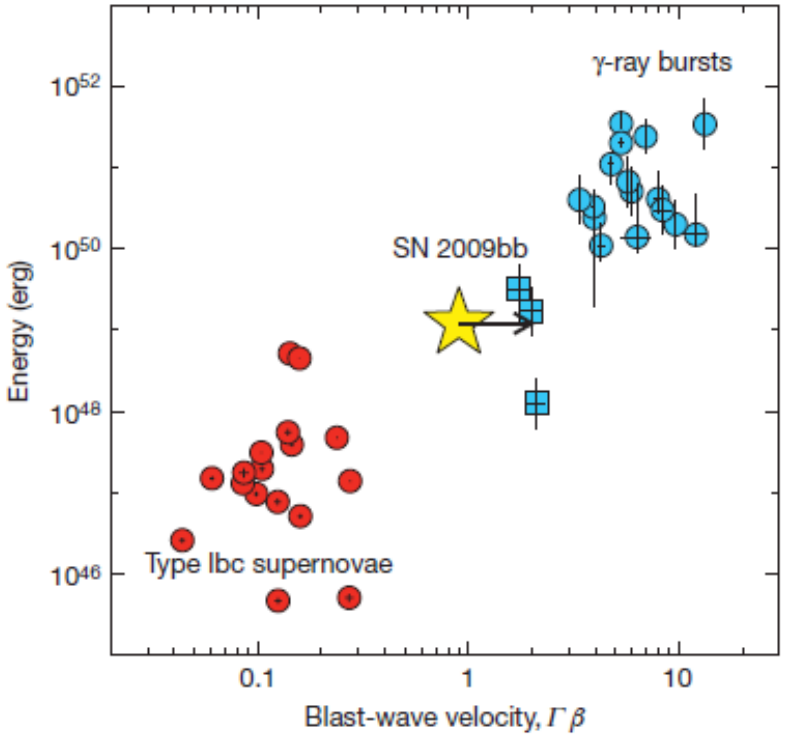

Soderberg + 2010

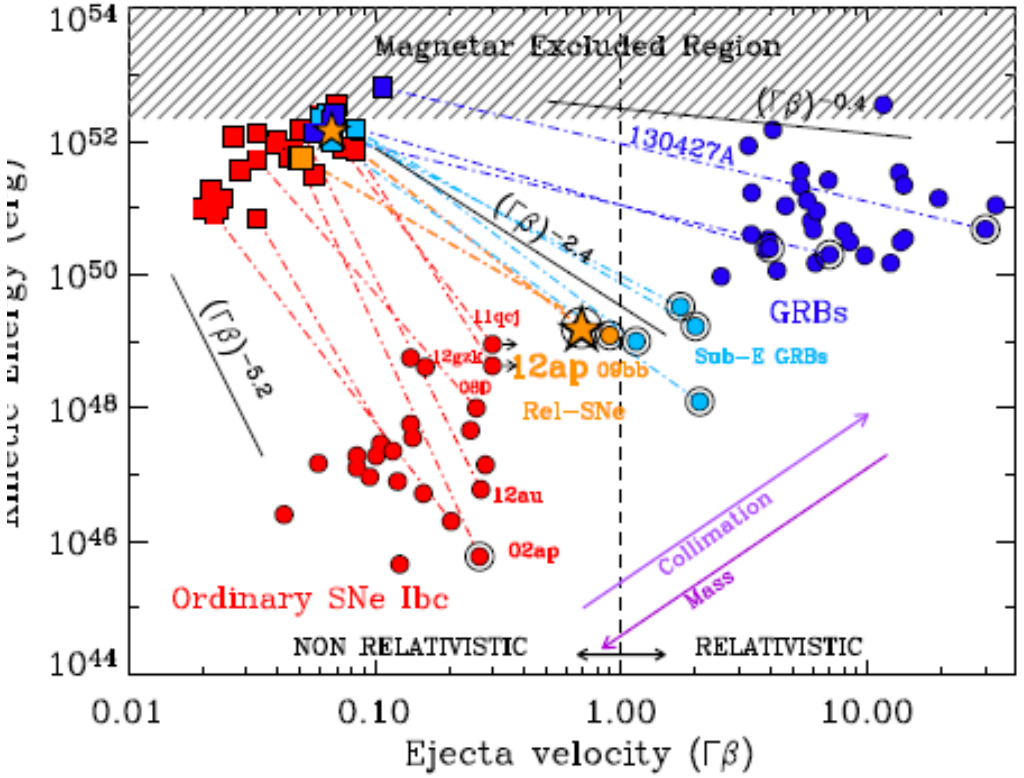

R.Margutti+ 2014

Distribution of kinetic energy over the ejecta 4-velocities derived from SNe & GRB observations

Relativistic SN 2009bb

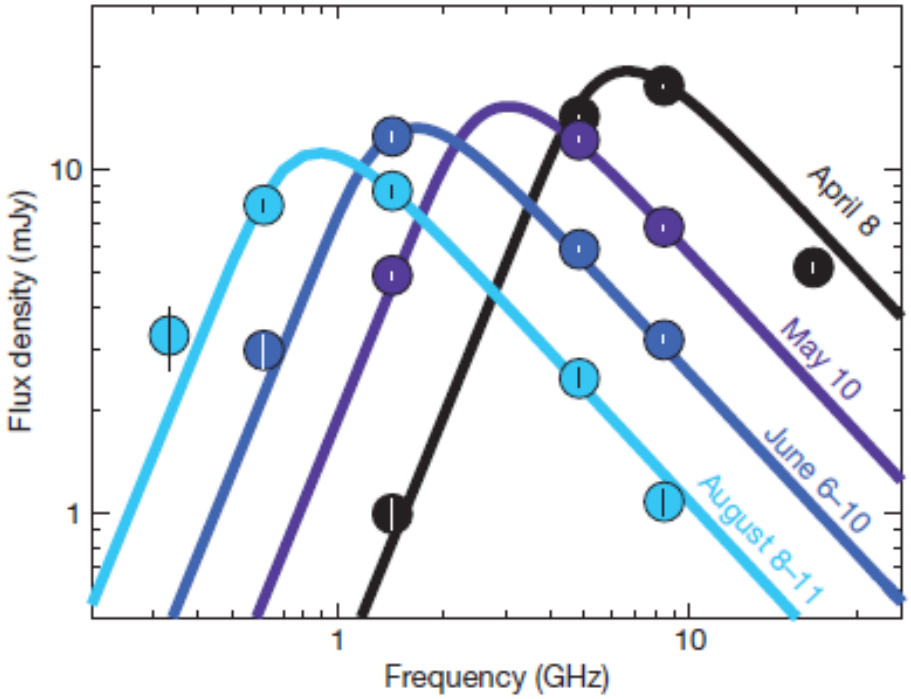

Derived equipartiton MF

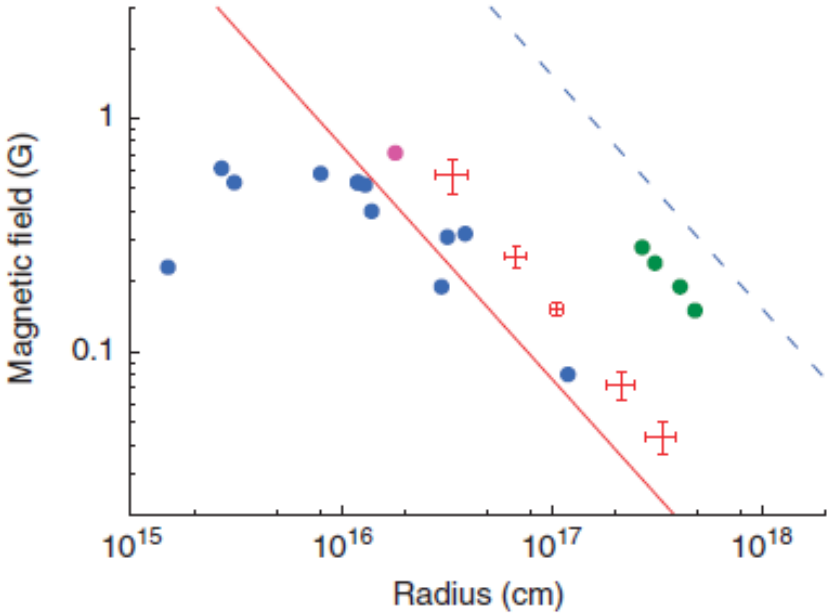

A.Soderberg + 2010; S.Chakraborti+ 2010

Table 1 | Radius-magnetic field evolution.

Hillas CR energy

Observation date (2009)	Age (days)	F_{op} (mJy)	ν_p (GHz)	R (10^{15} cm)	B (mG)	E_p (EeV)	E_{Fe} (EeV)
05 April	17	>24.53	—	—	—	>6.4	>166
08 April	20	17.87±0.95	7.63±0.63	34±3	570±48	5.7±0.1	148±3
10 May	52	13.69±0.79	3.33±0.17	68±4	256±14	5.2±0.1	134±3
08 June	81	10.82±0.34	1.93±0.07	106±4	152±5	4.7±0.1	123±1
10 August	144	9.82±0.65	0.90±0.06	216±16	72±5	4.6±0.1	119±3
27 October	222	8.35±0.59	0.53±0.04	337±28	43±3	4.3±0.1	112±3

Peak fluxes and peak frequencies of SN 2009bb are determined from VLA and GMRT observations by fitting a SSA spectrum to the observed fluxes. Fluxes until August can be found in Supplementary Information of ref. 19. The fluxes around 27 October 2009 are from new VLA (1.6±0.1 mJy at 8.46 GHz and 3.7±0.2 mJy at 4.86 GHz) and GMRT observations (4.4±0.3 mJy at 1.28 GHz, 8.7±0.7 at 617 MHz and 5.8±0.7 mJy at 332 MHz). Radius and magnetic fields are determined using equations (1,2) assuming equipartition (a possible source of systematic error). Quoted errors are statistical, see Methods for discussion on the equipartition assumption. Maximum energies to which protons and iron nuclei can be accelerated are computed using equation (5), ± are standard errors. Note that both E_p and E_{Fe} decrease slowly by only ~24% in a span of ~200 days.

Is the Hillas (maximal) CR energy achievable here?

We'll return back to the estimations of max CR energy in SN2009bb, but now lets discuss

Amplification of Magnetic Turbulence in SN Shocks

What can we learn from high resolution X-ray imaging of SNRs?

Tycho's Supernova Remnant (Type Ia SN)

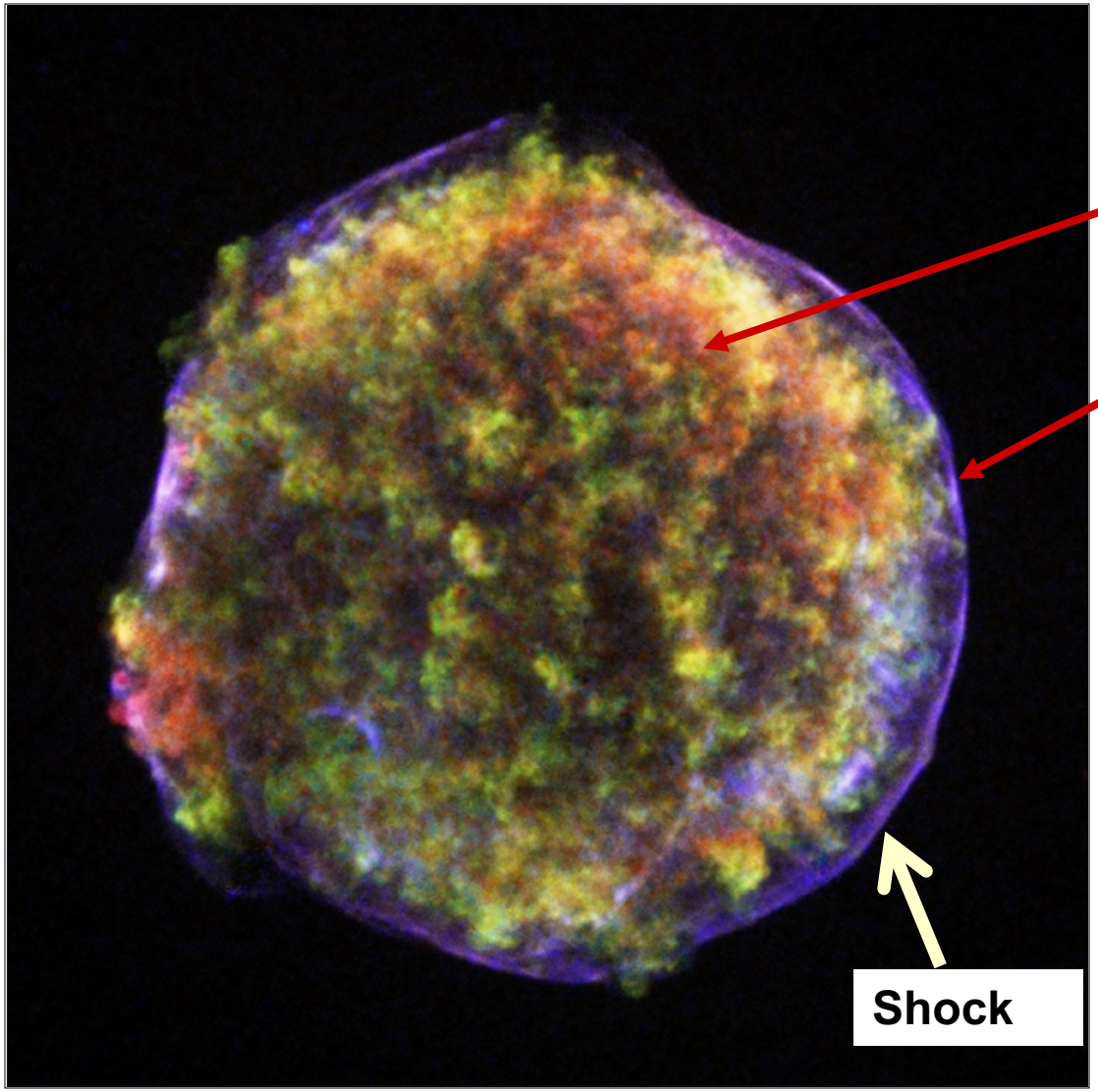

http://chandra.harvard.edu/photo/2005/tycho/

Exploded in 1572 and studied by Tycho Brahe

Chandra X-ray image

Shock heated gas inside 3000 km/s blast wave

Blue is nonthermal X-ray emission (synchrotron) from shock accelerated relativistic electrons.

No doubt that TeV electrons are produced by this shock !!

Evidence for TeV ions is less direct but very strong.

Chandra 4-6 keV Image of Tycho's SNR (mostly synchrotron photons)

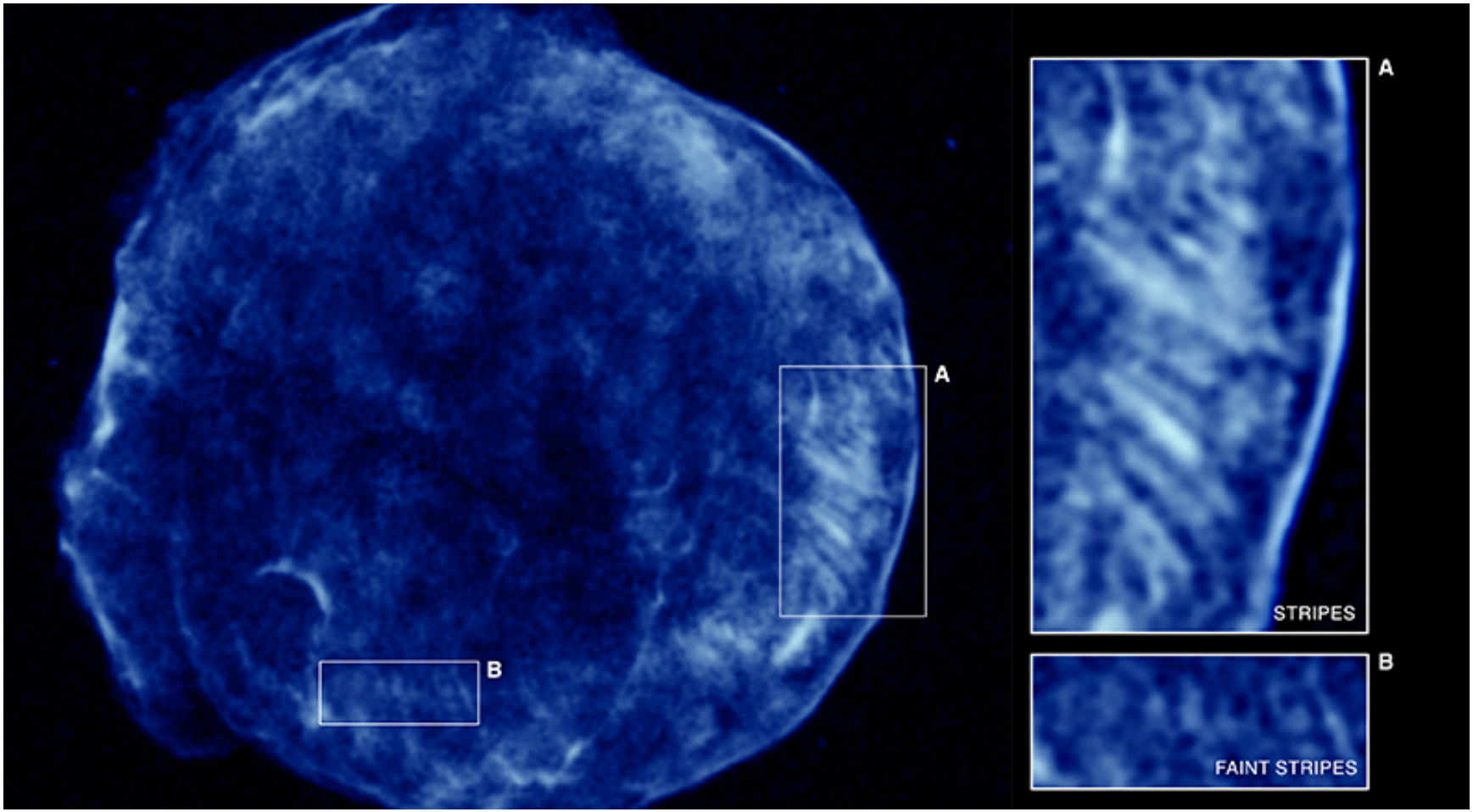

Eriksen + 2011

Sharp X-ray synchrotron edges in SNRs : one piece of evidence for high Magnetic fields

Tycho's Supernova Remnant

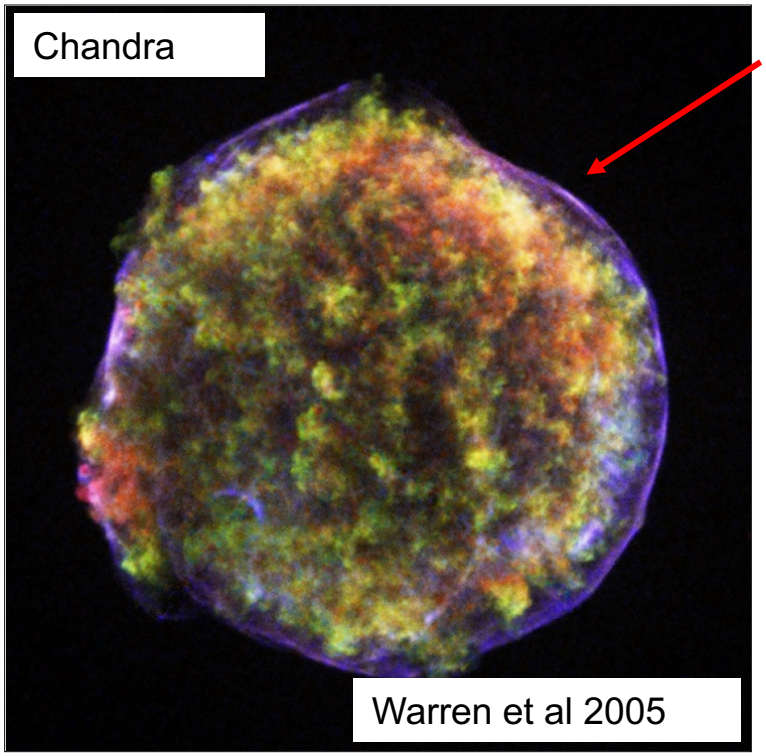

Sharp edge X-ray edges

Blue is synchrotron emission from TeV electrons.

Radial cuts: Sharp decline ➔ high B-field

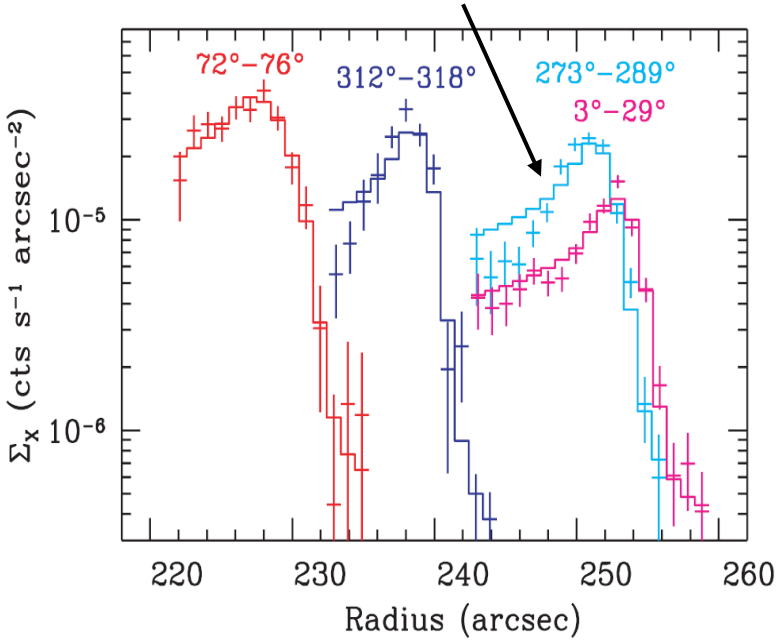

Tycho's SNR, 4-6 keV surface brightness profiles at outer blast wave (non-thermal emission)

Evidence for High (amplified) B-fields in SNRs

Sharp synch. X-ray edges

Cassam-Chenai et al. 2007

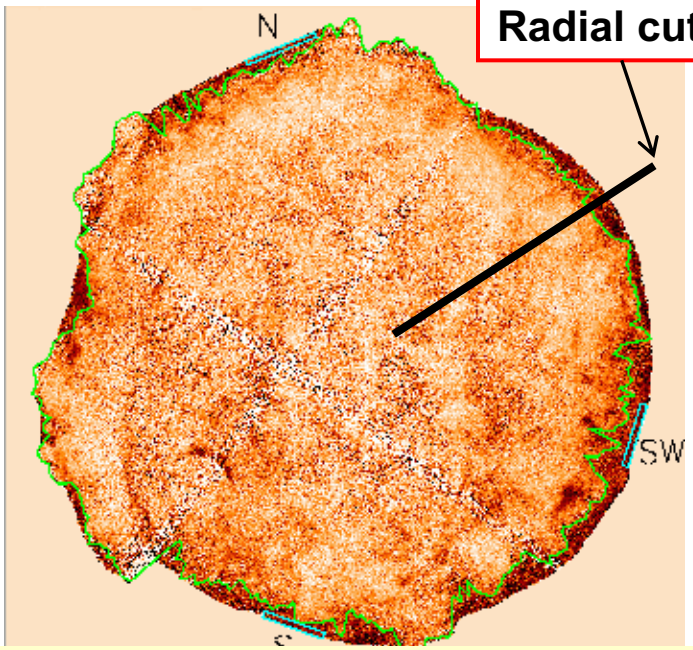

Radial cuts

Chandra observations of Tycho's SNR
(Warren et al. 2005)

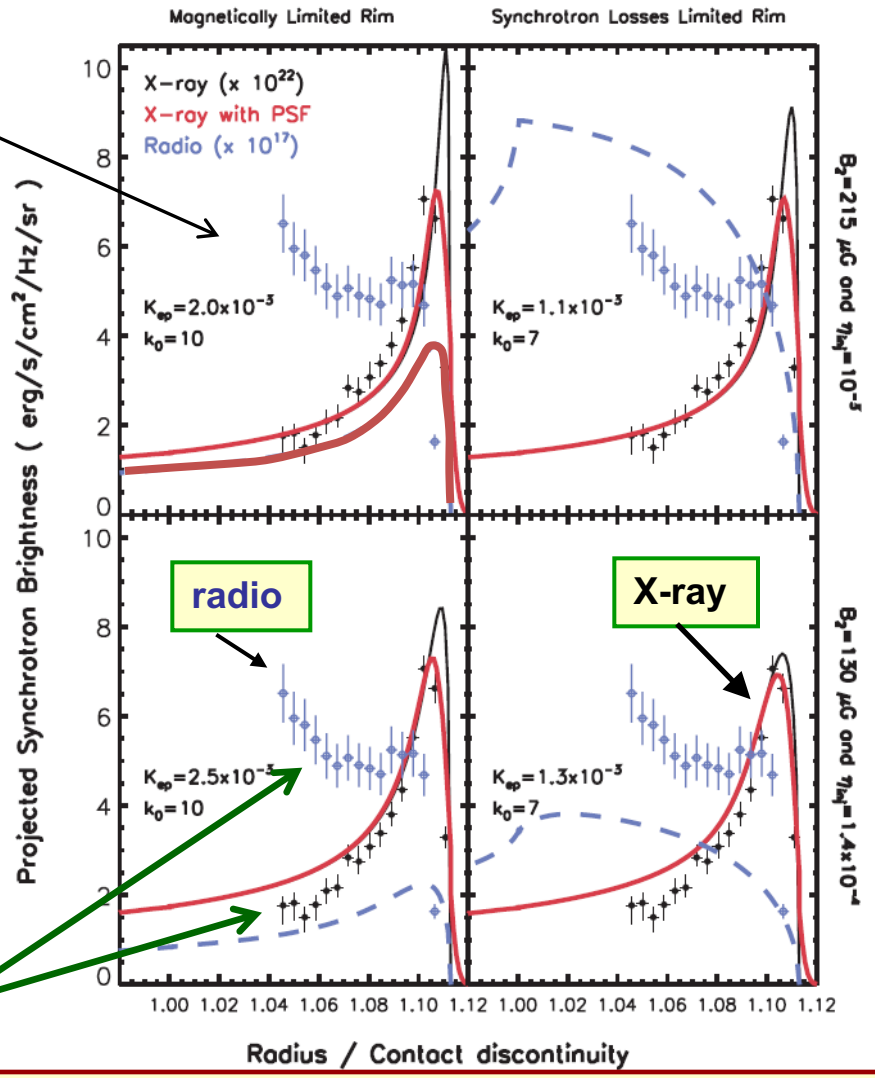

If emission drops from B-field decay instead of radiation losses, expect synch radio and synch X-rays to fall off together.

Thin structures: evidence for radiation losses and, therefore, large, amplified B-fields.
On order of 10 times higher than expected

Magnetic Field Amplification in the Thin X-Ray Rims of SN 1006 Ressler et al. 2014 ApJ 790 85

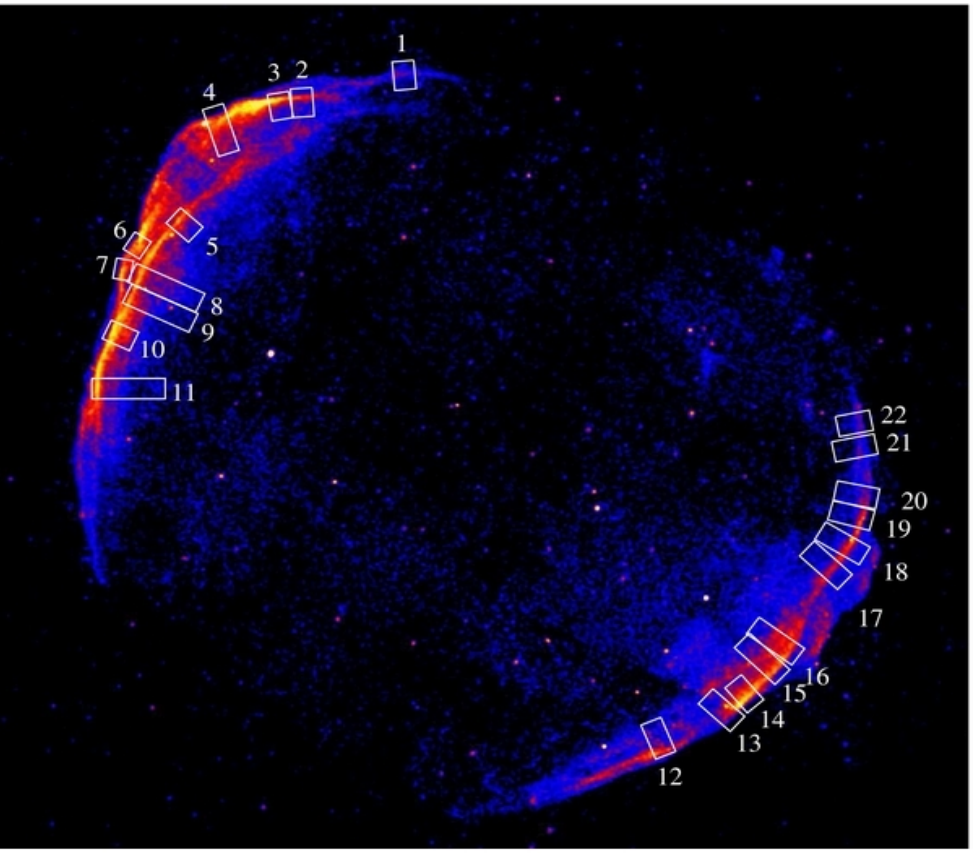

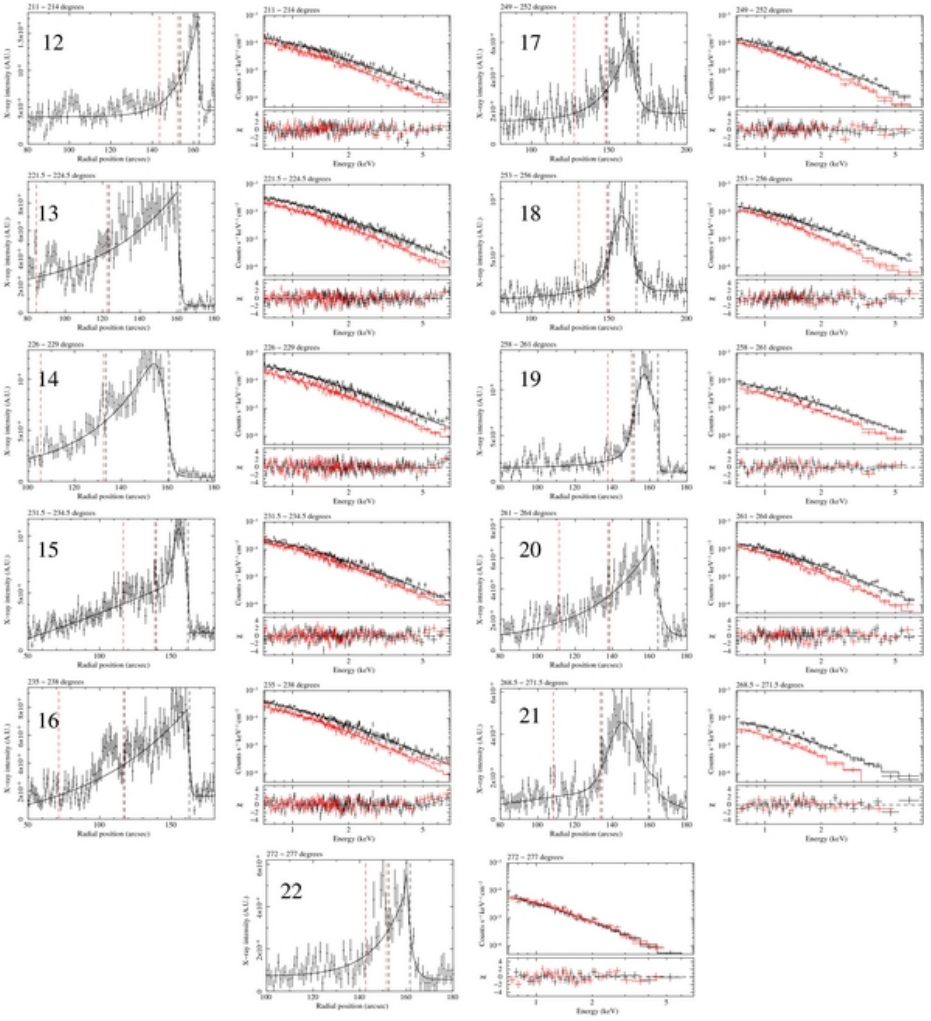

SNR name	τ_{syn}^{max}/t_{SNR} ($\times 4P/r$)	B_{adv} (μG)	B_{diff} (μG)	$\rho_B = \frac{\Delta R_{diff}^{(B)}}{\Delta R_{adv}}$
Cas A	<2.6%	210	230	1.1
Kepler	<2.8%	170	180	1.1
Tycho	<2.1%	200	230	1.2
SN 1006	<5.9%	57	90	2.0
G347.3–0.5	<3.3%	61	77	1.4

E. Parizot A.Marcowith J.Ballet Y.Gallant
A&A 453, 387, 2006

Chandra X-ray images of the western shell of SNR RX J1713.7-3946
Variable synchrotron structure!

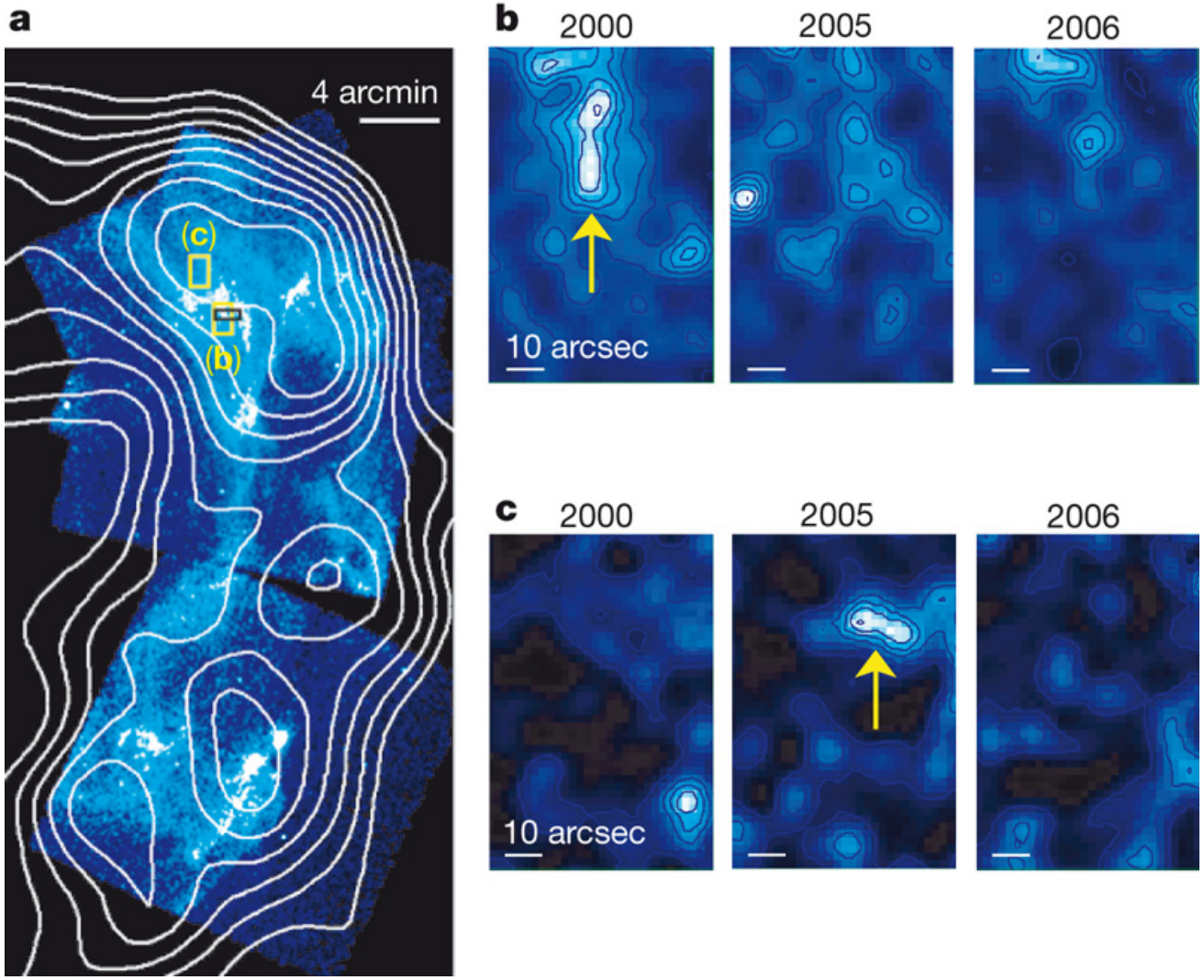

Uchiyama, Aharonian + 2007 Nature

Magnetic Field Amplification (MFA):

How we start with $B_{ISM} \sim 3$ μG and end up with B ~ 300 μG at the shock?

Cosmic ray driven instabilities are essential to amplify the field in strong shocks

MFA is connected to efficient CR production, so nonlinear effects essential

1-D: Model Type Ia or core-collapse SN with Pre-SN wind

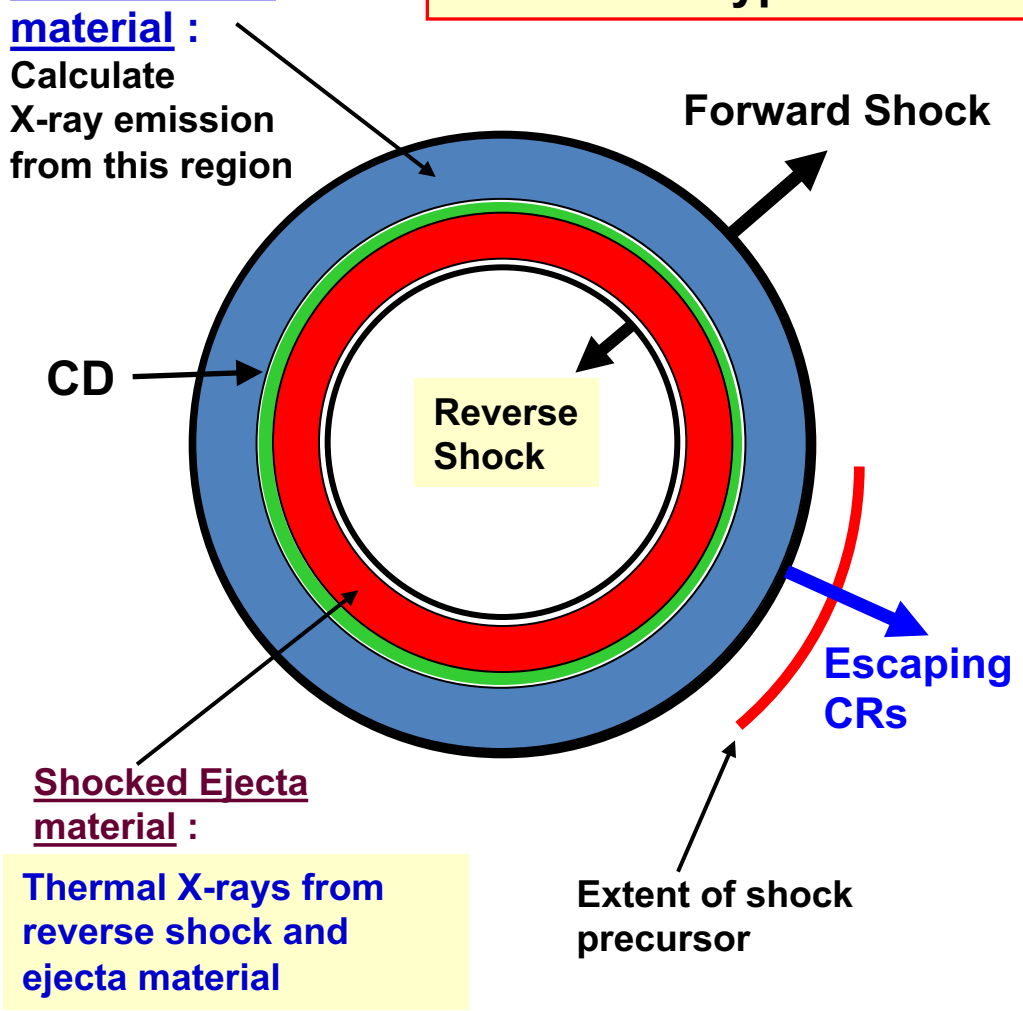

1) **CR electrons and ions accelerated at FS & RS**
   a) Protons give pion-decay γ-rays
   b) Electrons give synchrotron, IC, & non-thermal brems.
   c) High-energy CRs escape from shock precursor & interact with external mass

2) **Evolution of shock-heated plasma between FS and contact discontinuity (CD)**
   a) Electron temperature, density, charge states of heavy elements, and X-ray line emission
   b) Include adiabatic losses & radiation losses

3) X-ray lines from reverse shock:
   a) Connect SNR to SN explosion model

Spherically symmetric: We do not yet model clumpy structure

Ellison +

Diffusive Shock Acceleration: Shocks set up converging flows of ionized plasma

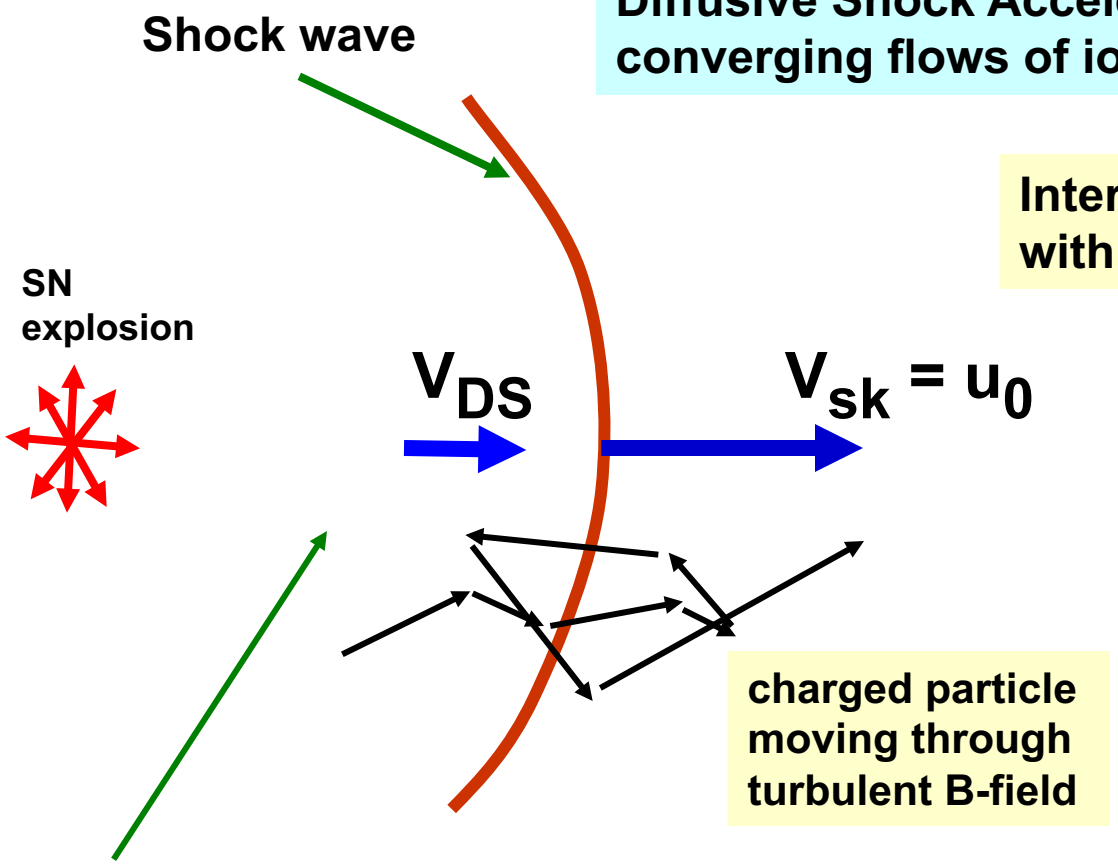

Interstellar medium (ISM), cool with speed $V_{ISM} \sim 0$

shock frame

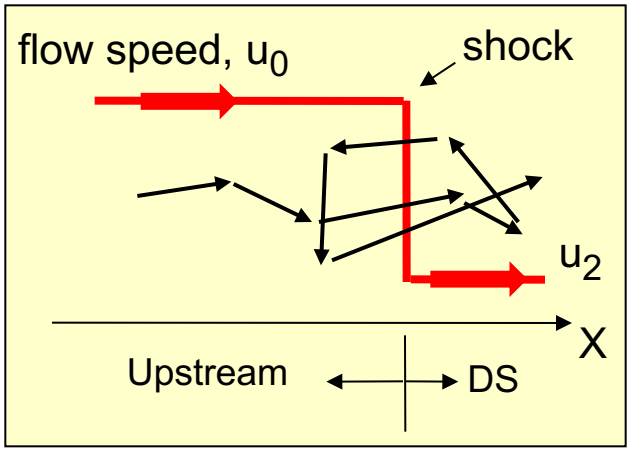

$u_2 = V_{sk} - V_{DS}$

Particles make nearly elastic collisions with background plasma → gain energy when cross shock → bulk kinetic energy of converging flows put into individual particle energy → some small fraction of thermal particles turned into (approximate) power law

You'll hear many more in the next few days about DSA…

Ellison +

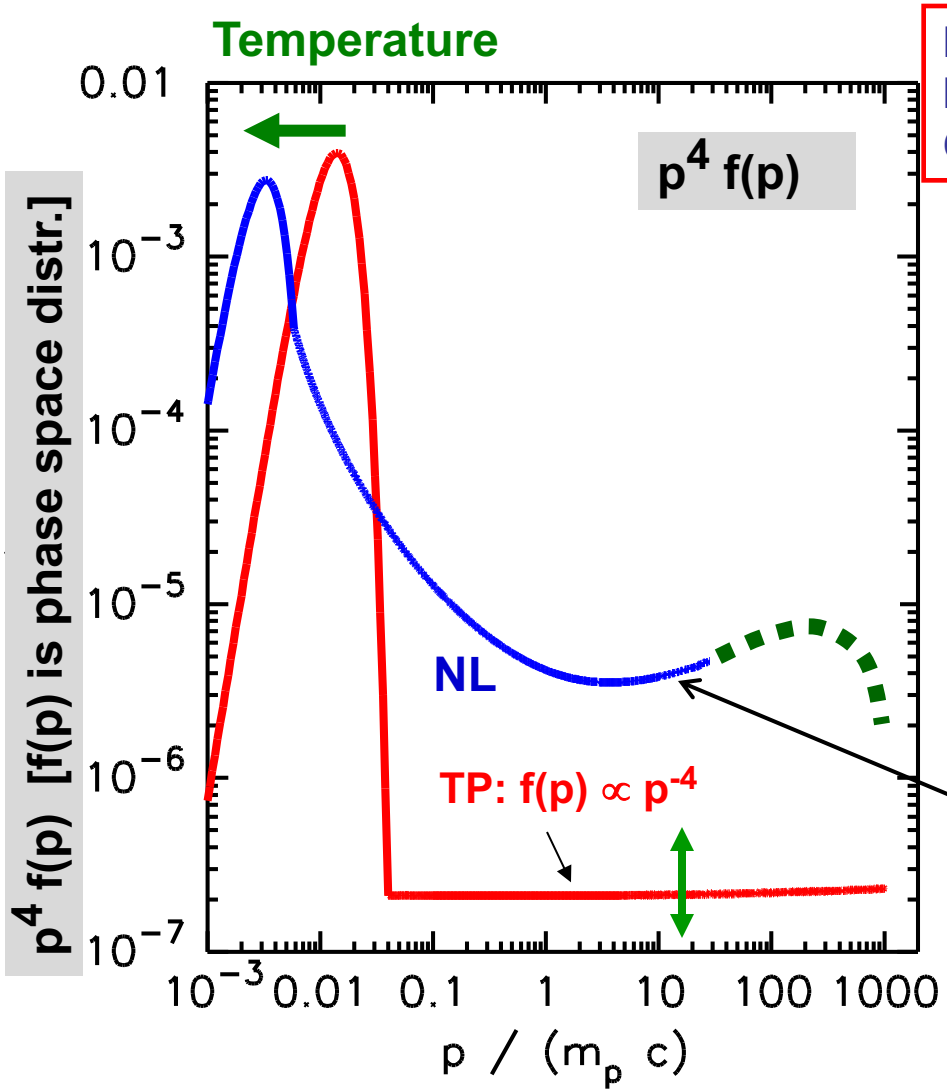

If acceleration is efficient, shock becomes smooth from backpressure of CRs

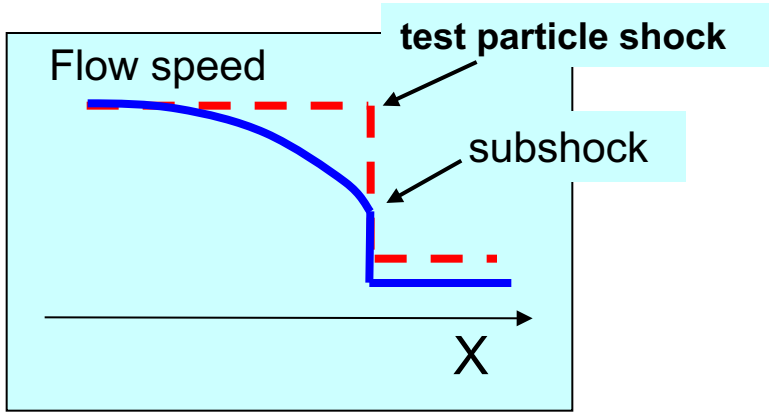

- Concave spectrum
- Compression ratio, $r_{tot} > 4$
- Low shocked temp. $r_{sub} < 4$

In efficient acceleration, entire particle spectrum must be described consistently, including escaping particles ➔ much harder mathematically

BUT, connects thermal emission to radio & GeV-TeV emission

Test particle spectra were calculated in seminal works by W.I. Axford ea, G.F.Krymskii, A.R.Bell, Blandford & Ostriker in 1977-78

Ellison +

Electron and Proton distributions from efficient (nonlinear) diffusive shock acceleration

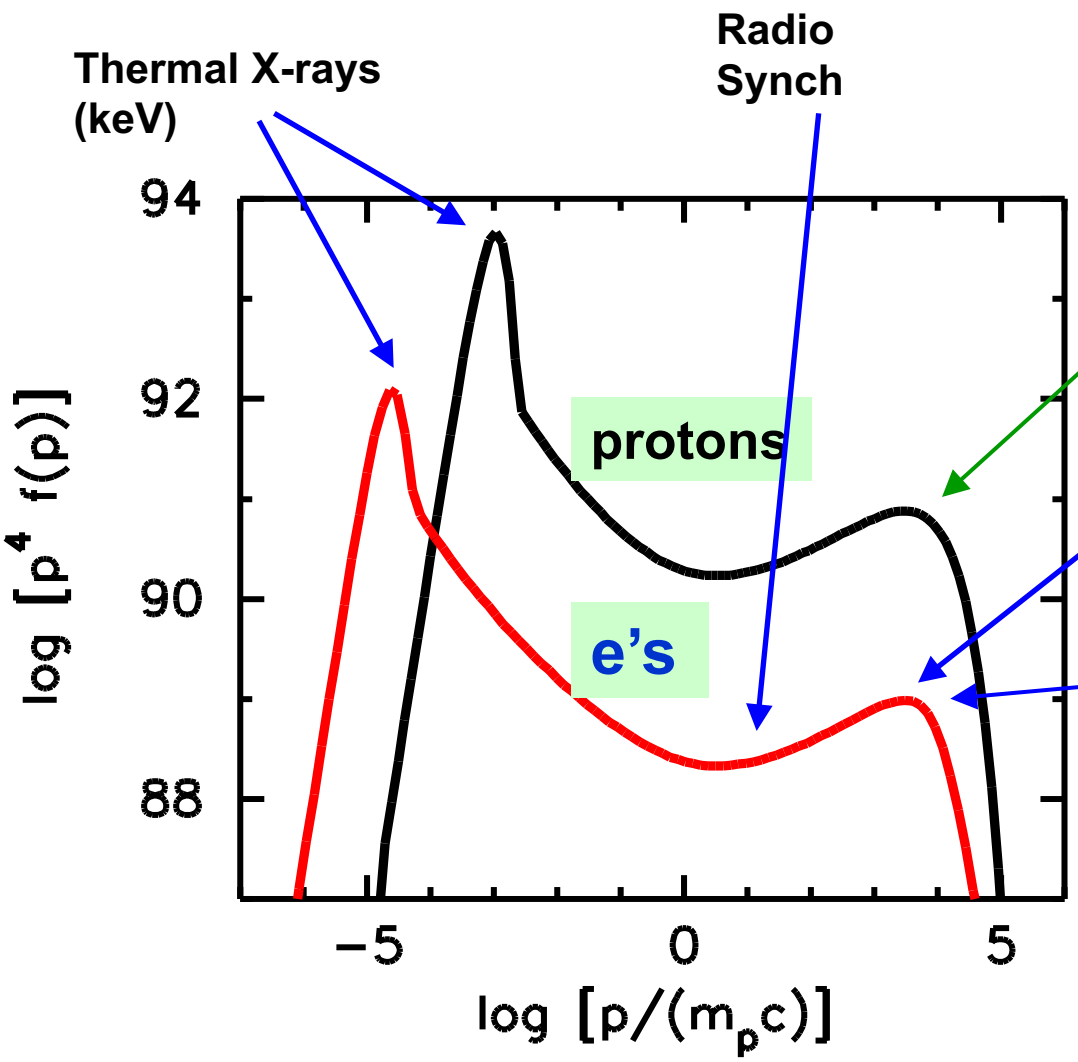

Pion-decay (GeV-TeV) only emission coming from protons

compete at TeV energies

X-ray Synch (keV X-rays)

Inverse Compton (GeV-TeV γ-rays) from electrons

Several free parameters required to characterize particle spectra, including B-field, e/p ratio, diffusion coefficient

Curvature not expected to be this pronounced for typical SNR parameters

Ellison +

Particle distributions

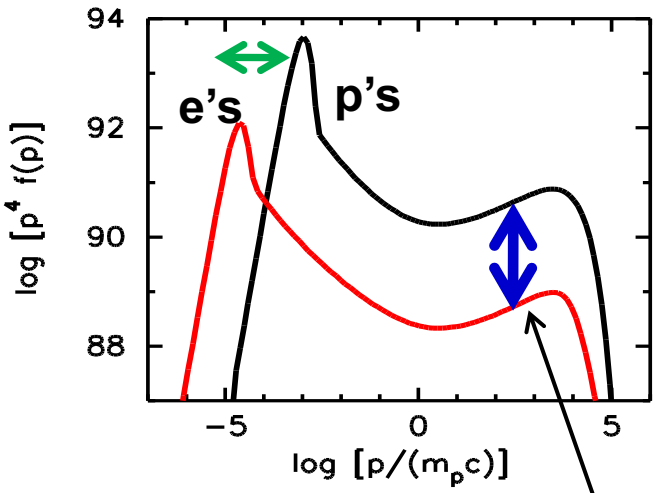

For electrons need two extra parameters: K_{ep} & T_e/T_p

Electron/proton ratio, K_{ep}

K_{ep} critical for p-p / IC ratio at GeV-TeV

K_{ep} and T_e/T_p not yet determined by theory or plasma simulations!

continuum emission

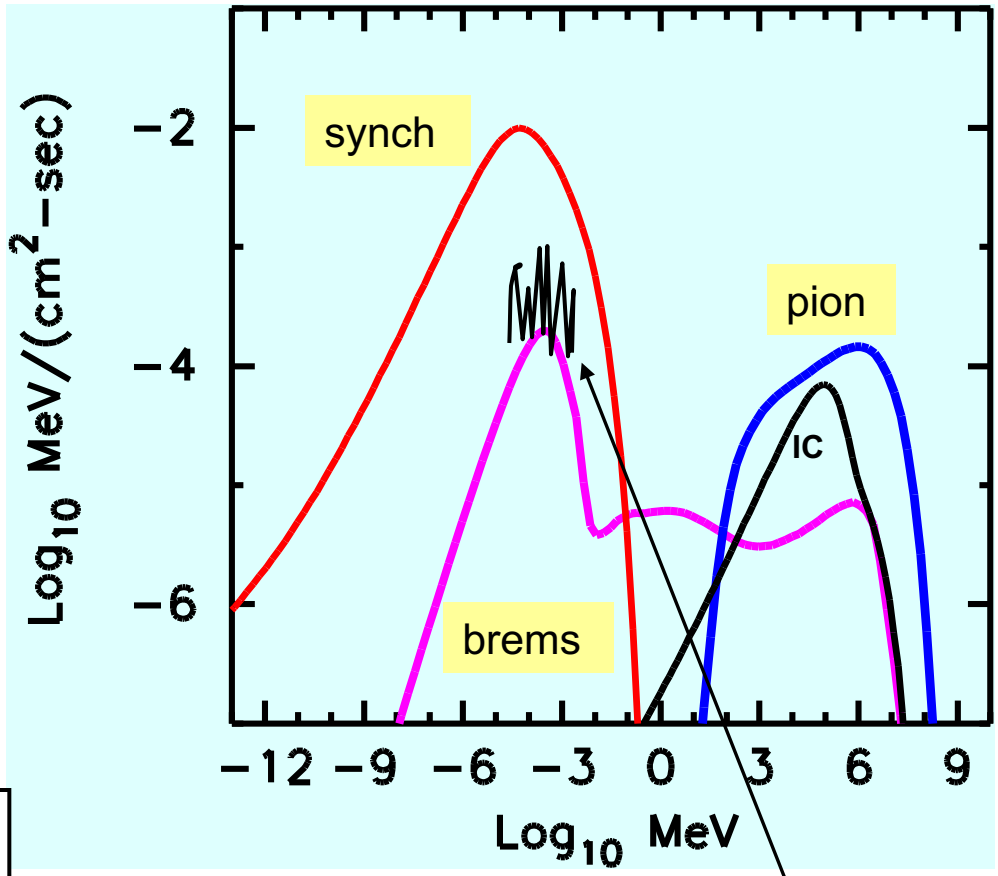

Thermal X-ray emission lines ➔ depend on T_e/T_p and electron equilibration
➔ Coupling with NL DSA helps to constrain parameters

Ellison +

Diffusion-convection equation for particle transport

$$\frac{\partial}{\partial x}\left[D(x,p)\frac{\partial}{\partial x}f(x,p)\right] - u\frac{\partial f(x,p)}{\partial x} + \frac{1}{3}\left(\frac{du}{dx}\right) p \frac{\partial f(x,p)}{\partial p} + Q(x,p) = 0$$

u_0 is shock speed, f(x,p) is phase distribution function

This equation requires that $v_{part} >> u_0$ so distributions f(x,p) on either side of shock are nearly isotropic (this is why it doesn't hold for relativistic flows).

In many cases, observations and PIC simulations show that shocks can inject thermal particles

Particle-in-cell simulations demonstrated injection of CRs from the thermal pool

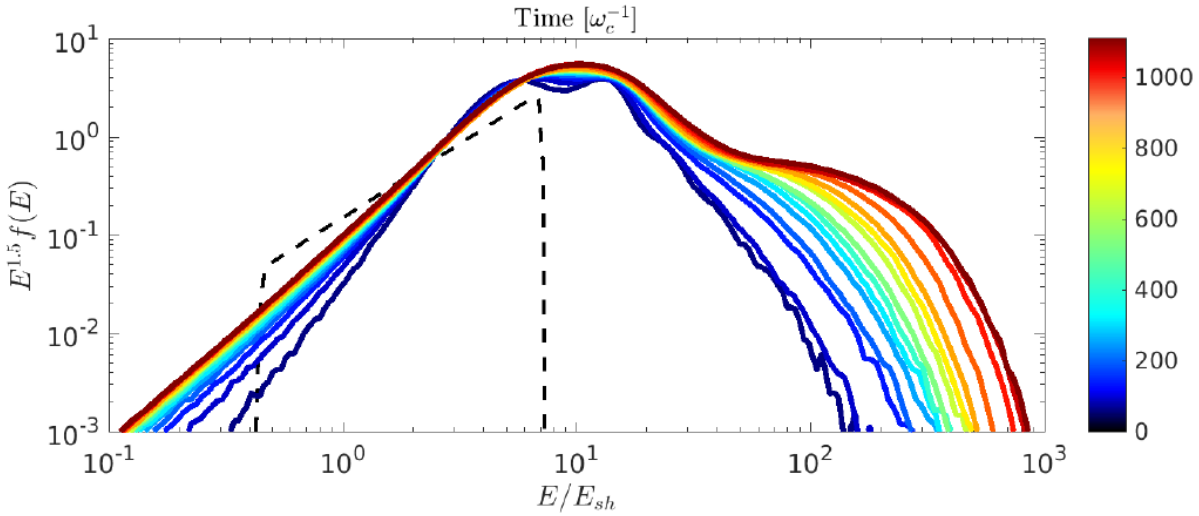

Caprioli Spitkovsky

Nonlinear Monte Carlo modeling of DSA and SDSA with Magnetic Field Amplification

Using approximate plasma physics (quasi-linear theory, Bohm diffusion, etc.)

Monte Carlo code iteratively solves nonlinear DSA problem with MFA

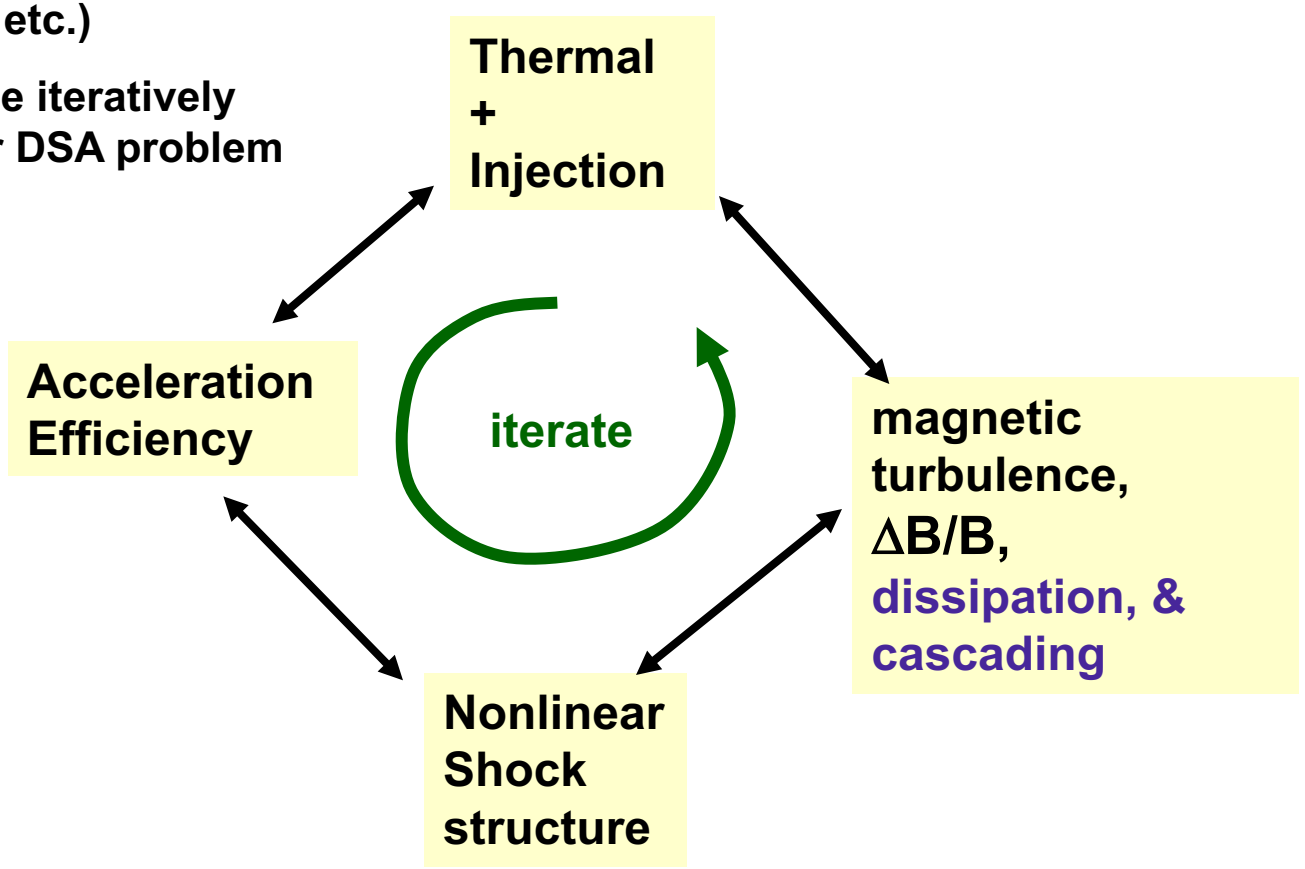

If acceleration is efficient, all elements feedback on all others

Monte Carlo model of Nonlinear Diffusive Shock Acceleration

k – wavenumber of turbulent harmonics

$W(x,k)$ – spectrum of turbulent fluctuations, (energy per unit volume per unit Δk).

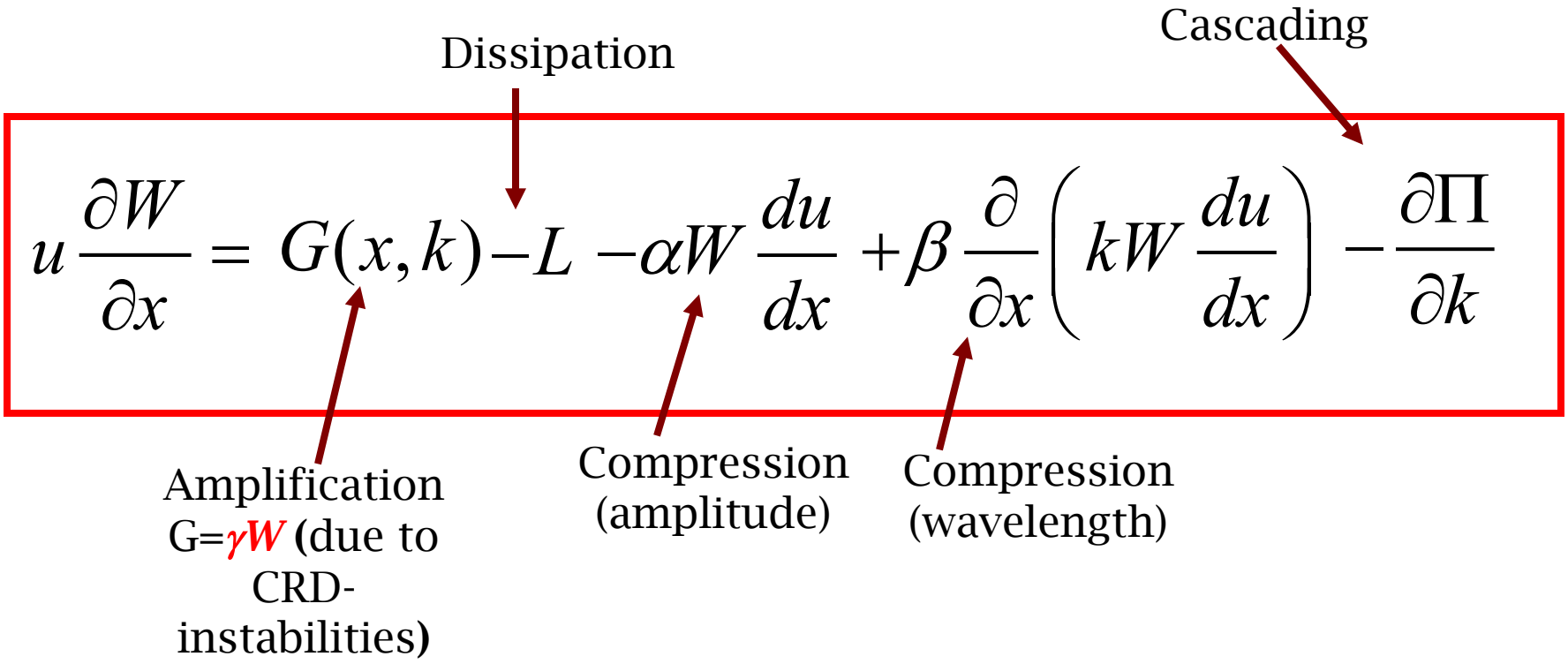

In non-linear MC models the growth rates and the CR anisotropy – the driving source are derived consistently and simultaneously…

Magnetic turbulence spectra in a MC model with 3 instabilities

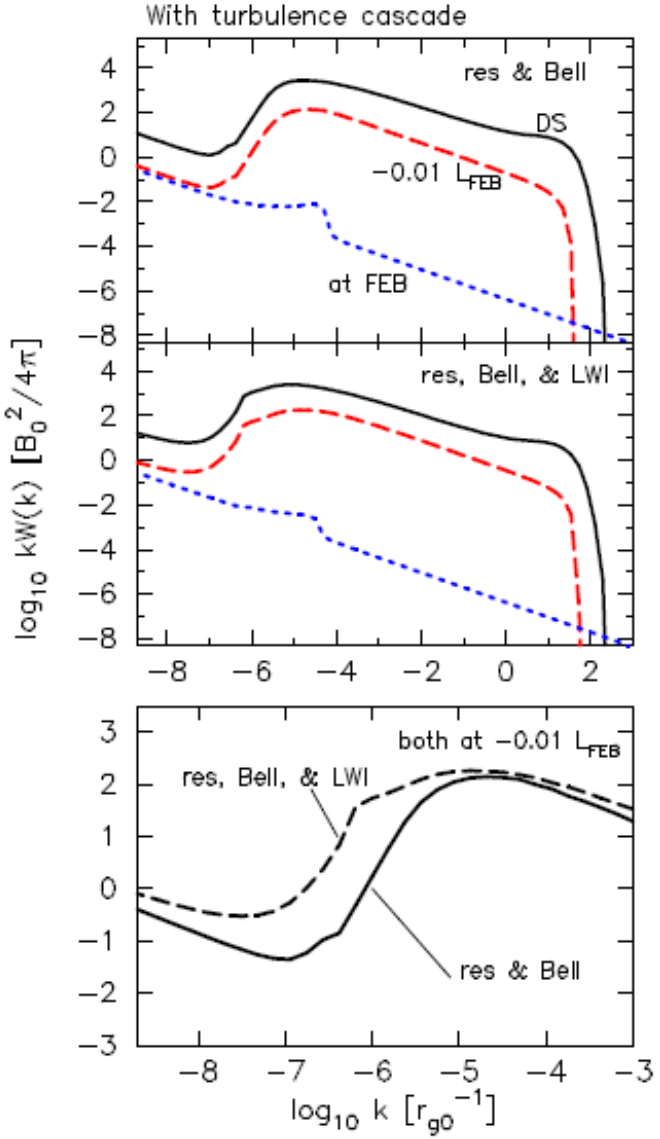

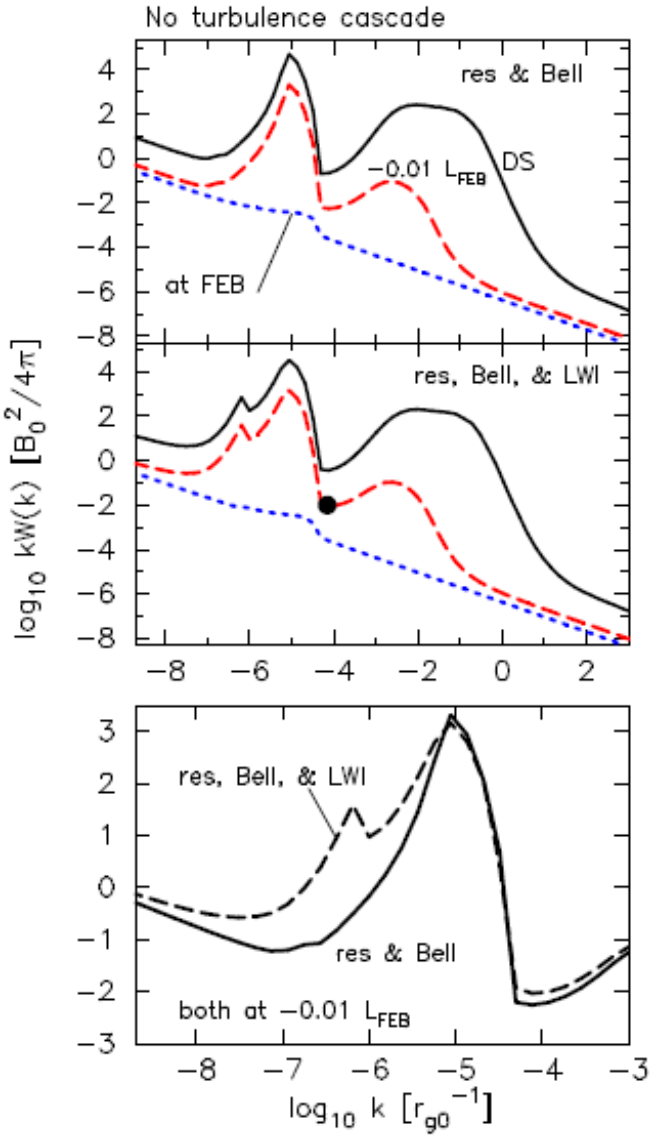

ApJ, 789:137, 2014.

$$n_0 = 0.3\ см^{-3};\ u_0 = 5000\ \frac{км}{с};\ B_0 = 3\ мкГс$$

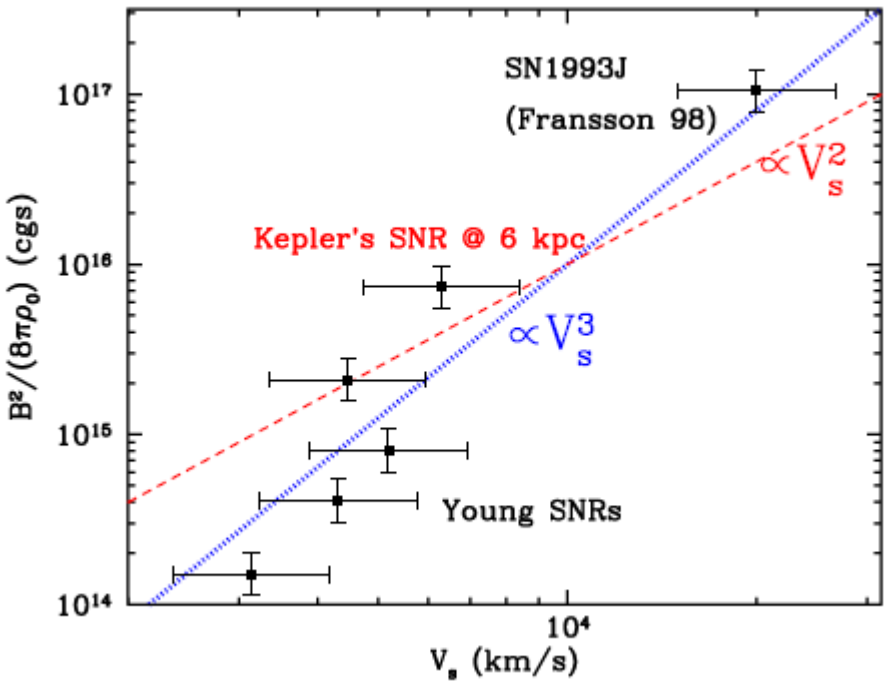

Jacco Vink AARv12

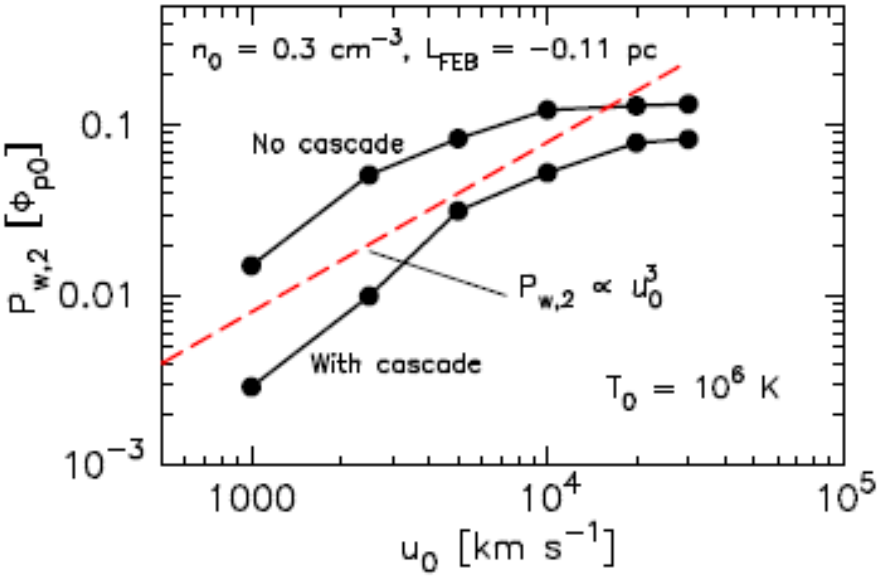

ApJ, 789:137, 2014

Magnetic Field in supernova shells is highly turbulent with quasi-regular field much smaller than the fluctuating field

What about the sychrotron radiation in this field?

The strongest field fluctuations have scales longer than the synchrotron photon radiation length

Then the shell images are intermittent with structures e.g. dots, clumps and filaments some of these are highly polarized in X-rays

Simulated synchrotron X-ray polarized image of young supernova shells at 5 keV XIPE

X-ray polarization can be used to study strong turbulence in SNR!

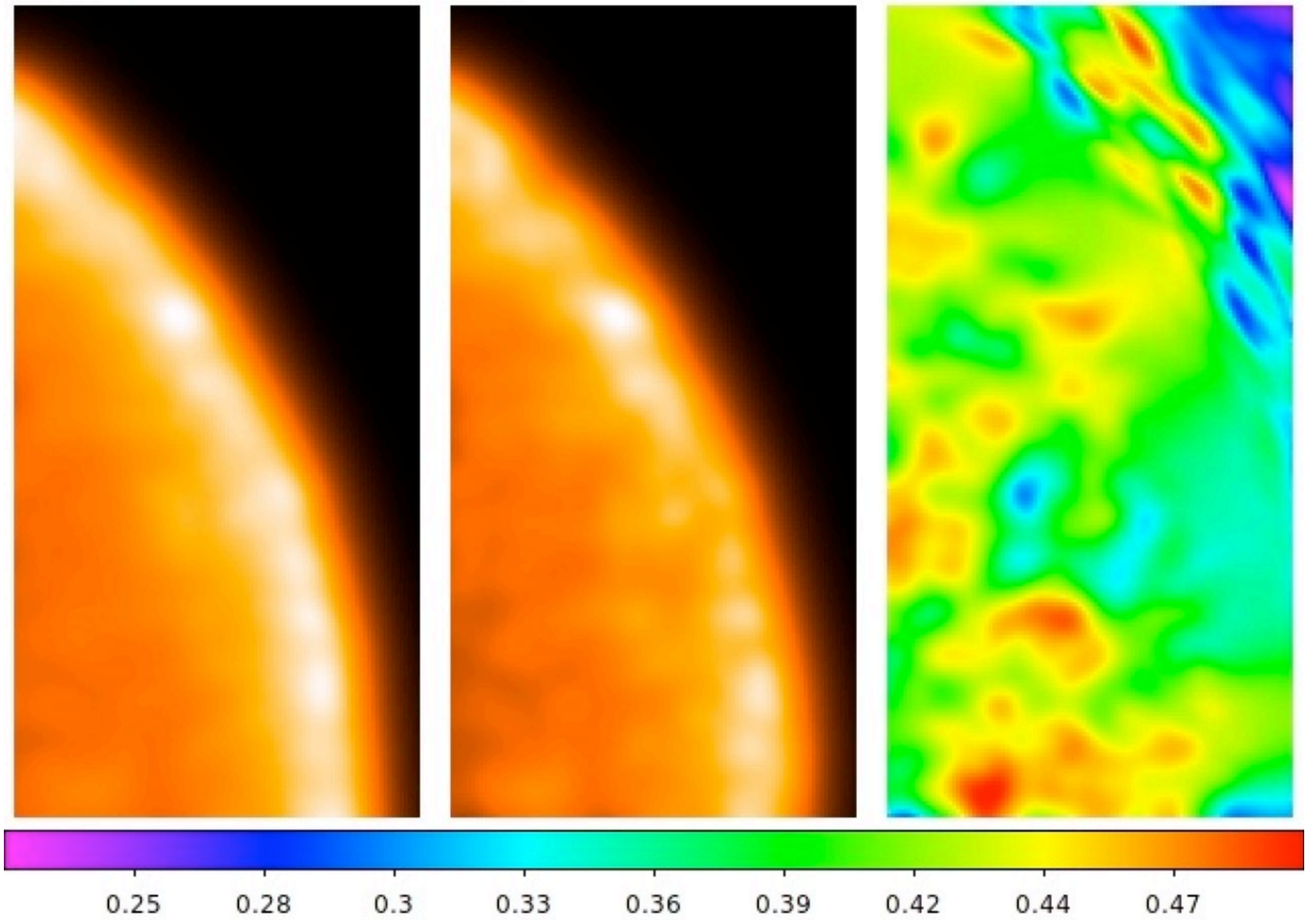

anisotropic magnetic turbulence K^{-5/3} (Kolmogorov model)

AB + MNRAS v.399, p1119, 2009

Simulated synchrotron X-ray polarized image of young supernova shells at 5 keV XIPE PSF resolution

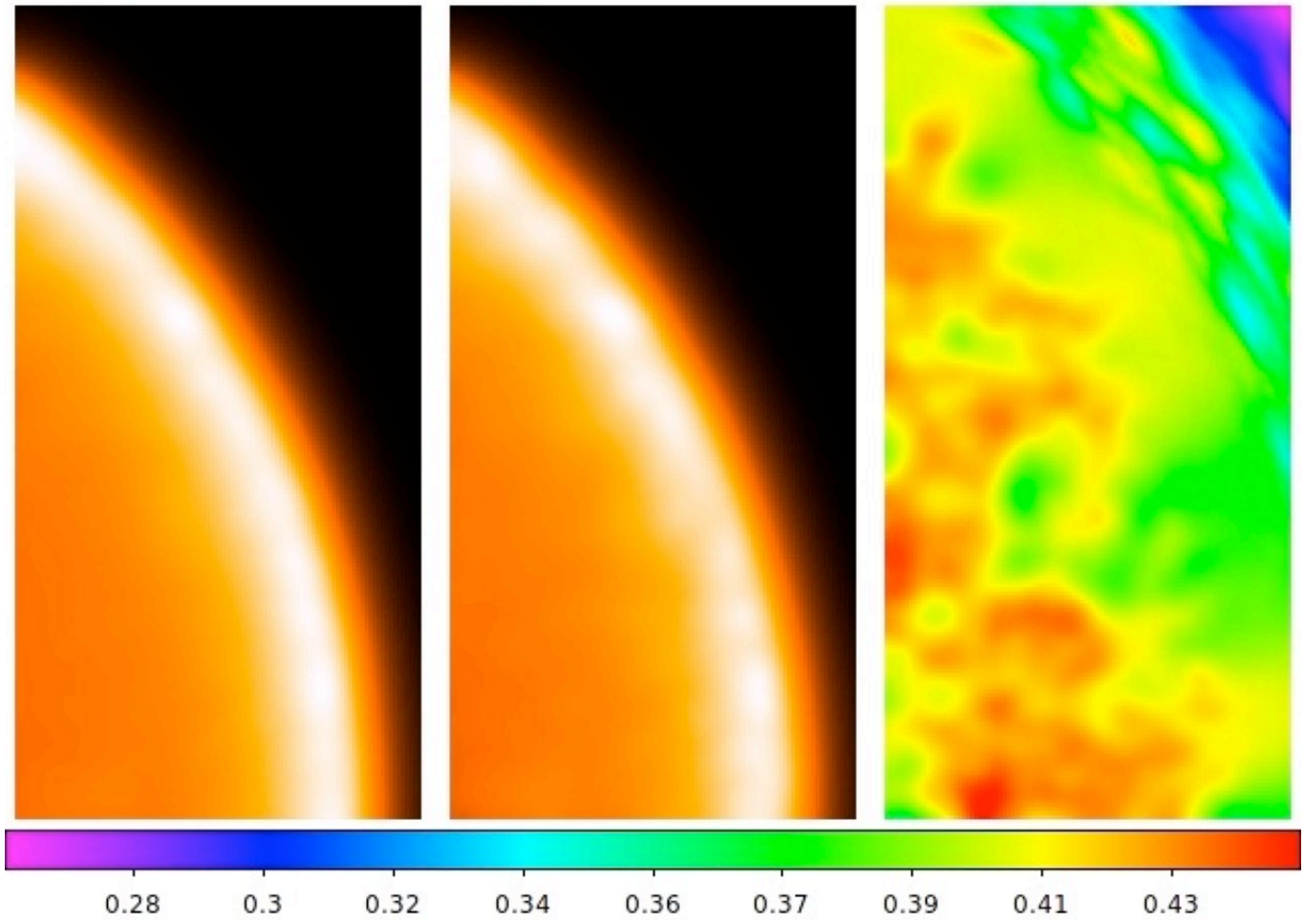

anisotropic magnetic turbulence K^{-1}
(Bohm diffusion model)

AB + MNRAS v.399, p1119, 2009 and
AB and Uvarov 2017

AB+ ApJL v735, L40, 2011

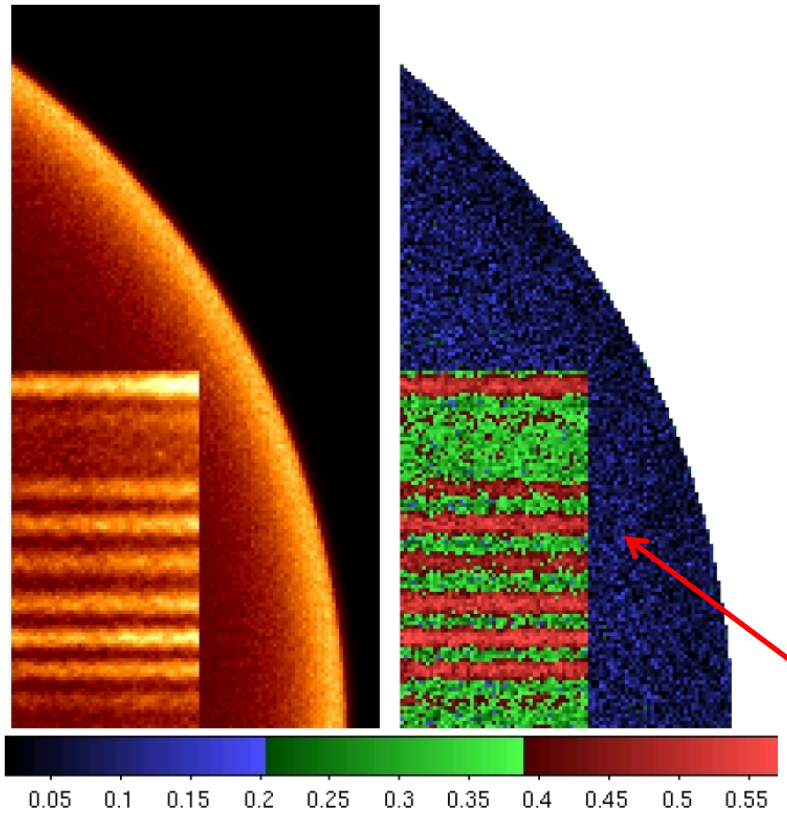

Polarization fraction

DSA is a possible explanation of Tycho's strips

➔ **Some shock and turbulence properties must come together to produce coherent structure on this scale. Transverse part of the shock, anisotropic cascade, high Pmax**

Strong predictions:
Quasi-perpendicular upstream B-field

Strong linear polarization in strips

AB+ ApJL v. 689, L133, 2008

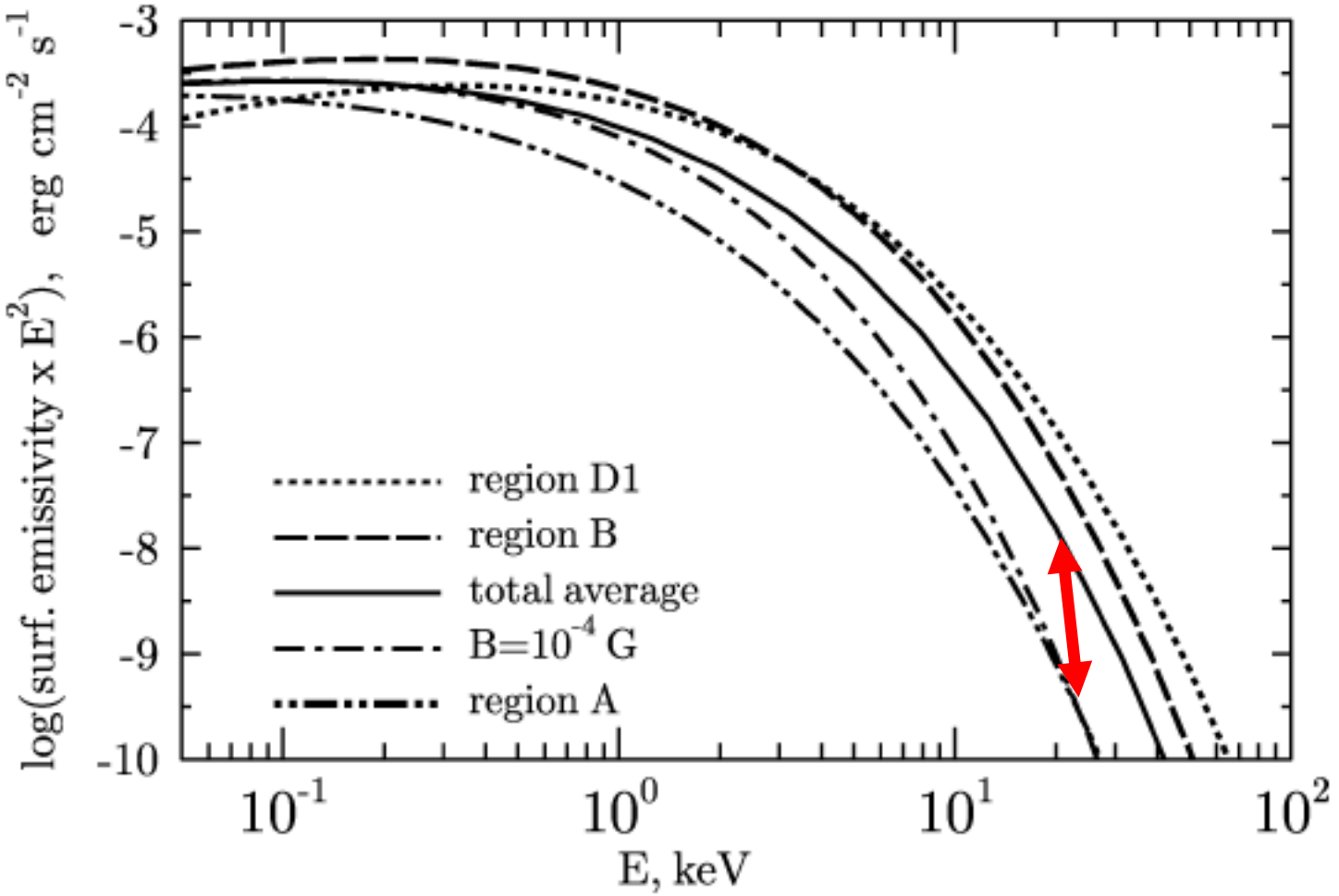

Important feature of the synchrotron SN shells with strongly turbulent magnetic field is the spectral redistribution of photons with the enhanced flux in the spectral cut-off region.
The dot-dashed line corresponds to radiation in homogenious field
Solid line is for random field of turbulent field where $B_0 = \sqrt{\langle B^2 \rangle}$.

Non-linear Relativistic Shock Monte Carlo modeling

(DSA with magnetic field amplification) SN2009bb case

so the model is getting close to the Hillas energy

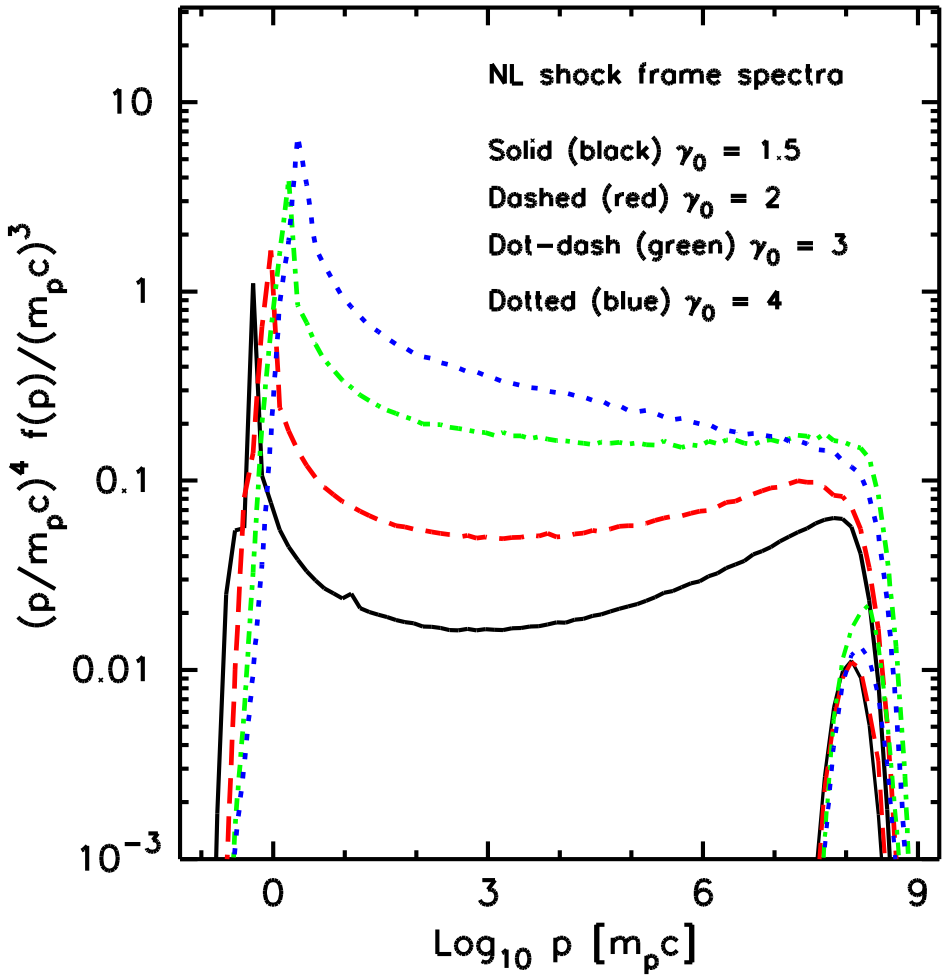

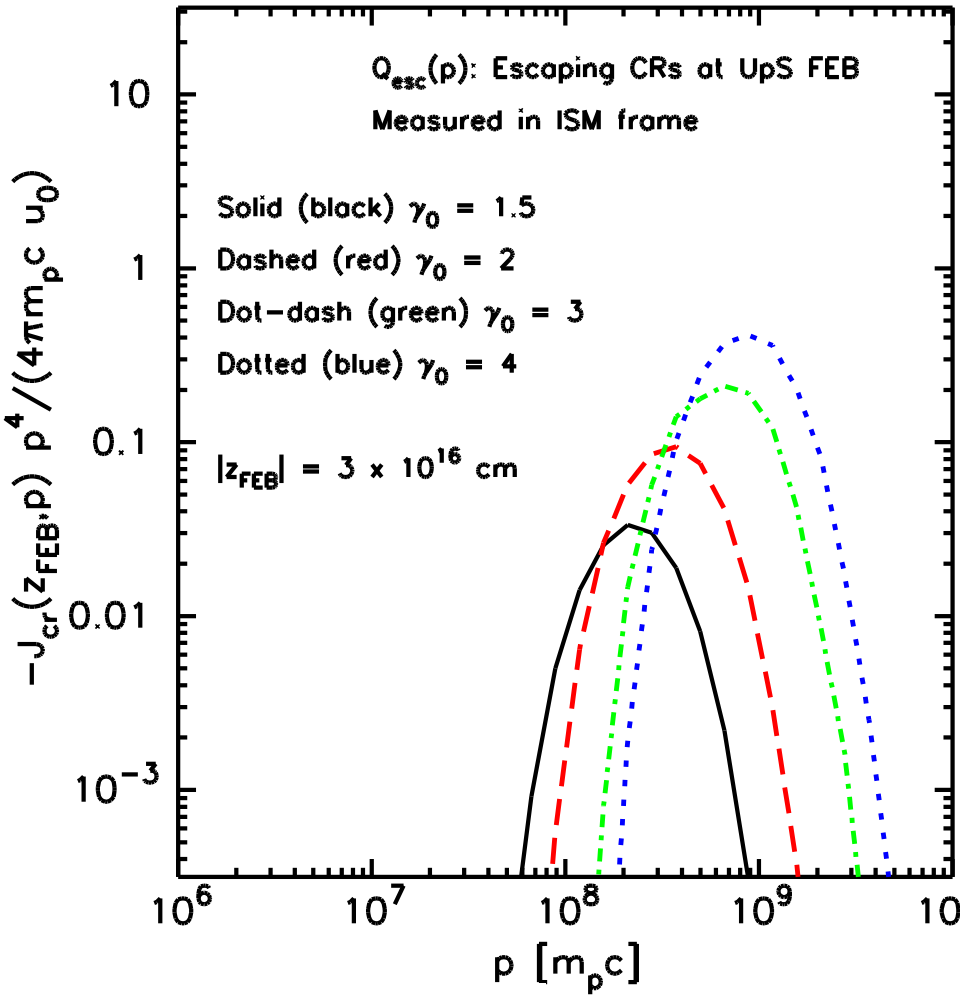

Space Science Reviews v214, id41 2018

Nonlinear Monte Carlo modeling of SuperDiffusiveSA with Magnetic Field Amplification

CR transport in the shock precursor

Diffusion **vs** **Levy walks**

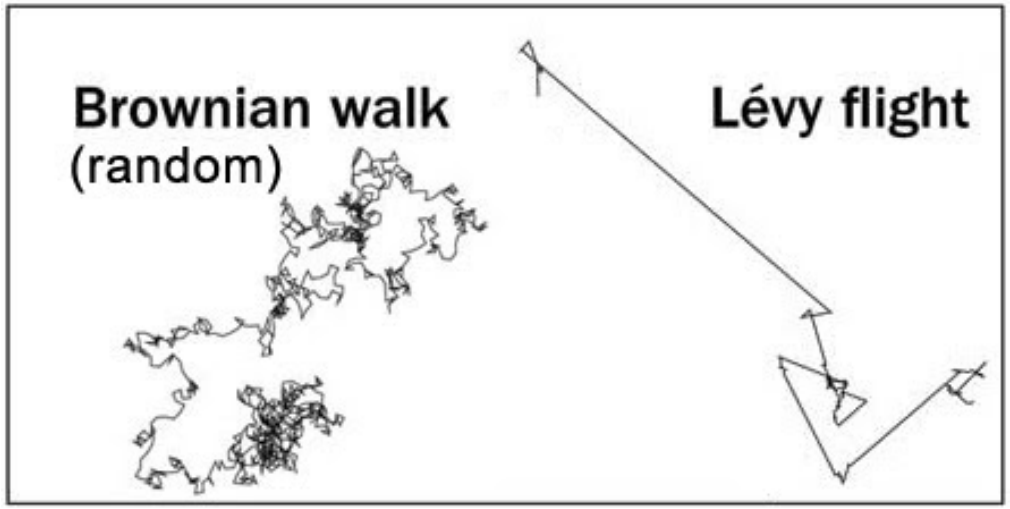

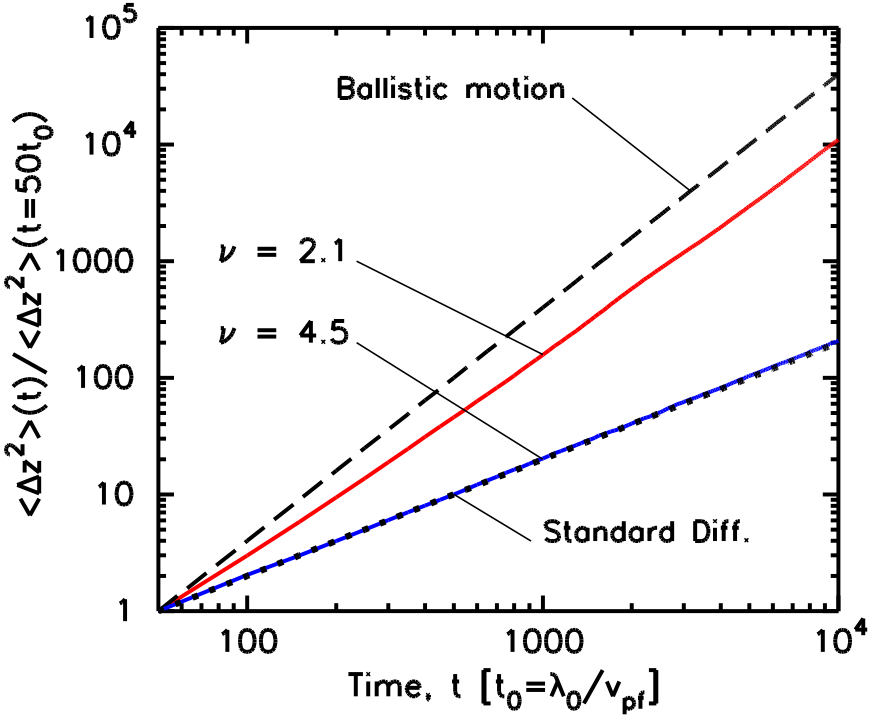

AB+ PHYSICAL REVIEW E 95, 033207 (2017)

Super-diffusion in the CR shock shock precursor ($x < -10^4 r_{g0}$) where turbulence onset

CR spectra downstream f(p) and CR escaping flux at FEB $Q_{esc}(p)$

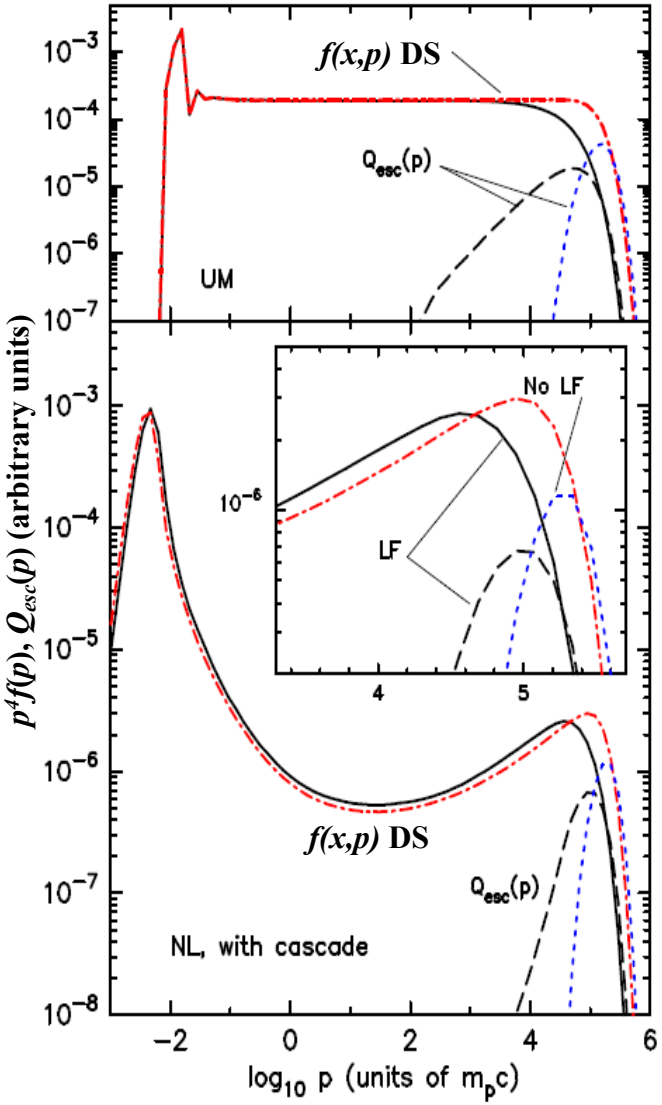

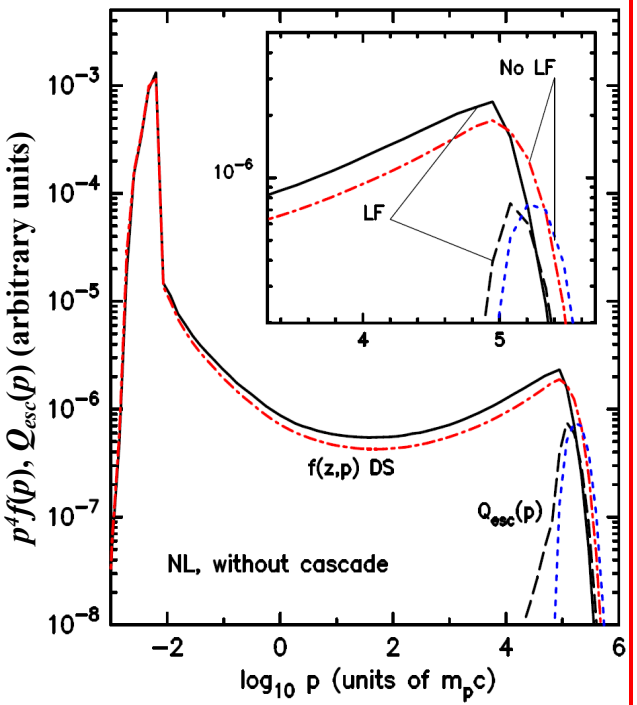

$$J(x,p) = 2\pi \int_{-1}^{1} v\mu f_{pf}^{cr}(x,p,\mu) d\mu$$

$f_{pf}^{cr}(x,p,\mu)$ - функция распределния ускоренных частиц в ситеме покоя фоновой плазмы

$$Q_{esc}(p) = -\frac{J(x_{FEB},p)\,p^4}{4\pi m_p c u_0}, \quad x_{FEB} = 10^8 r_{g0}$$

Turbulence spectra:(a) at FEB $x=-10^8 r_{g0}$, (b) at $x=-10^6 r_{g0}$, (c) at shock downstream

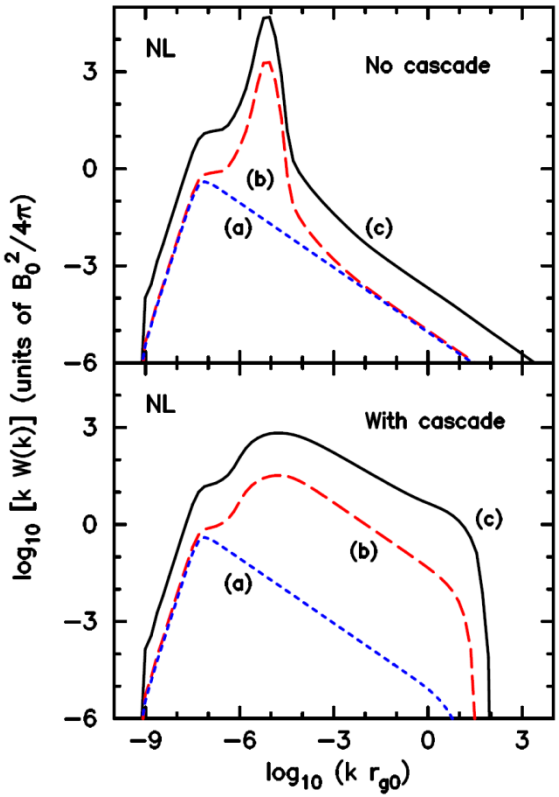

AB+ PHYSICAL REVIEW E 95, 033207 (2017)

What can we learn from gamma-ray observations of SNRs?
How can they contribute to Galactic CRs?

Supernova remnants as CR accelerators

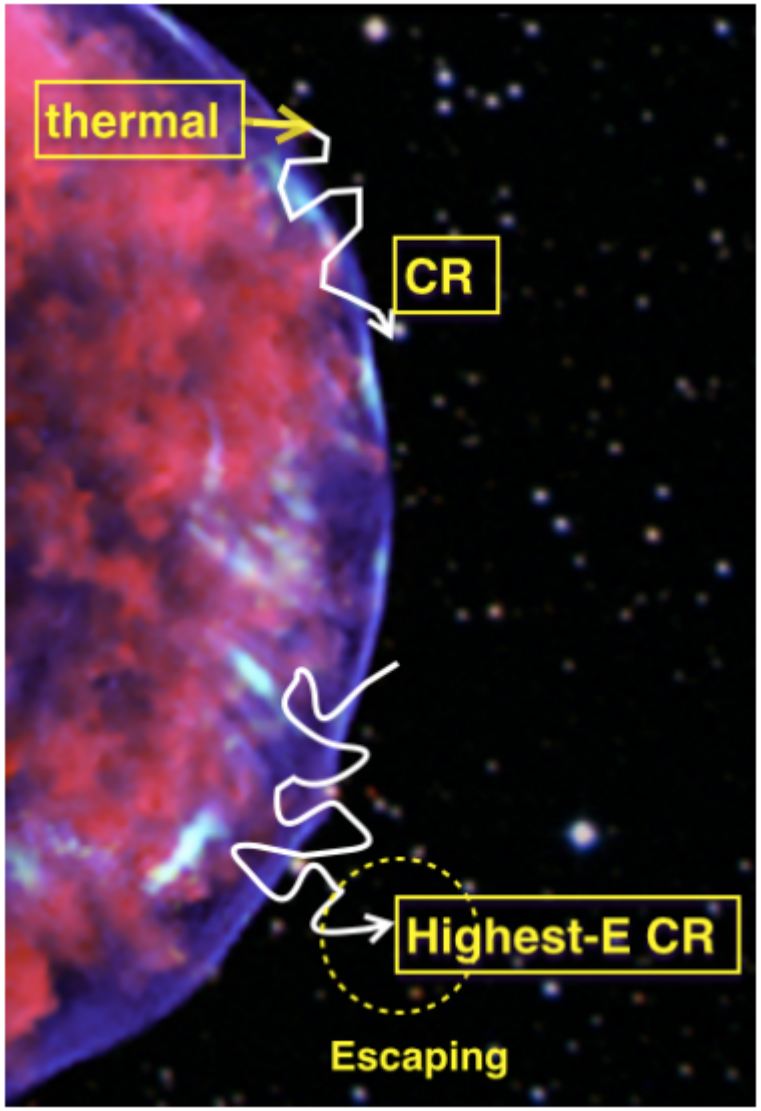

Supernova remnants (SNRs)

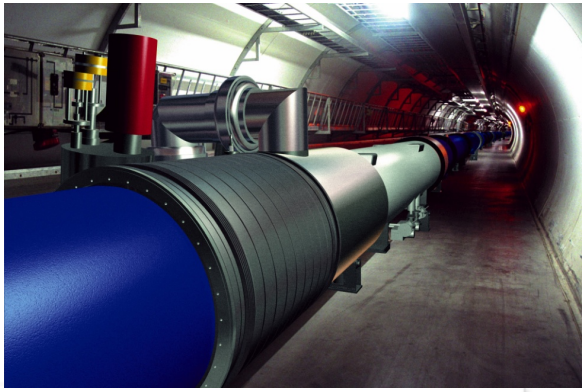

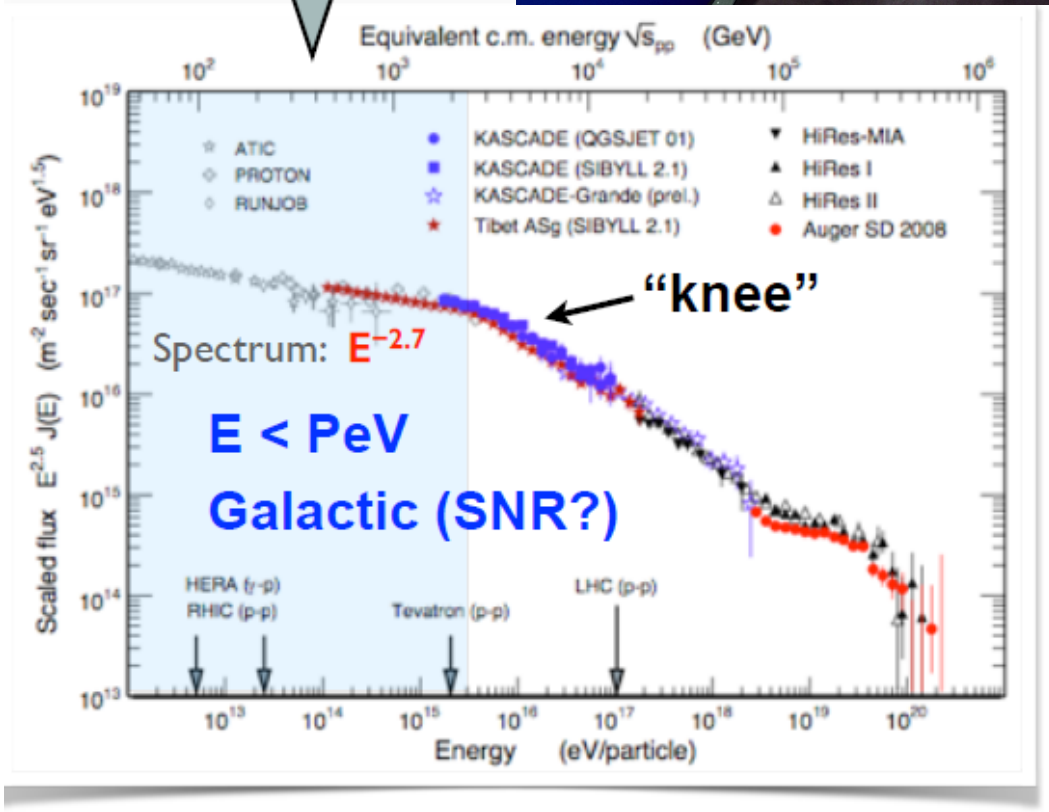

TeV gamma rays from RXJ1713.7-3946

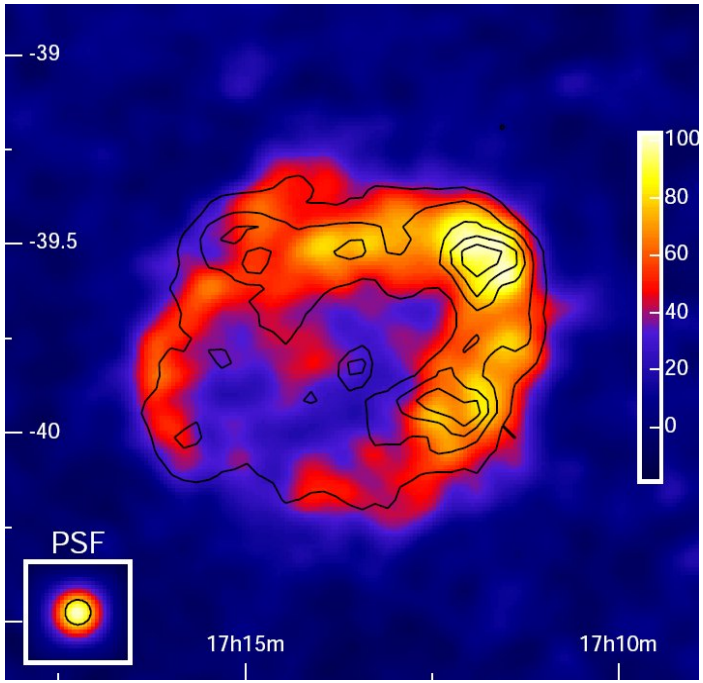

RXJ1713.7-3946 (HESS)

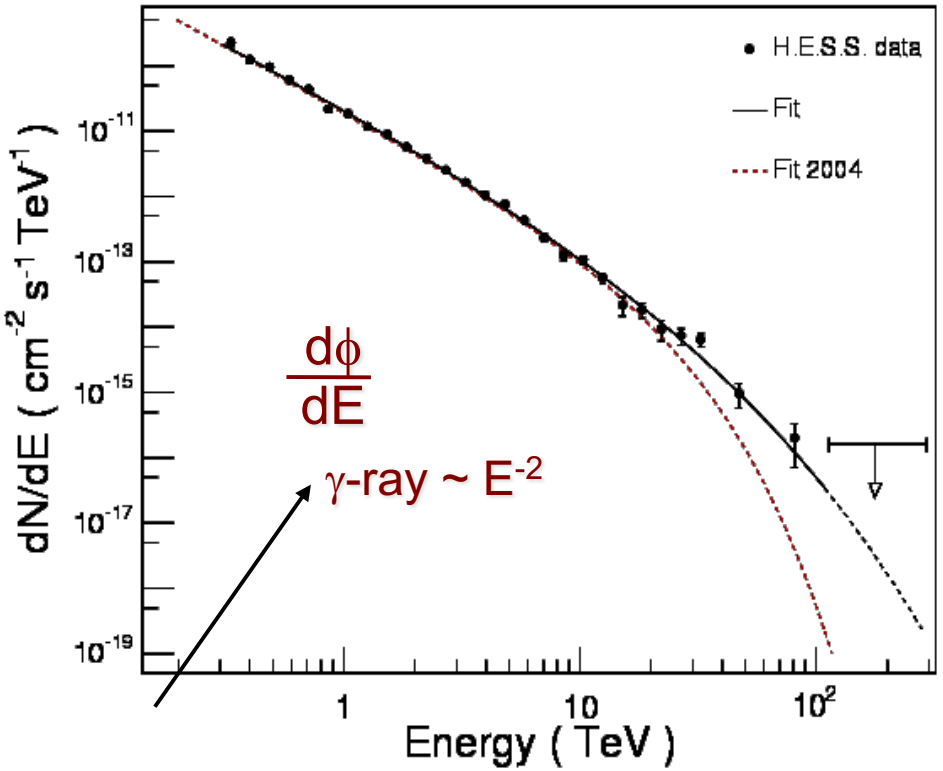

F.Aharonian+, *Astron.Astrophys.***464**, 235 (2007)

Fermi images of young SNRs

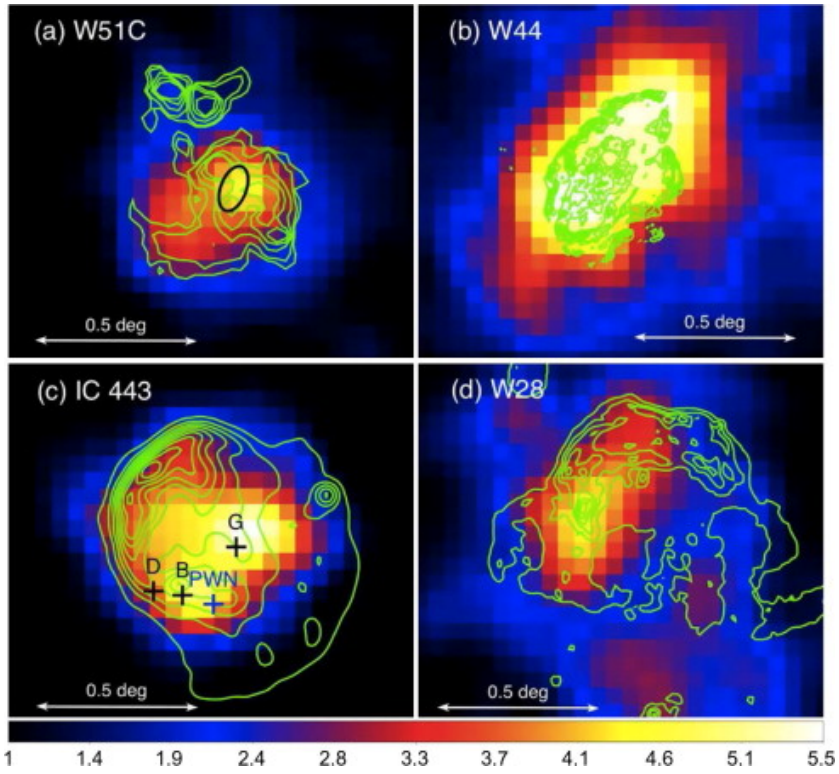

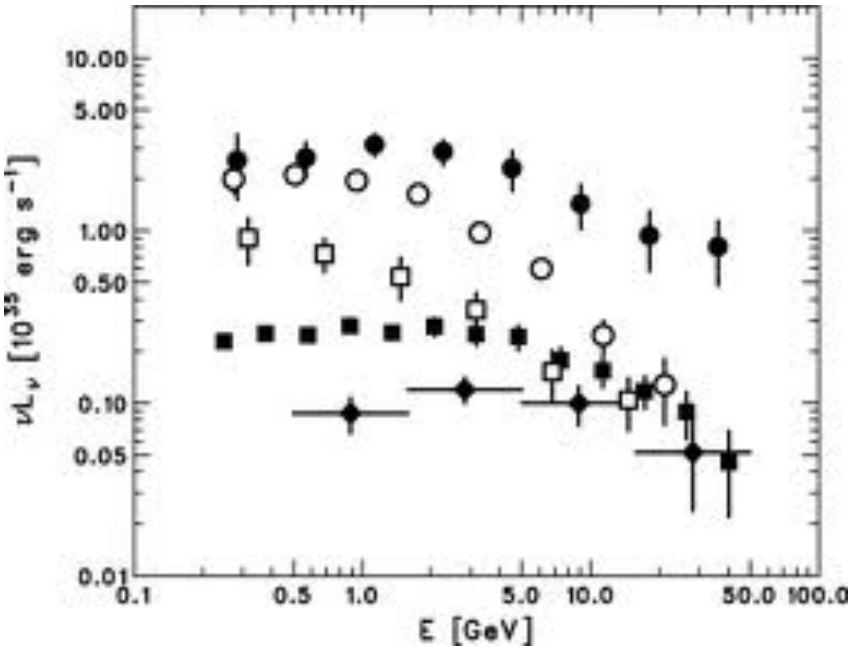

$$L_\gamma \sim 10^{34} - 10^{36}\, erg/s$$

W51C (filled circles) W44 (open circles);
IC 443 (filled rectangles); W28 (open rectangles)
Cassiopeia A (filled diamonds).

Thompson Baldini Uchiyama 2012

Ackermann et al., Tavani ea

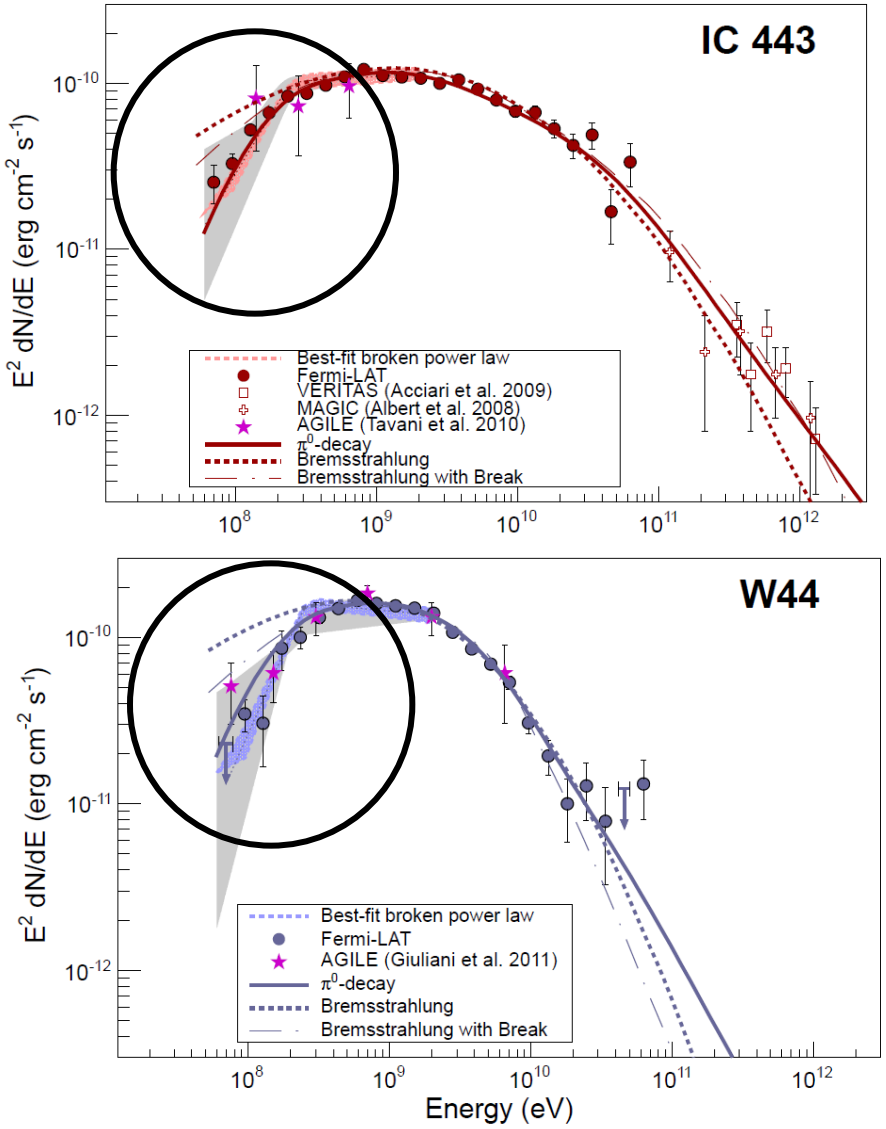

Fermi LAT observations of SNRs interacting with dense material (molecular clouds)

➔ Strong case for pion-decay gamma-rays dominating GeV-TeV emission

➔ Smoking gun for SNRs being a primary source of galactic CR ions,

but are there other compelling reasons to believe SNRs are primary source of the bulk of CRs?

Energy budget and Ionic composition are most compelling reasons

IC 443 SNR interacting with a molecular cloud

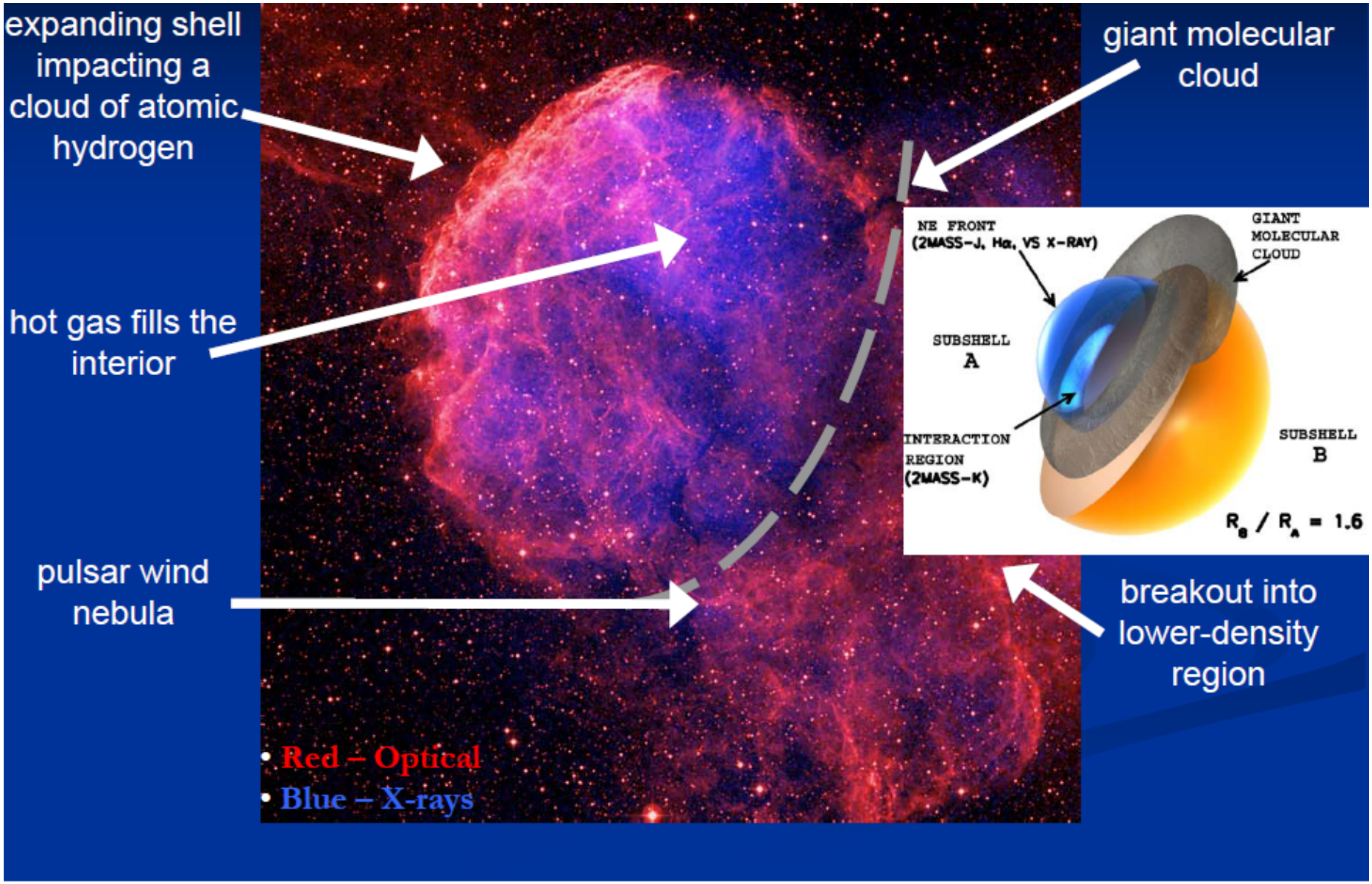

Fermi-LAT and MAGIC spectra of Cas A SNR (2017)

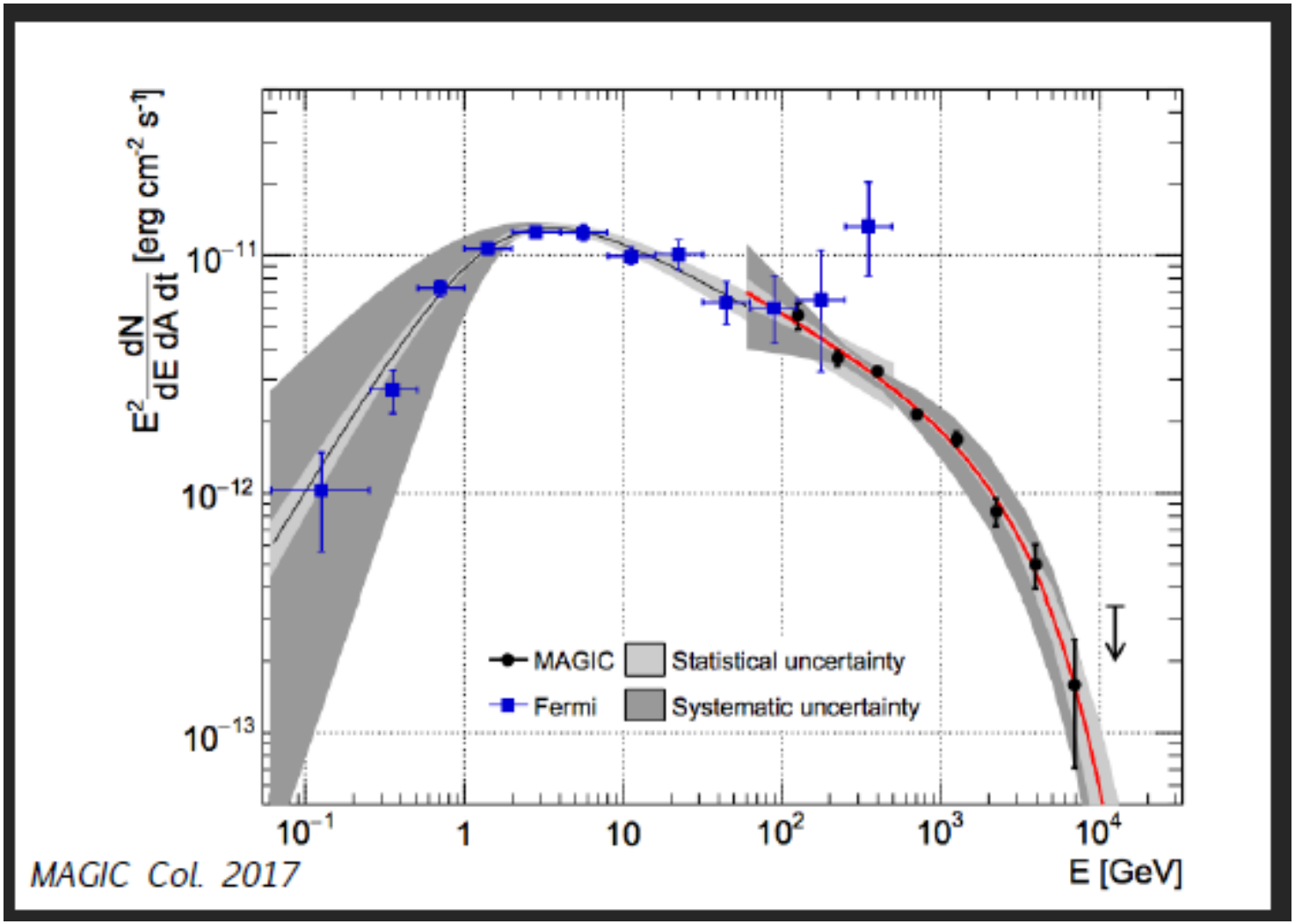

Spectral energy distribution of the Tycho SNR with Fermi-LAT and VERITAS data (2015) in filled red squares and circles, respectively.

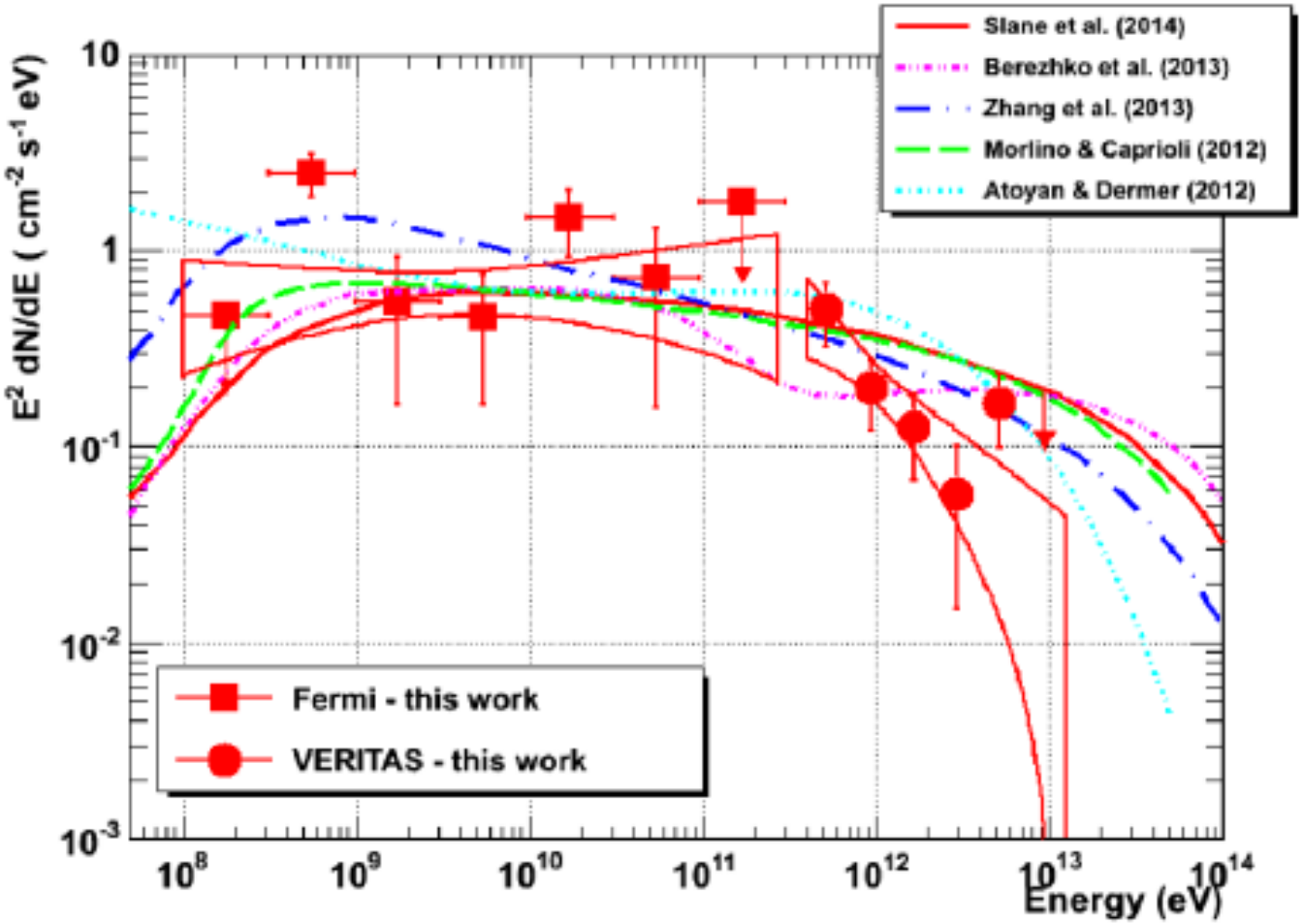

Observed gamma-ray spectra of SNRs

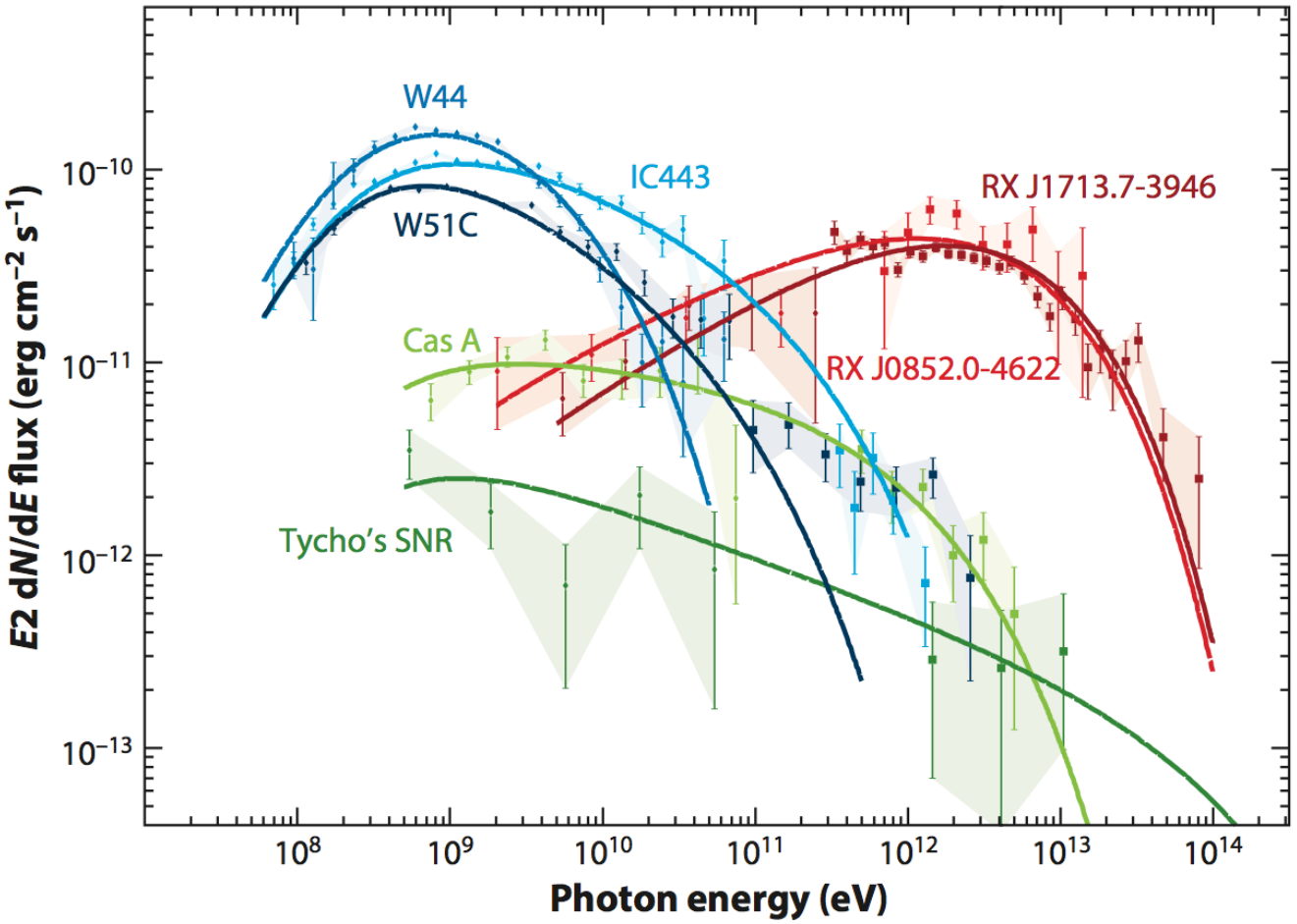

S. Funk 2015

However what are the sources of PeV regime CRs?

PeV CRs are likely accelerated in the Galaxy…

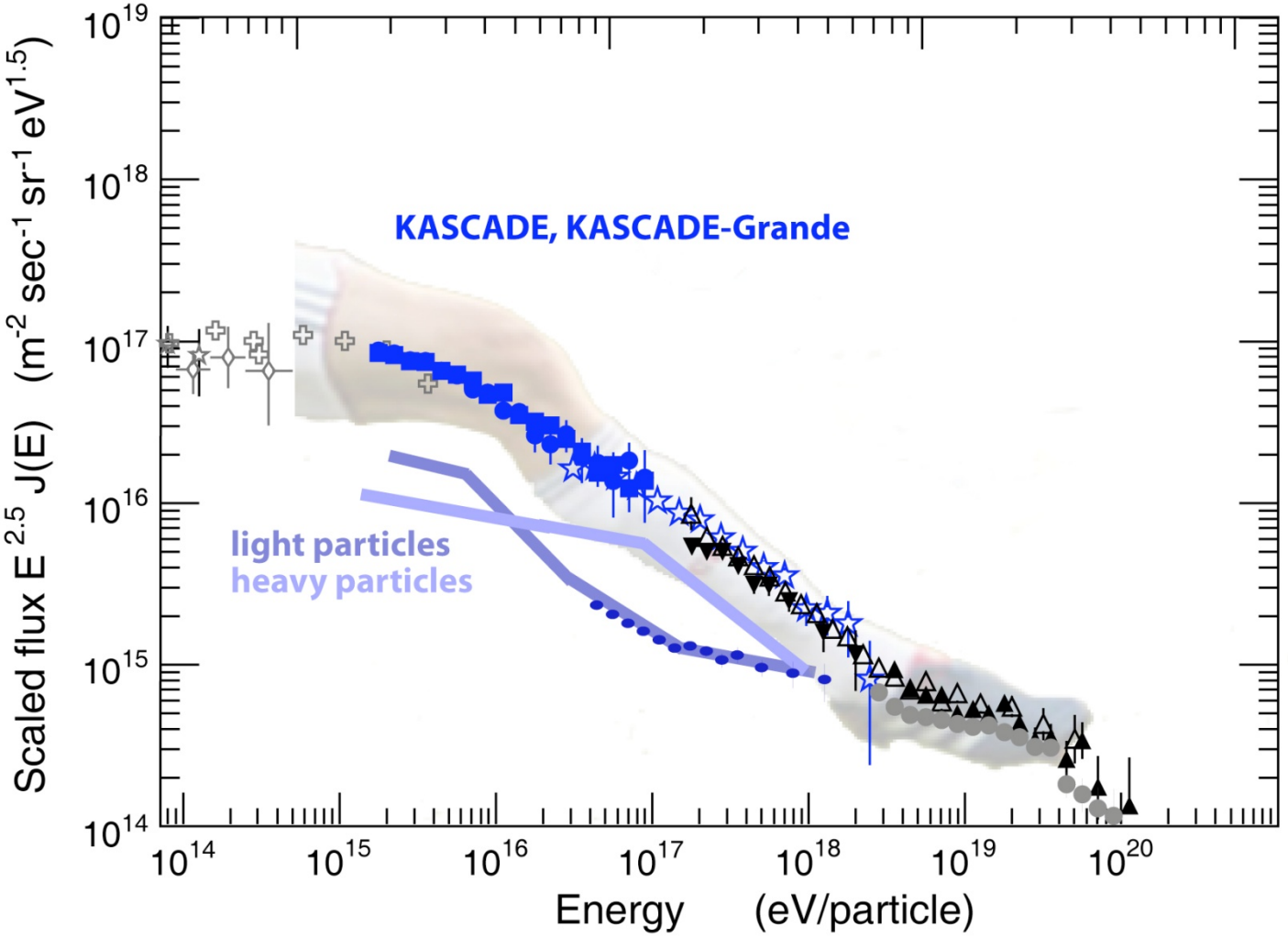

… but how and where?

What else one could expect in galaxies and in the starbursts?

Superbubbles - caverns blown by multiple SN and stellar wind shocks around OB associations

VLT view of superbubbles in LMC

N40

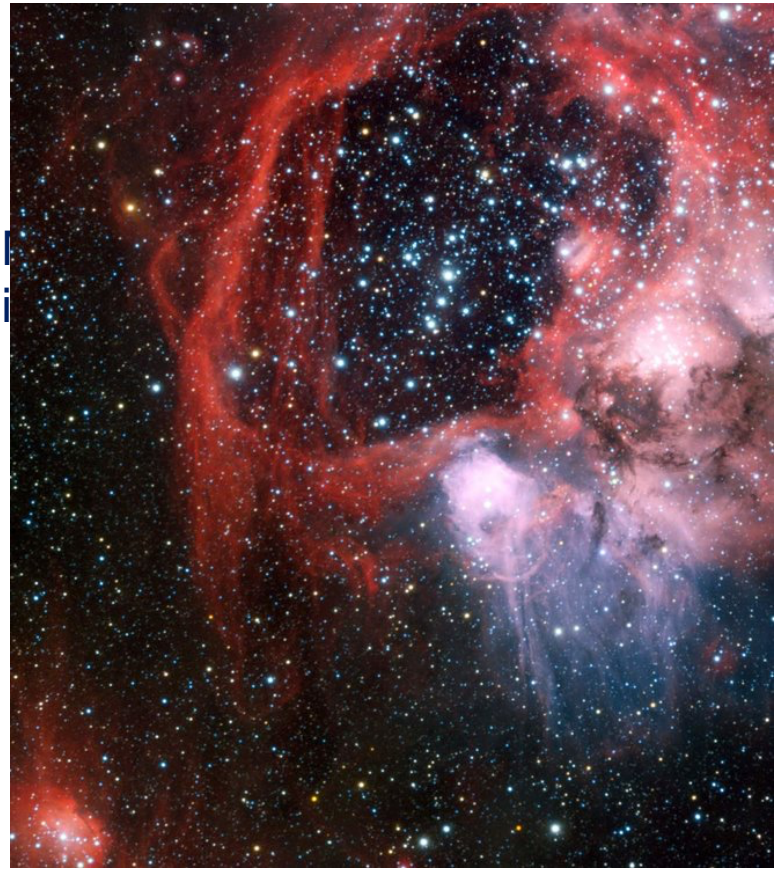

N70

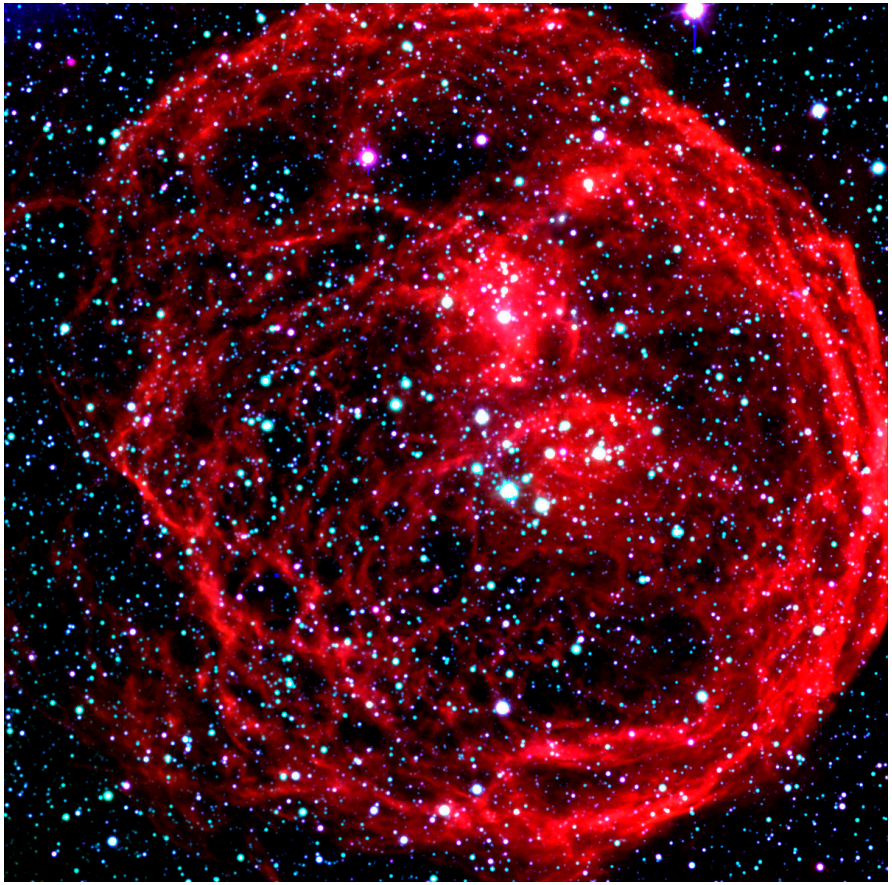

Intermittent structures in hot ~ MK plasma
shocks and rarefactions
~ 100 pc scale size supershell
See Wikipedia

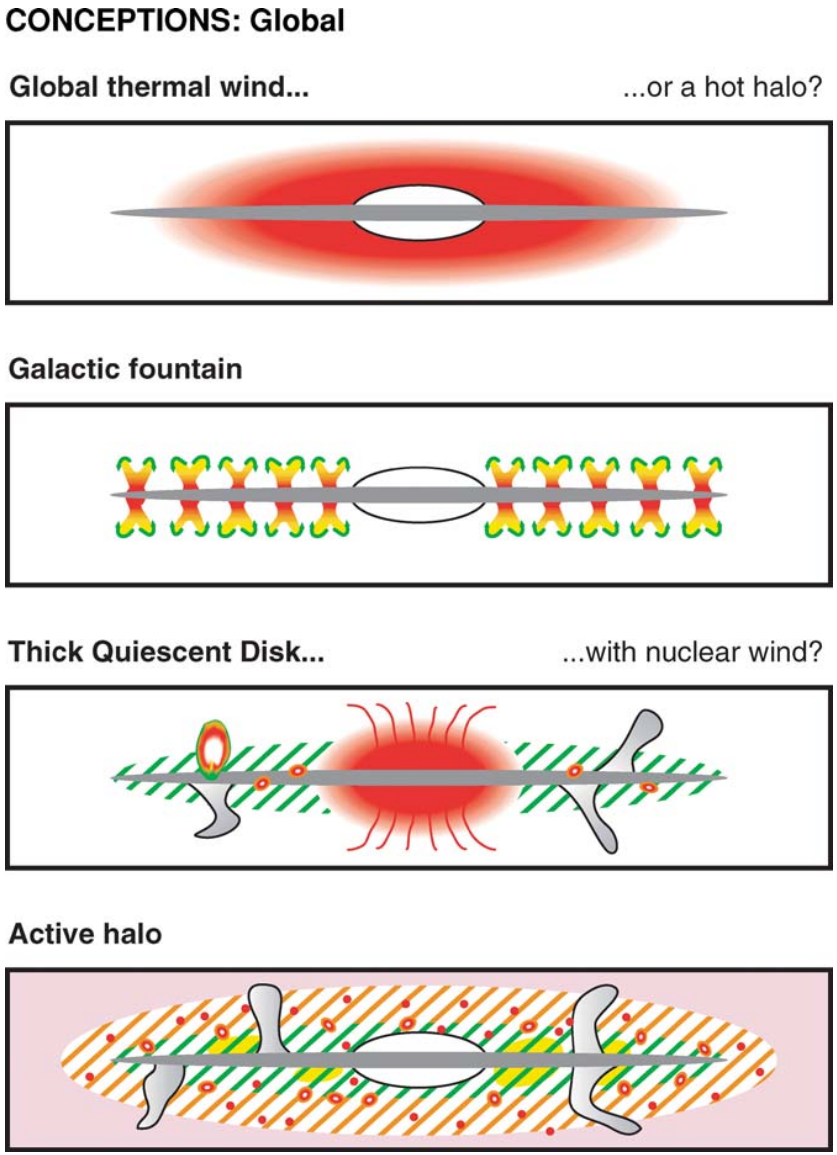

Figure 10 Various conceptions of the larger scale structure of the Galactic atmosphere. In this figure, *hatched green* indicates warm HI; *hatched green on yellow background*—diffuse warm HII; *orange*—hotter gas bearing OVI; *red*—material hot enough to emit X rays; *gray*—plumes of escaping cosmic rays; and *red dots*—microflares. Problems with the *top two panels* are discussed in the text. The *lower two panels* contain some elements of potentially greater realism.

Cox ARAA

NB: Superbubble LECRs can easily reach halo. Different to isolated SNRs

Fermi image of Cygnus superbubble

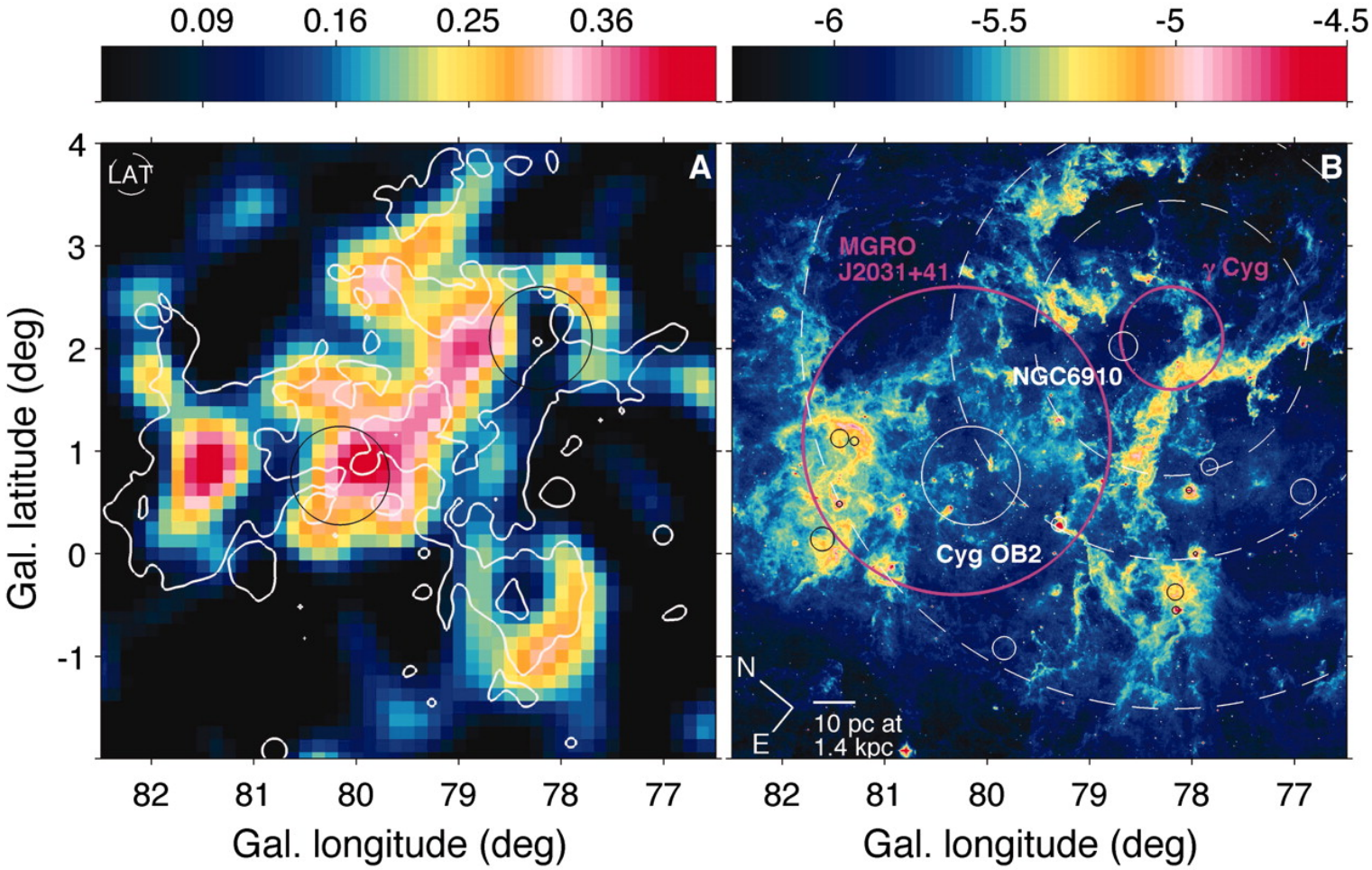

Ackermann + 2011

See also: Katsuta, Uchiyama & Funk Extended Gamma-Ray Emission from the G25.0+0.0 Region: A Star-forming Region Powered by the Newly Found OB Association? ApJ, v.839, id.129, (2017)

Fermi spectrum of Cygnus superbubble

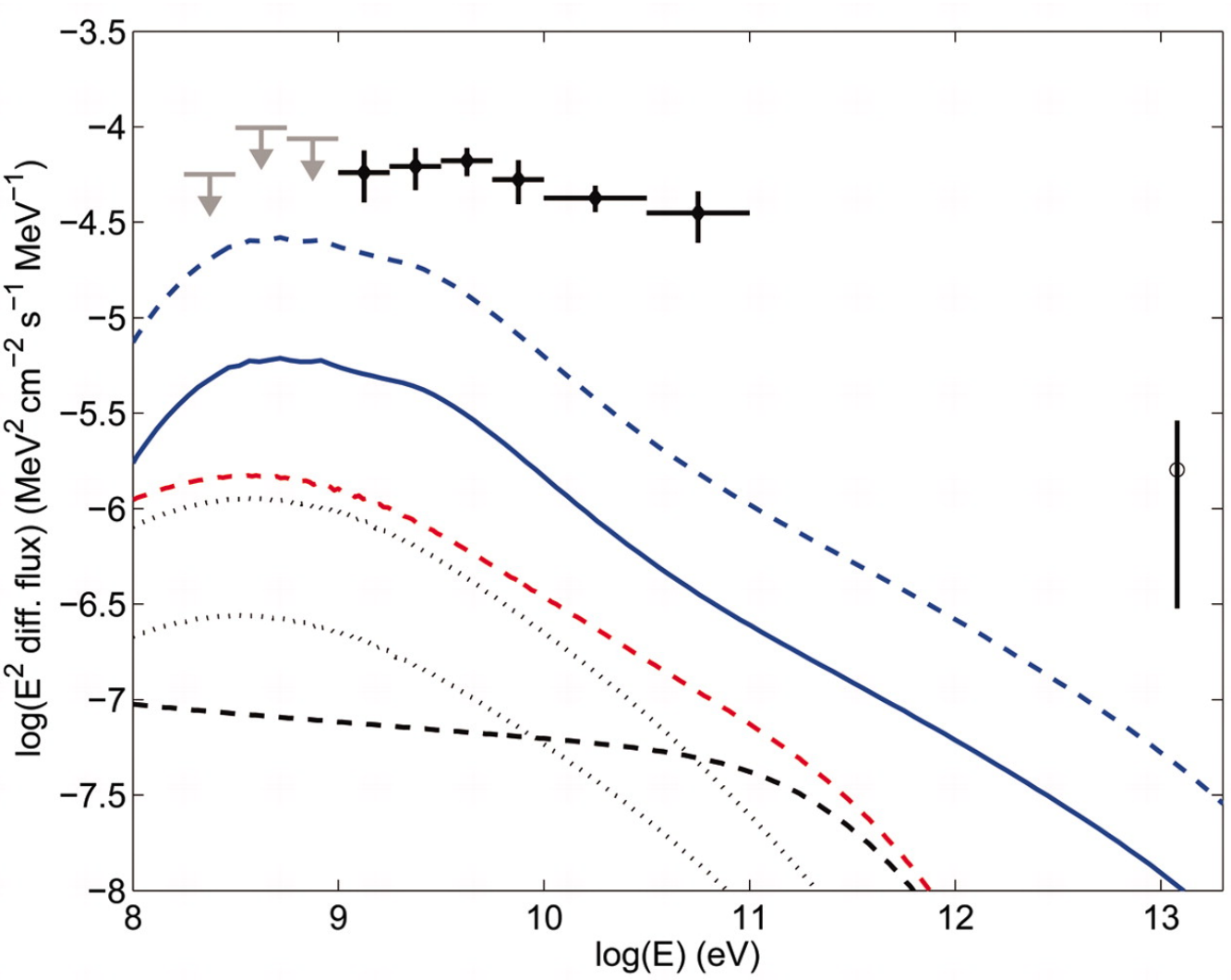

Ackermann + 2011

The Fermi source is extended of about 50 pc scale size and anti-correlate with MSX

Cygnus X is about 1.5 kpc away. Contain a number of young star clusters and several OB associations. Cygnus OB2 association contains 65 O stars and more than 500 B stars. There is a young supernova remnant Gamma-Cygni and a few gamma-pulsars.

Simulations with a non-linear kinetic model of relativistic particle acceleration accounting for particle acceleration by multiple shocks and long-wavelength strong turbulence predicted temporal evolution of CR spectrum

Space Science Reviews v.99, p. 317, (2001)

Astron. Astrophys. Reviews v.22, id.77, (2014)

MHD-turbulence and CR acceleration in SBs

The energy sources are OB-star winds and SNRs

The turbulence generation mechanism:

Multiple shocks interacting with cloudlets linear transformations, nonlinear cascade, wave damping including CR acceleration.

Particle acceleration by multiple shock ensemble with accompanied rarefactions

Kinetic equation for the mean distribution function F(**r**,**p**,t) (phase space) in a highly intermittent system

$$\frac{\partial F}{\partial t} - \frac{\partial}{\partial r_\alpha} \chi \alpha \beta \frac{\partial F}{\partial r_\beta} - \frac{1}{p^2} \frac{\partial}{\partial p} D(p) \frac{\partial F}{\partial p} =$$

$$G\hat{L}F + A\hat{L}^2 F + 2B\hat{L}\hat{P}F$$

This equation

$$\hat{L} = \frac{1}{3p^2} \frac{\partial}{\partial p} p^{3-\gamma} \int_0^p dp' p'^{\gamma} \frac{\partial}{\partial p'}$$

$$\hat{P} = \frac{p}{3} \frac{\partial}{\partial p}$$

AB 2001

Turbulence model

$$\frac{\partial W_i}{\partial t} + \frac{\partial \Pi_i(k)}{\partial k} = \sum \gamma_{ij} W_j - \gamma^d W_i$$

The turbulence spectra $W_i(k,t)dk = dE$

Vortex $W_1(k,t) = T(k,t)$ (incompressible)

Acoustic $W_2(k,t) = S(k,t)$ (compressible)

Turbulence model spectra

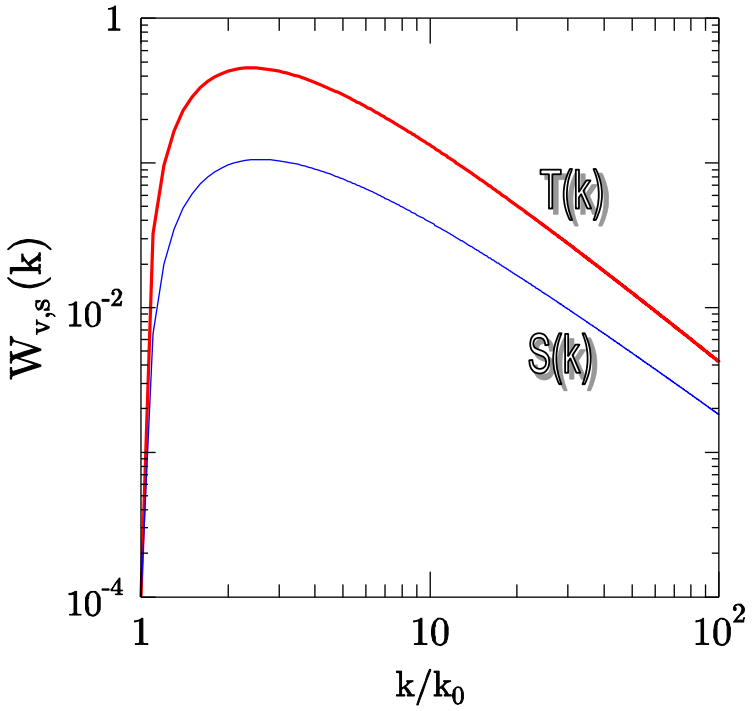

Temporal Evolution of Particle Spectrum

Soft-Hard-Soft

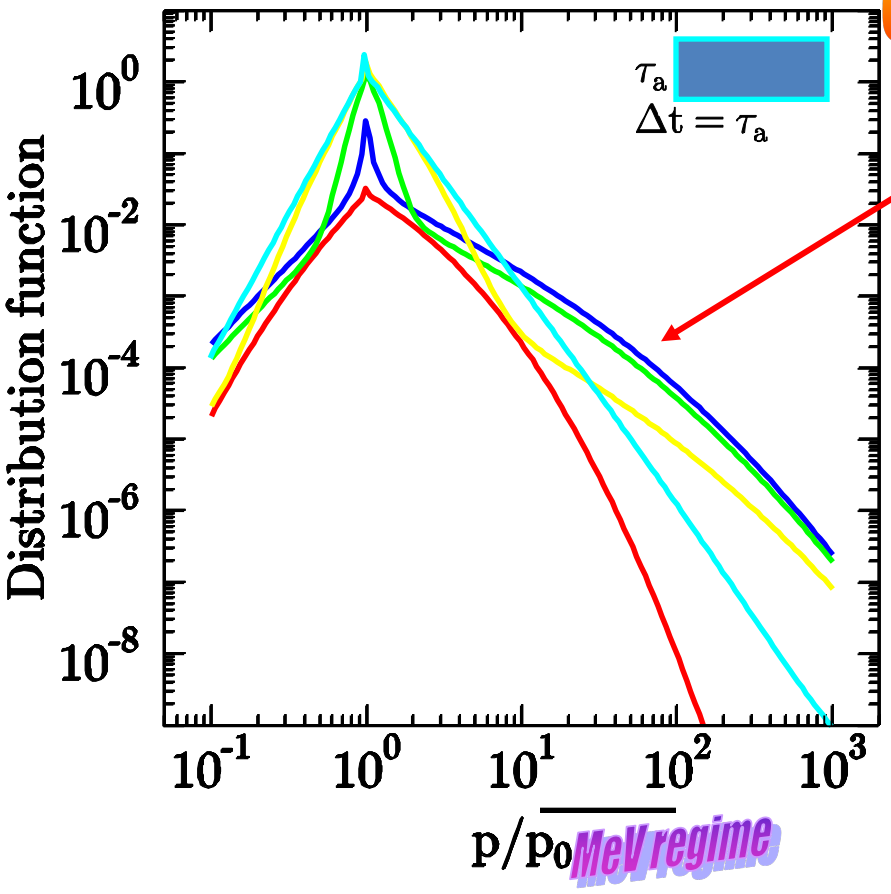

Space Sci. Rev. v.99, 317

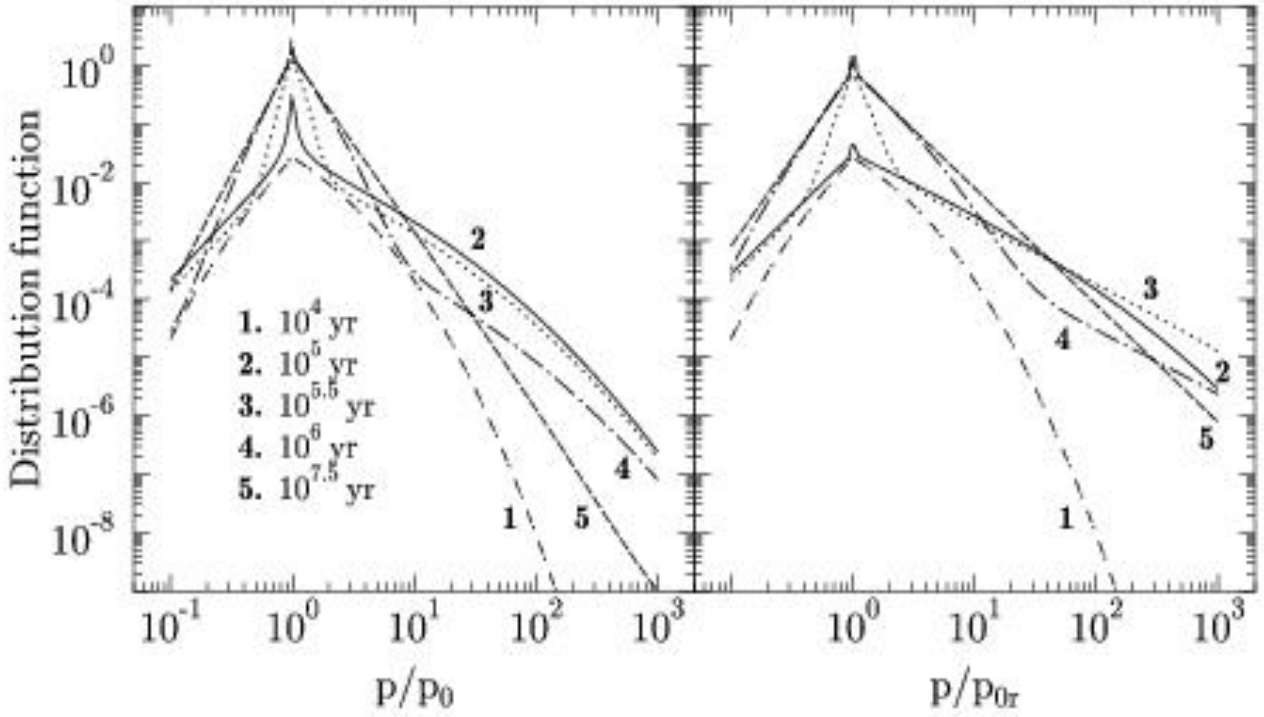

Space Sci. Rev. v.99, 317

Astron. Astrophys. Reviews v.22, id.77, (2014)

MHD Shock-Turbulence Power Conversion to CRs

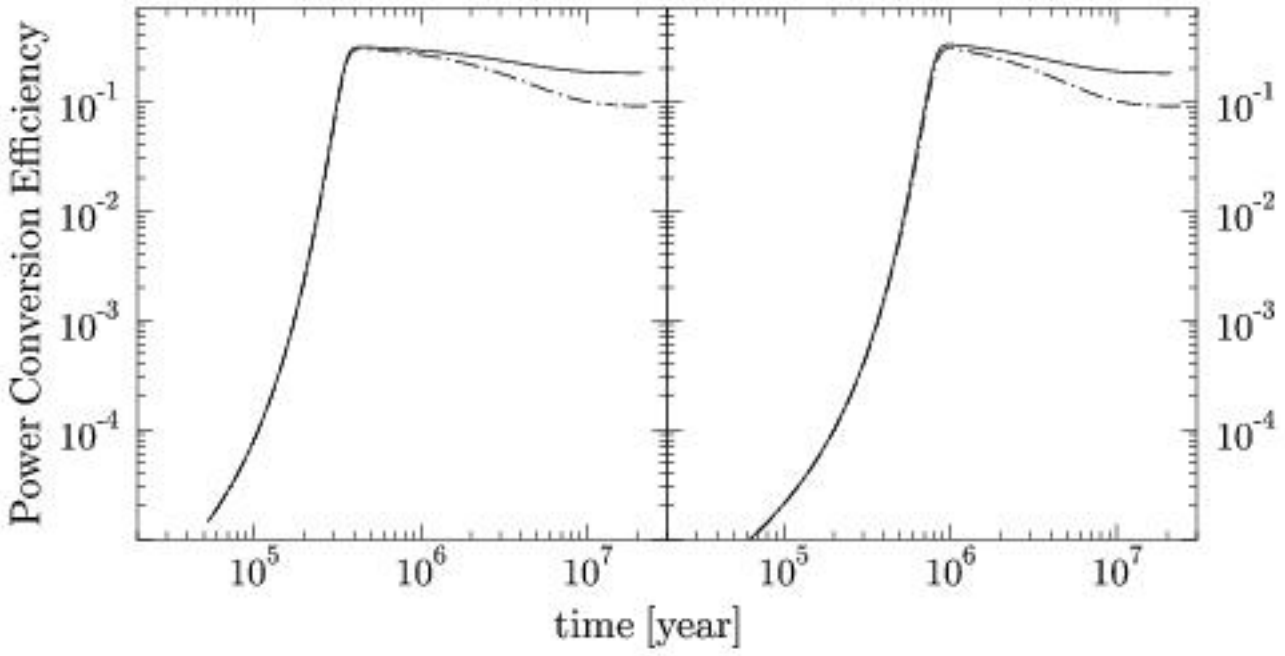

Space Sci. Rev. v.99, 317, 2001

HECR Spectra in the SB model

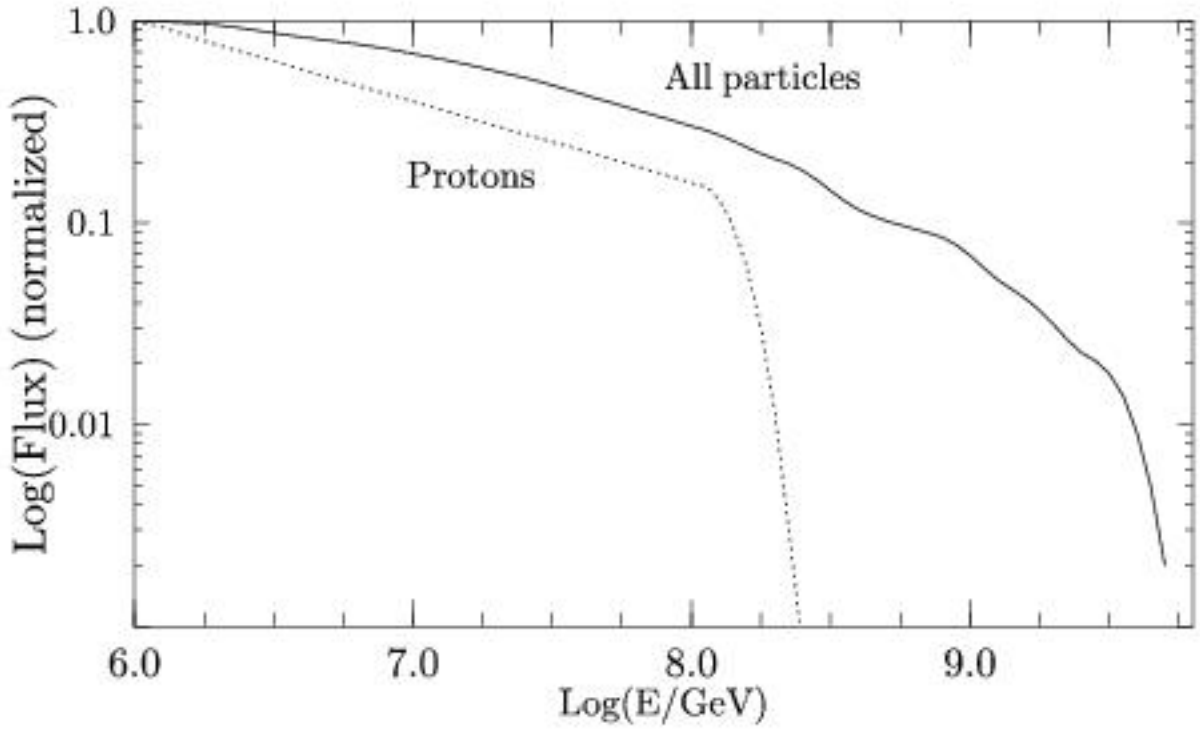

Astronomy Letters, v.27, pp.625-633 (2001)

PeV proton acceleration by SNe and stellar winds in starbursts

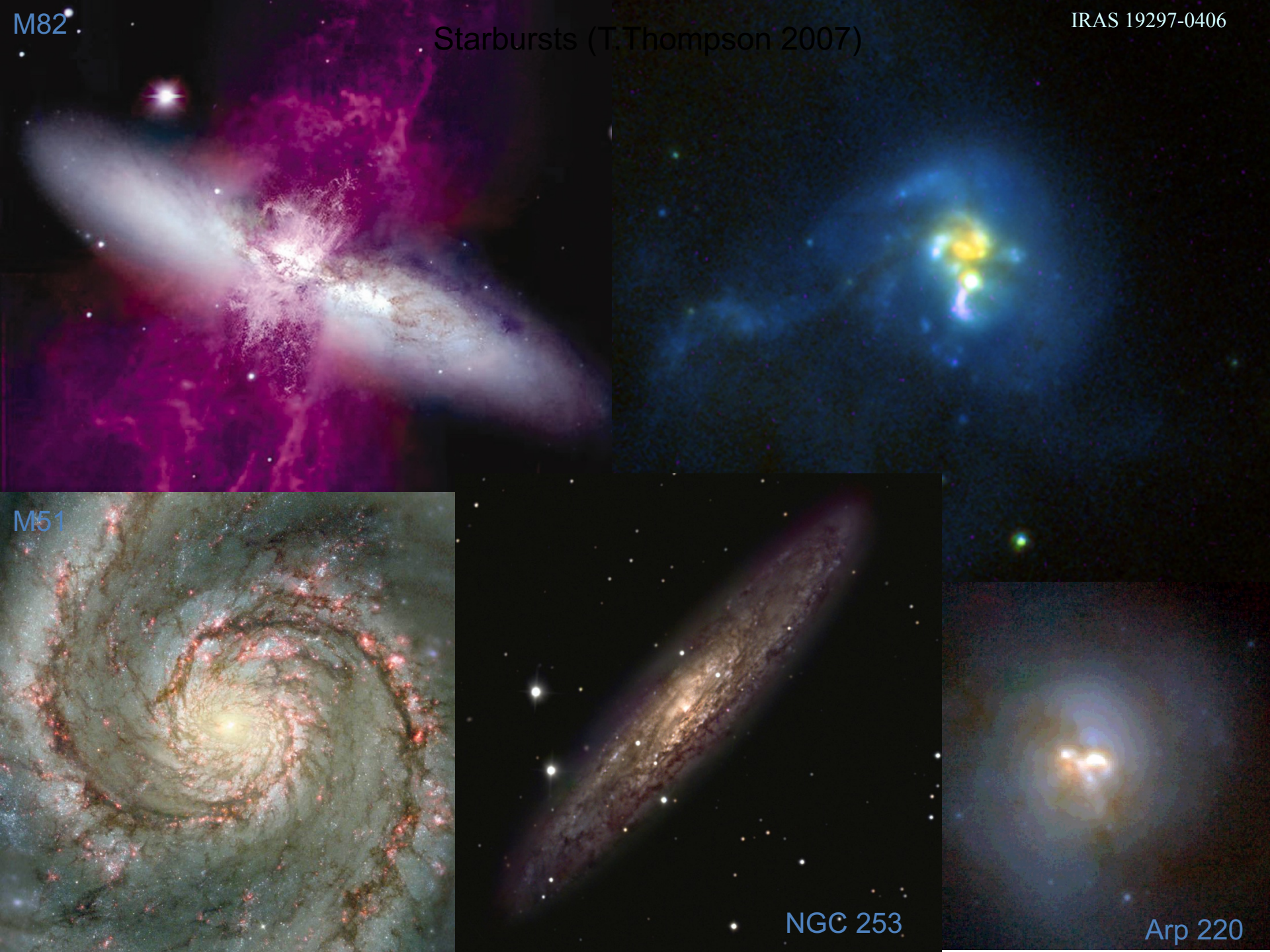
M82
Starbursts (T.Thompson 2007)
IRAS 19297-0406
M51
NGC 253
Arp 220

Nearest Merger—The “Antennae”

- WFPC2, with CO overlay (Whitmore et al. 1999; Wilson et al. 2000)
- VLA 5 GHz image (Neff & Ulvestad 2000)

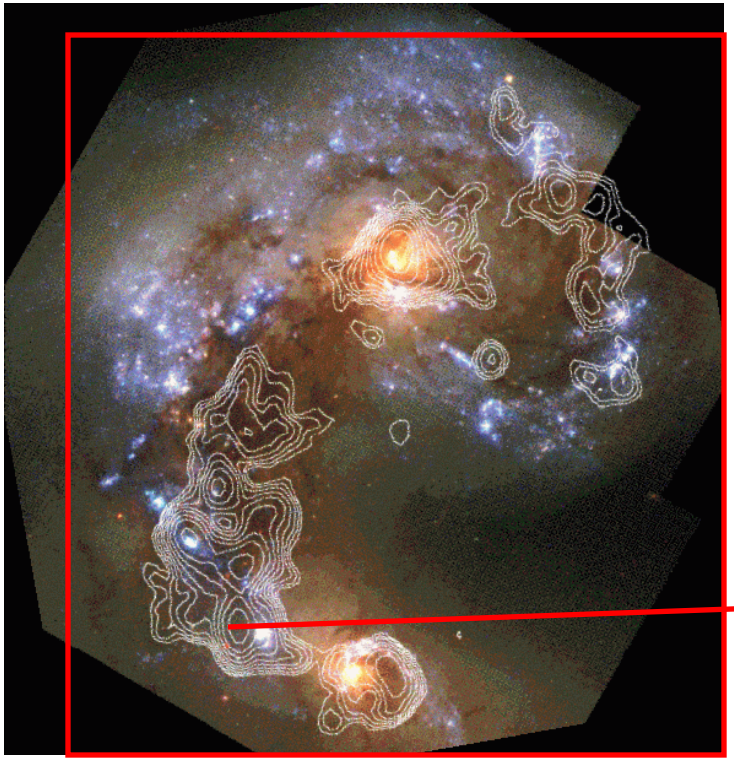

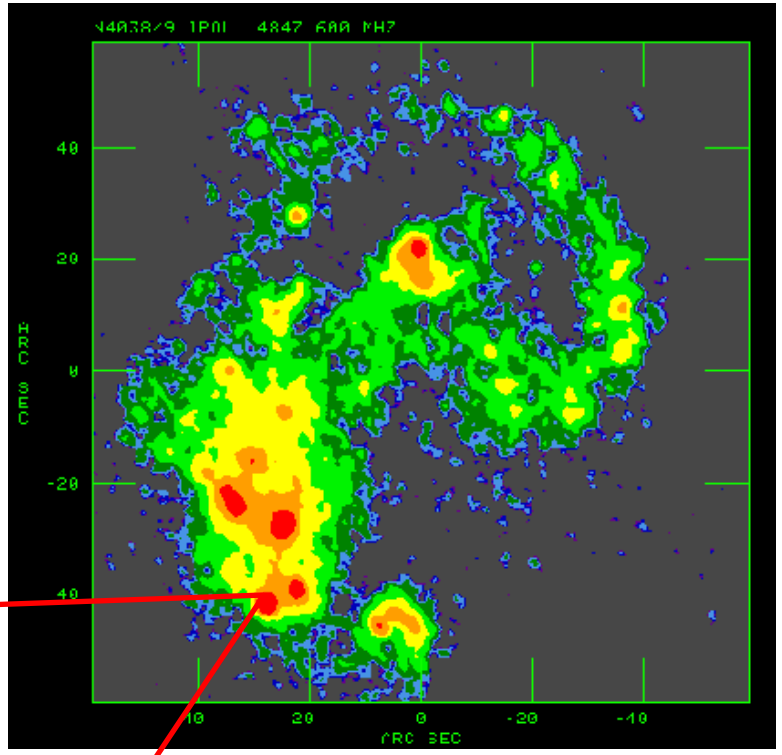

5 mJy ≙ 30,000 O7-equivalent stars

PeV proton acceleration by SNR in young compact stellar clusters & starbursts

CR acceleration in colliding shock flows
[between the colliding shock]
is the most efficient
version of Fermi I acceleration

SNR - cluster wind accelerator

CR acceleration in colliding shock flows

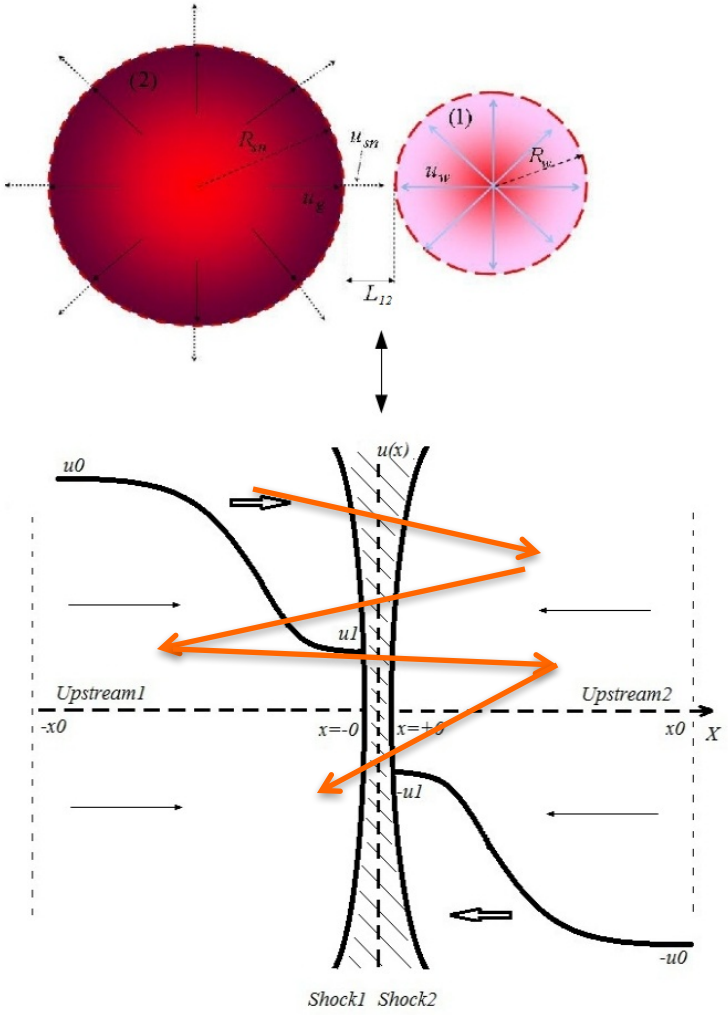

MNRAS V. 429, 2755, 2013

A Galactic Super Star Cluster

2MASS Atlas Image from M.Muno

- Distance: 5kpc
- Mass: 10^5 M_{sun}
- Core radius: 0.6 pc
- Extent: ~6 pc across
- Core density:~10^6 pc^{-3}
- Age: 4 +/- 1 Myr
- Supernova rate: 1 every 10,000 years

Chandra Observations

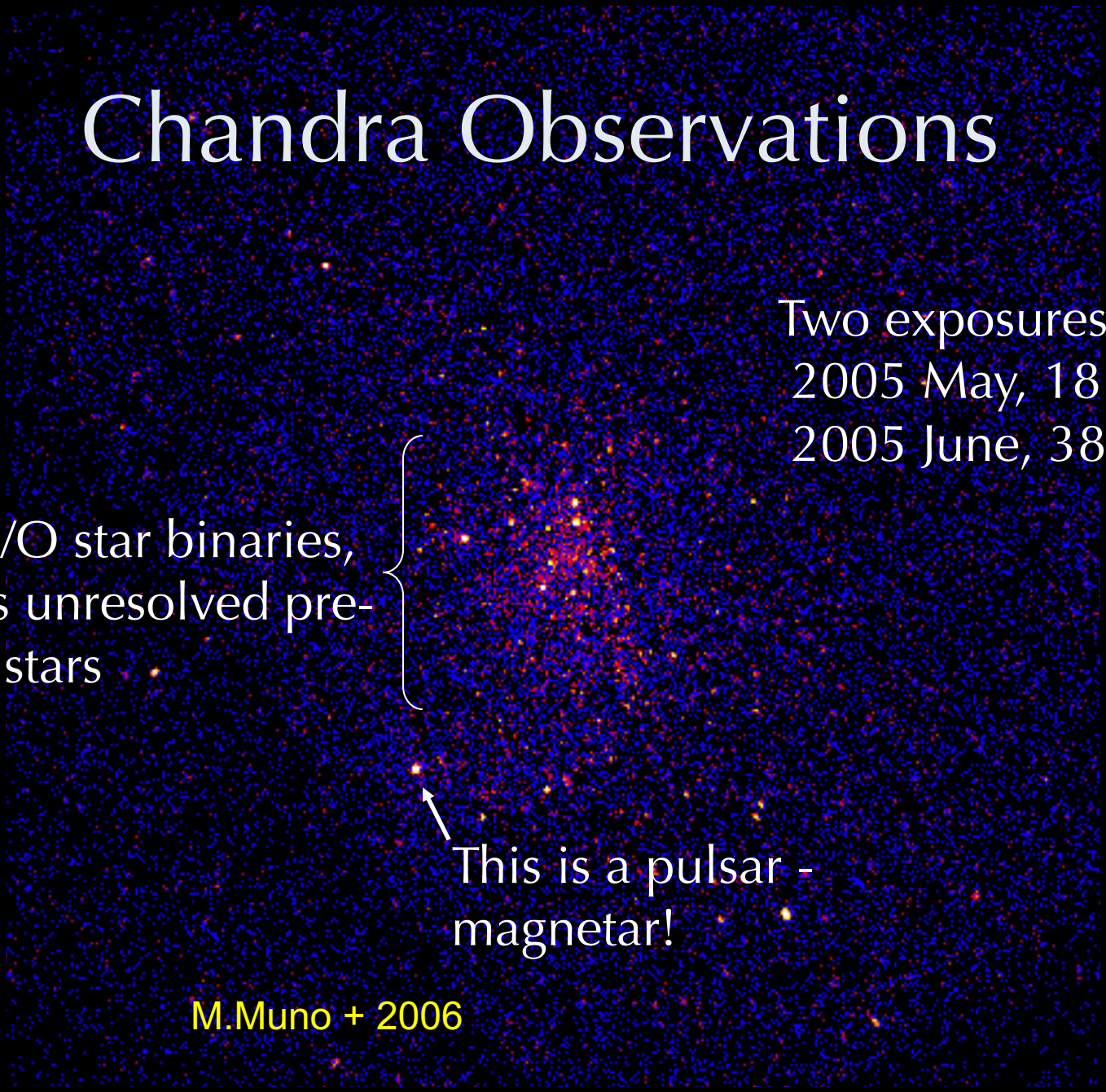

Westerlund 1

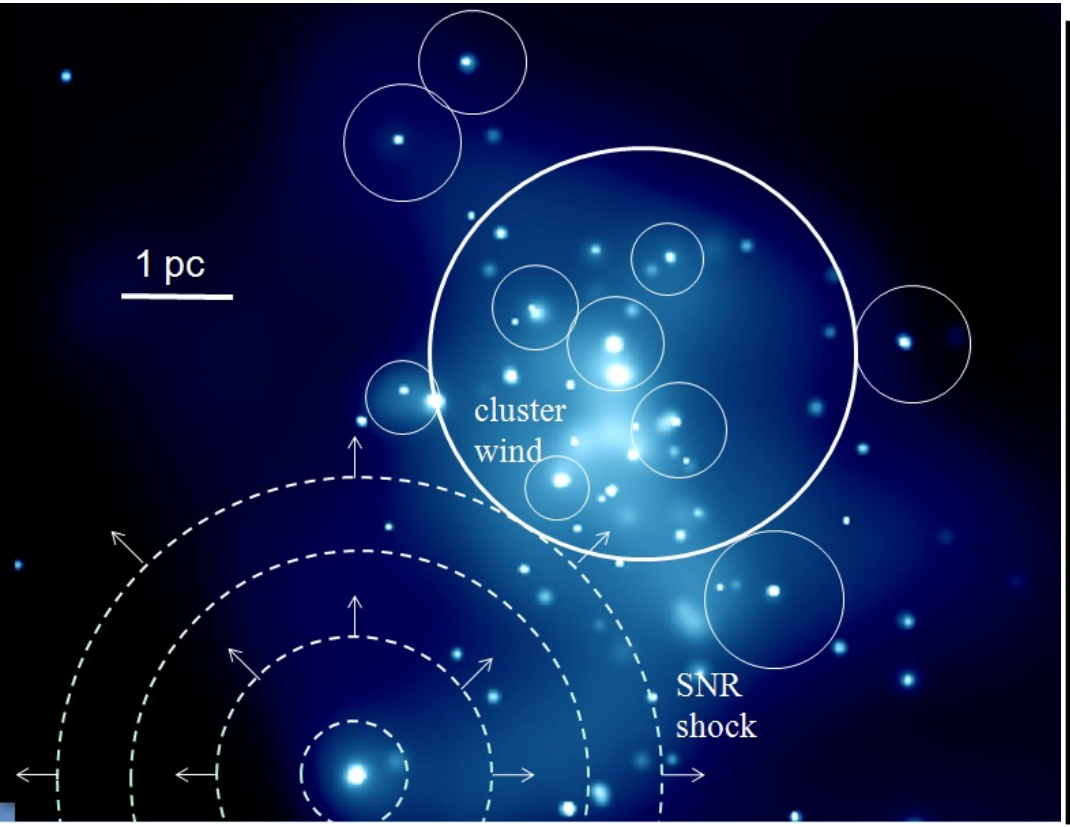

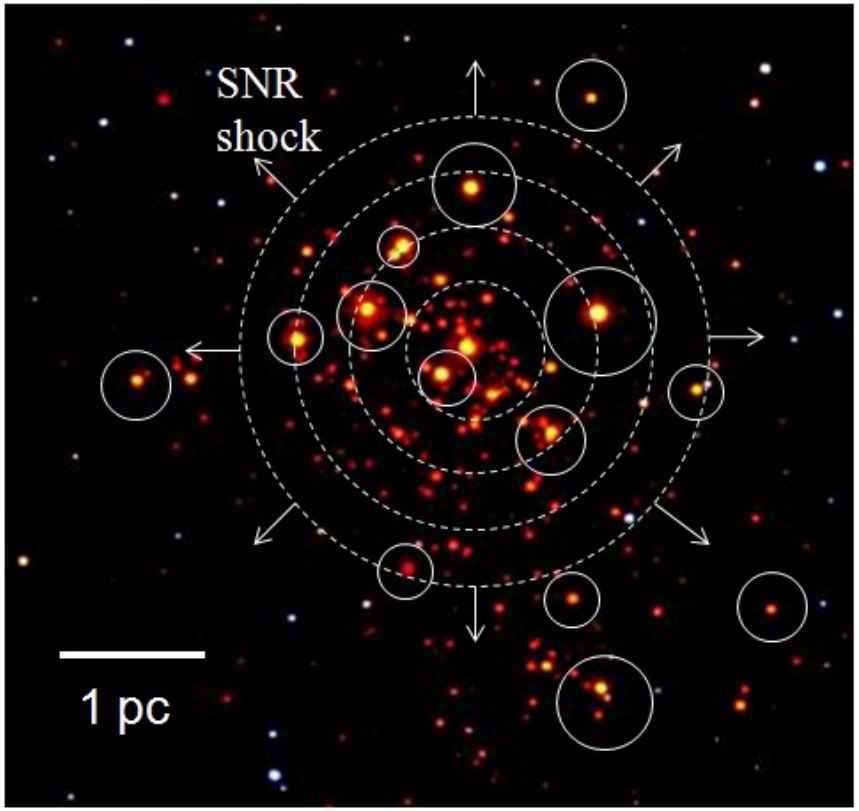

Muno+ 05

Clark+ 05

Colliding shock flow geometry used
Shock was divided in a few sections

Stellar wind shock
(thin shell approximation)
Wilkin 1996

$$R(\theta) = \sqrt{\frac{\dot{m} V_w}{4\pi \rho_a V_*^2}} \cdot \frac{\sqrt{3(1-\theta ctg\theta)}}{sin\theta}$$

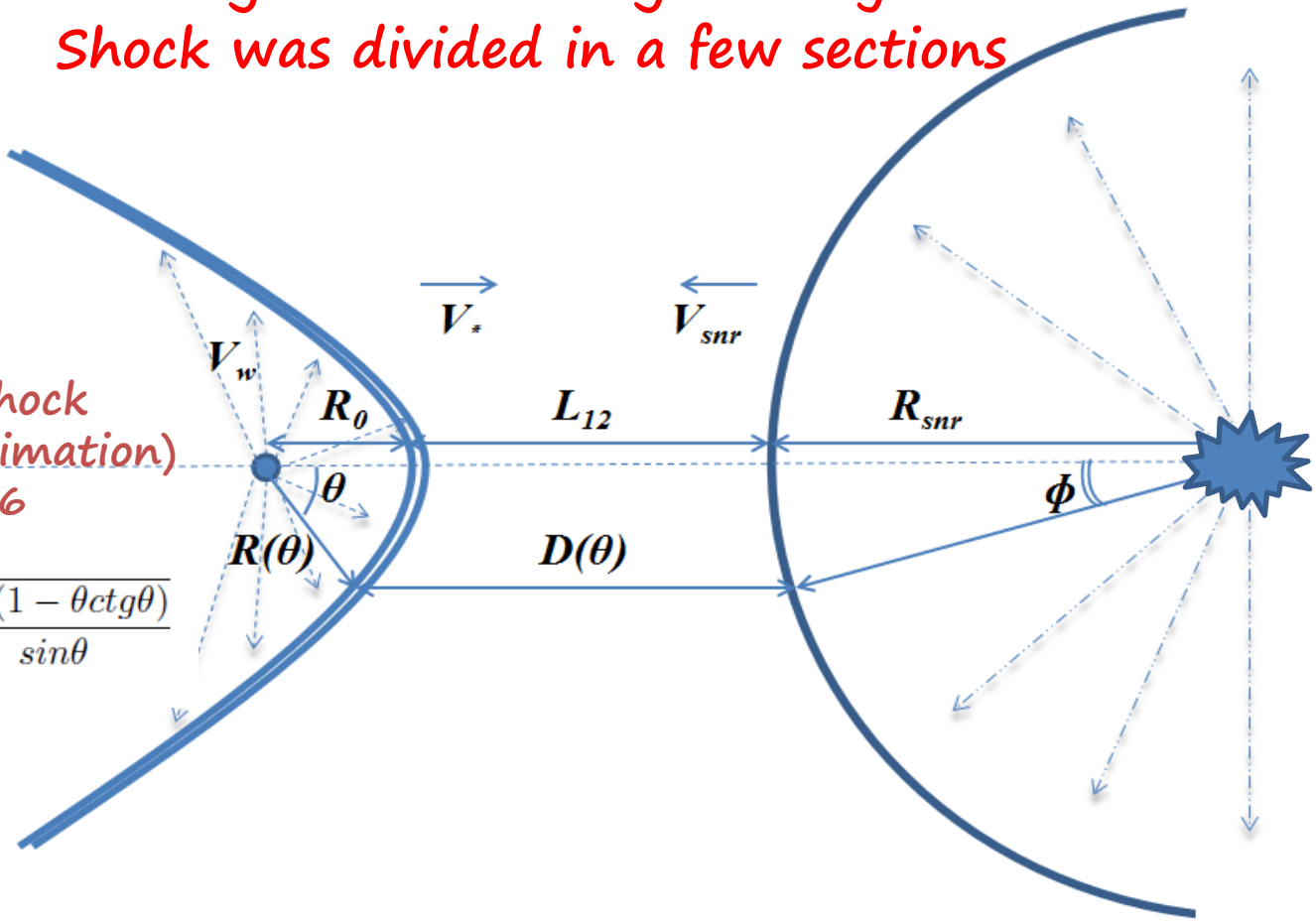

CR acceleration time in the colliding shocks SNR-cluster wind

$$\tau_a \approx \frac{cR_g(p)}{u_s\, u_w}.$$

Acceleration time is about 500 yrs for 10-40 PeV

$$\tau_a \approx 2 \cdot 10^{10}\, \mathcal{E}_{\rm PeV}\, (\eta_b n)^{-0.5}\, u_{s3}^{-2}\, u_{w3}^{-1}\ ({\rm s})$$

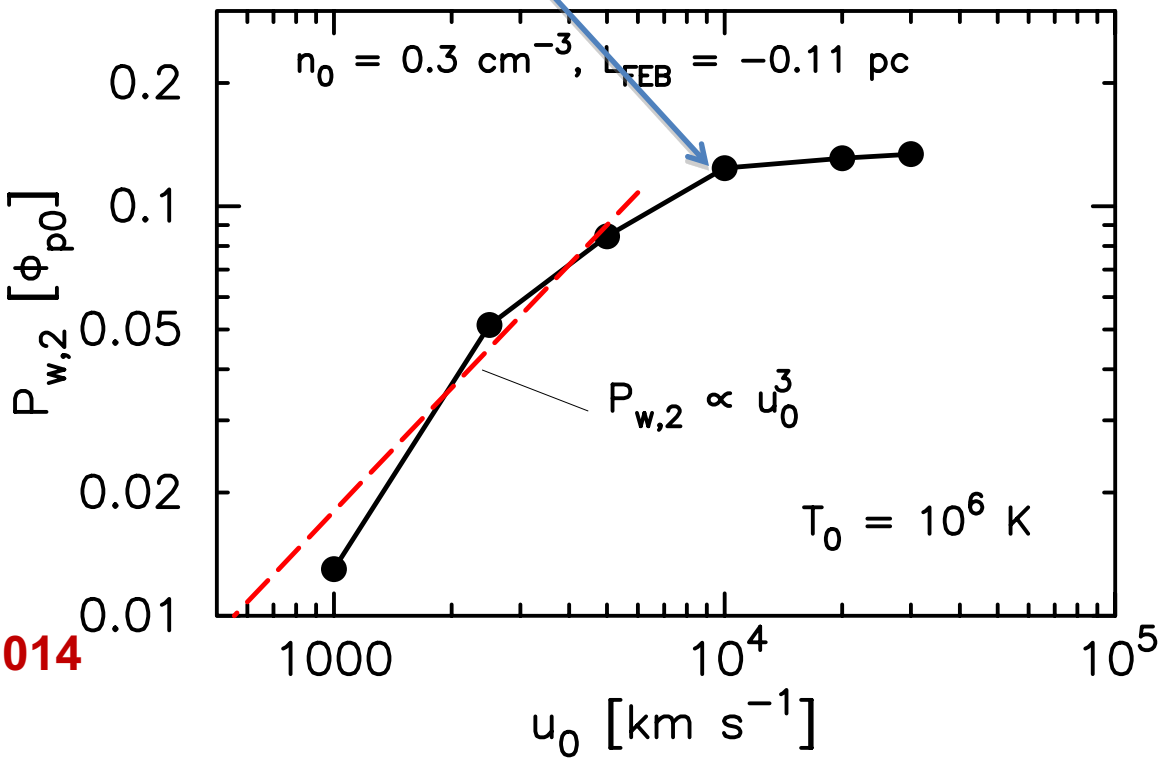

Magnetic field amplification by CR current driven instabilities: Bell's and LW

ApJ v.789, 137, 2014

CR distribution functions with the very hard energy spectra (upturn) is a specific feature of particle acceleration in colliding shock flows

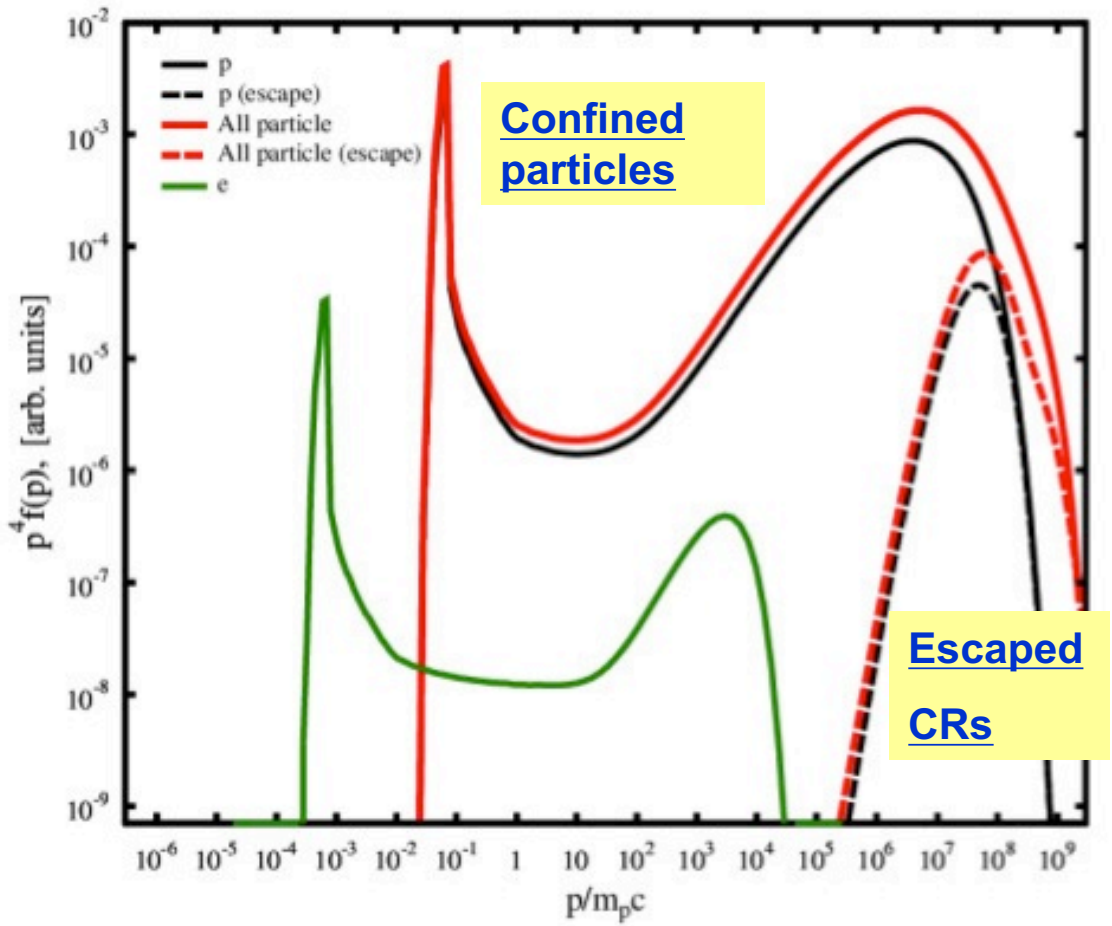

Gamma-rays from a Pevatron

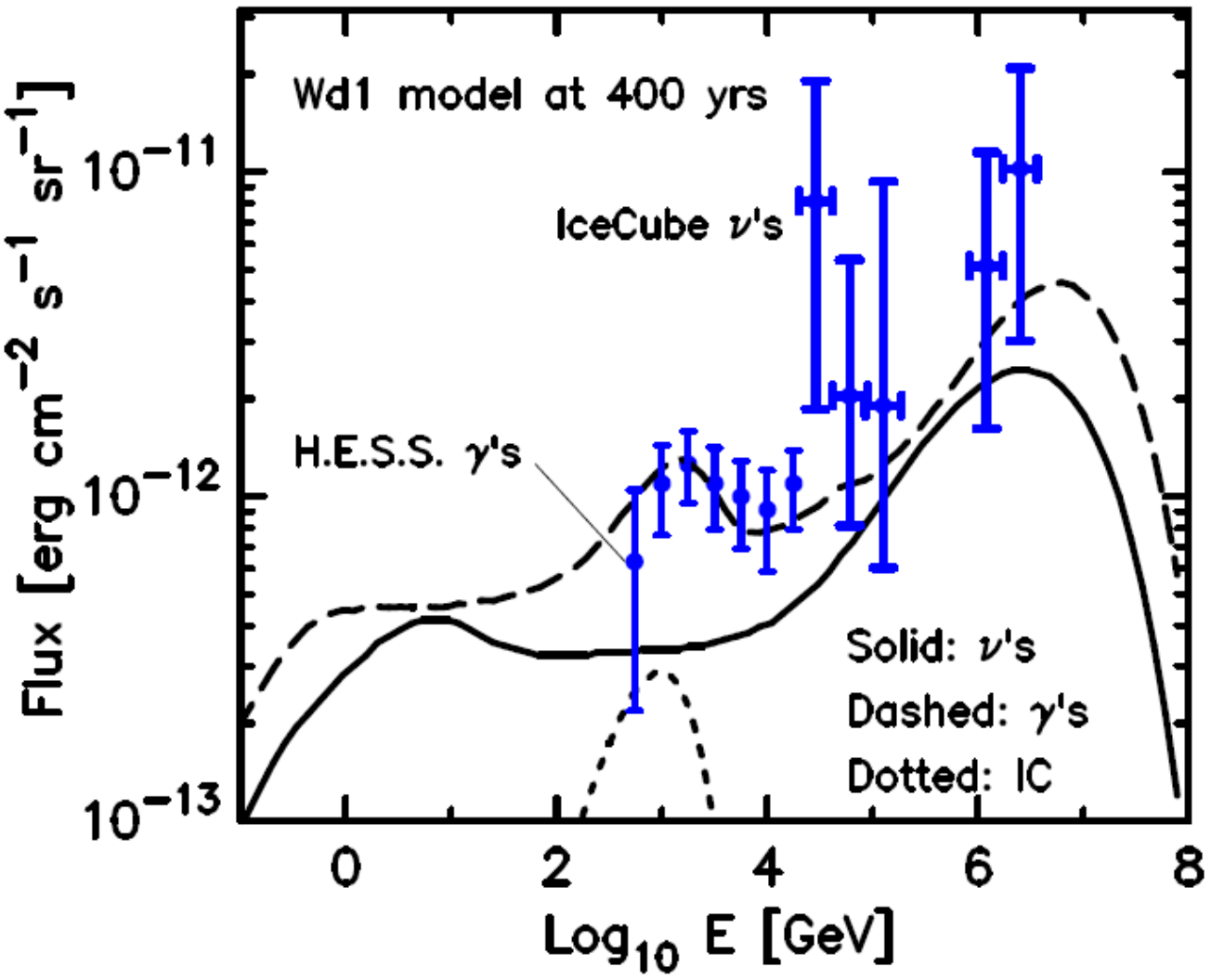

AARv v.22, p.54, 2014

MNRAS V. 453, p. 113, 2015

Gamma-rays from the Pevatron surrounding clouds

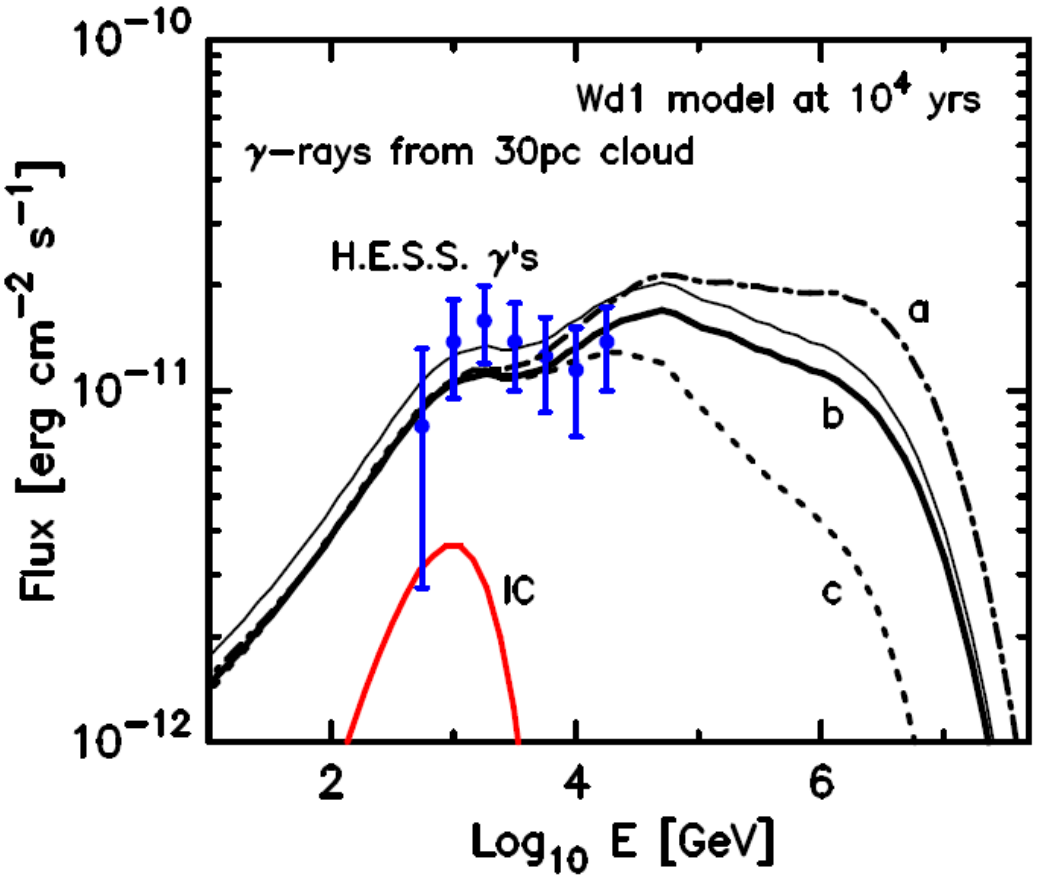

MNRAS V. 453, p. 113, 2015

H.E.S.S. image of Westerlund I

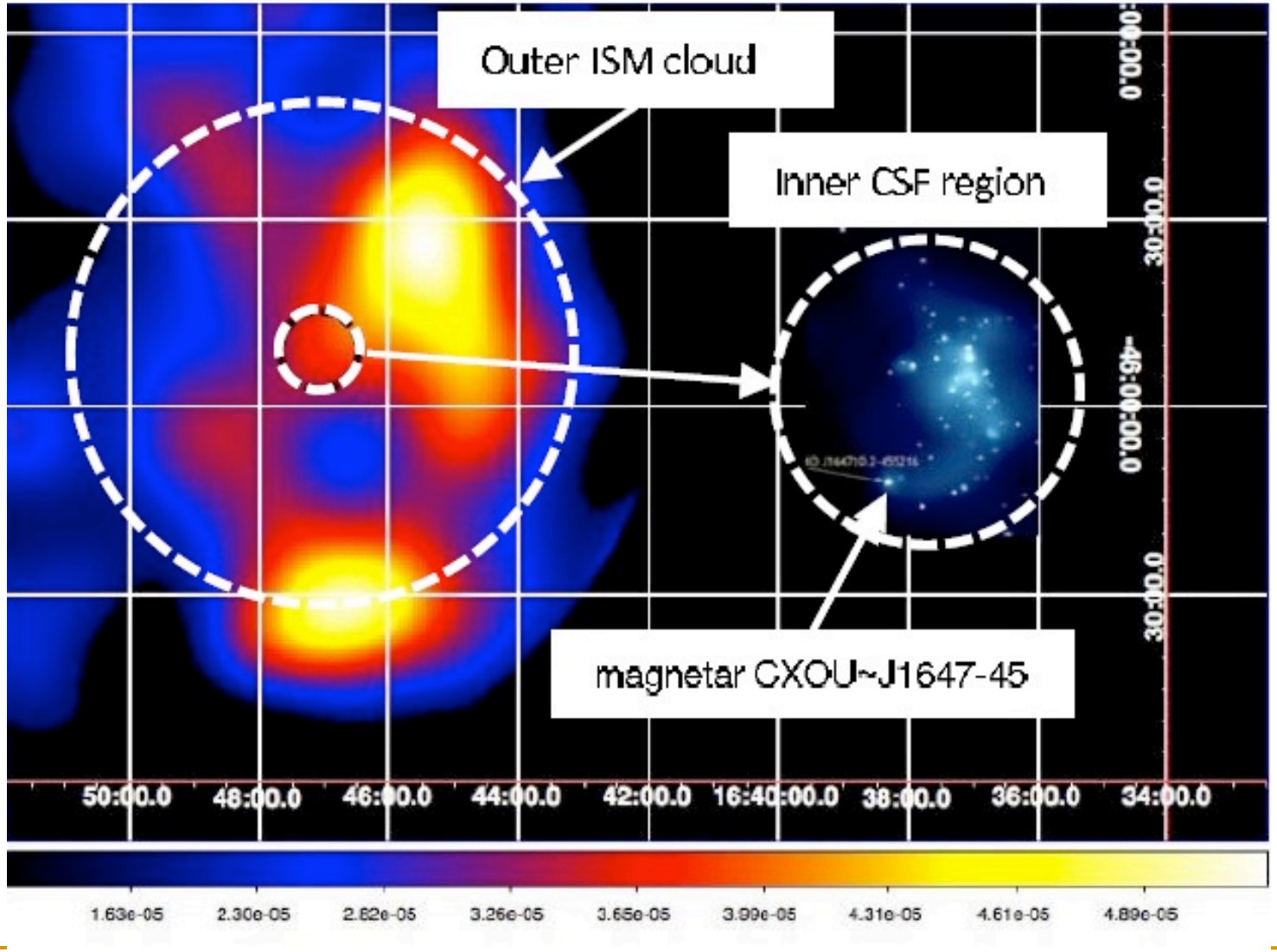

MNRAS v. 453, p. 113, 2015

Neutrinos from a 140 pc vicinity of a Westerlund I like Pevatron

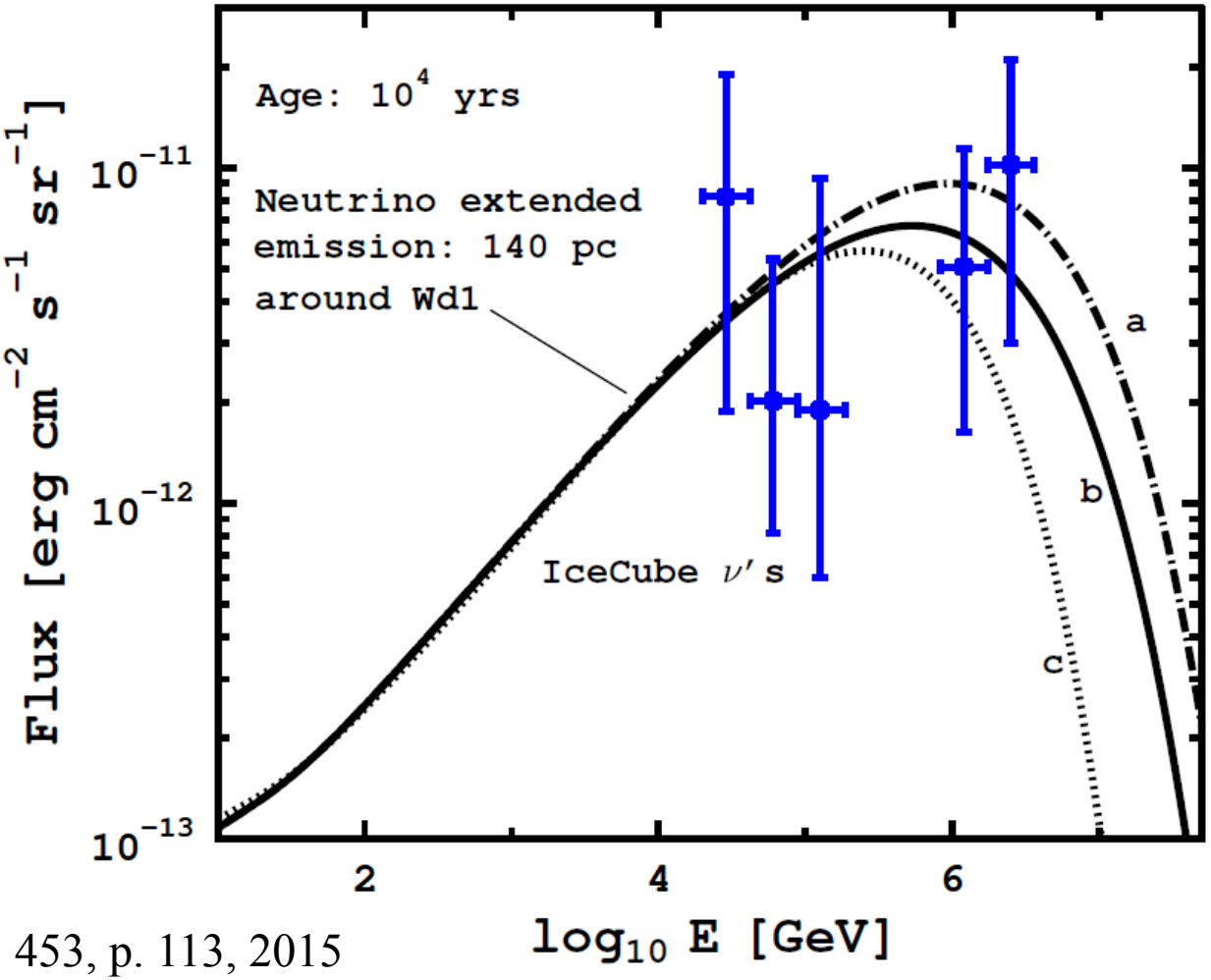

MNRAS V. 453, p. 113, 2015

H.E.S.S. J1808-204

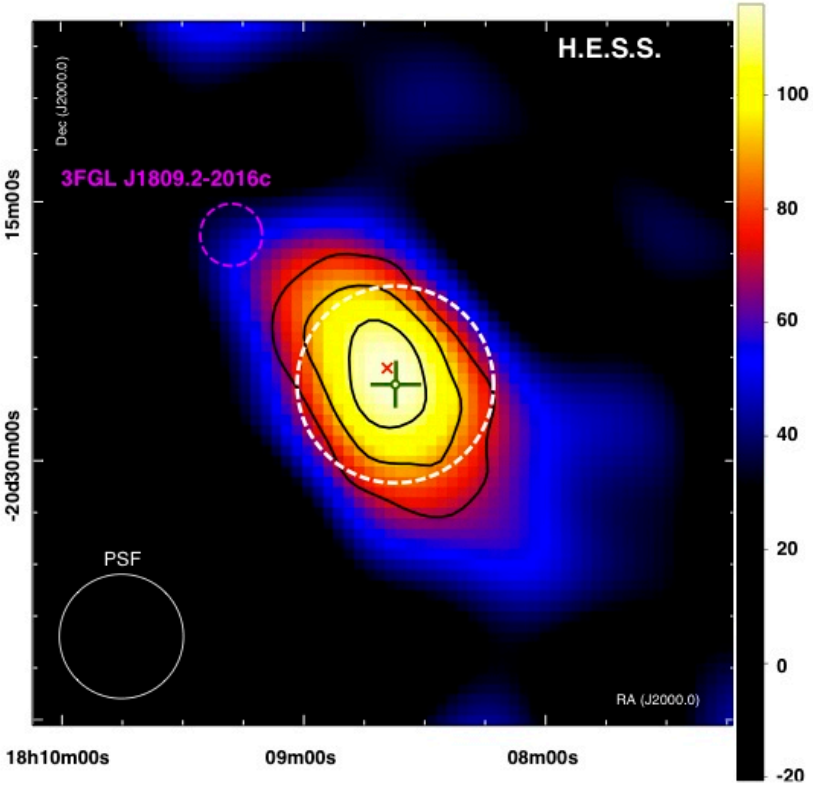

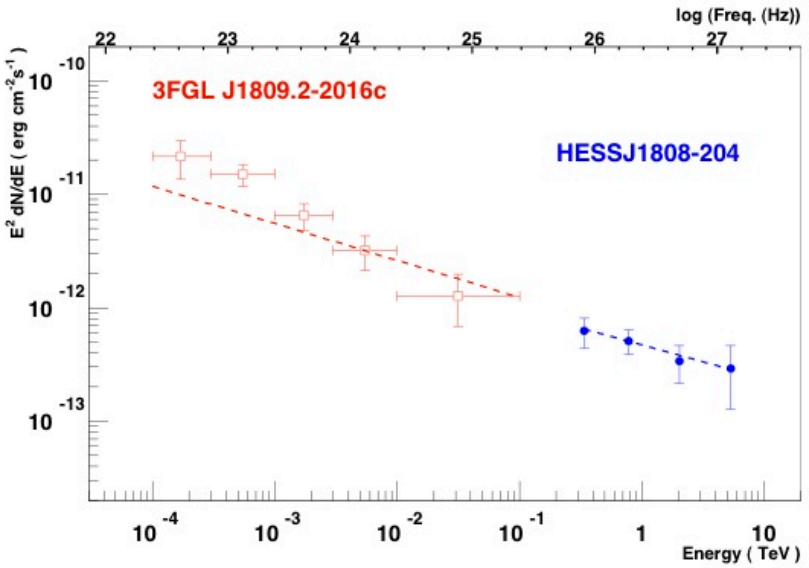

Fig. 2. Energy fluxes, 1 σ statistical errors, and fitted pure power-law fits for HESS J1808−204 (blue solid points and blue dashed line) and the *Fermi-LAT* source 3FGL J1809.2−2016c (red open squares and red dashed line) from Acero et al. (2015).

power-law photon index of 2.3 ± 0.2stat ± 0.3sys

Lvhe ~ 1.6 × 10^(34)[D/8.7 kpc]^2 erg/s

Extended very high-energy gamma-ray source towards the luminous blue variable candidate LBV 1806−20, massive stellar cluster Cl* 1806−20, and magnetar SGR 1806−20 of estimated age about 650 years.

H.E.S.S. collaboration arxiv 1606.05404 2016

H.E.S.S. J1808-204 model

with gamma-rays from the H.E.S.S. imaged region and total "calorimeter" neutrinos

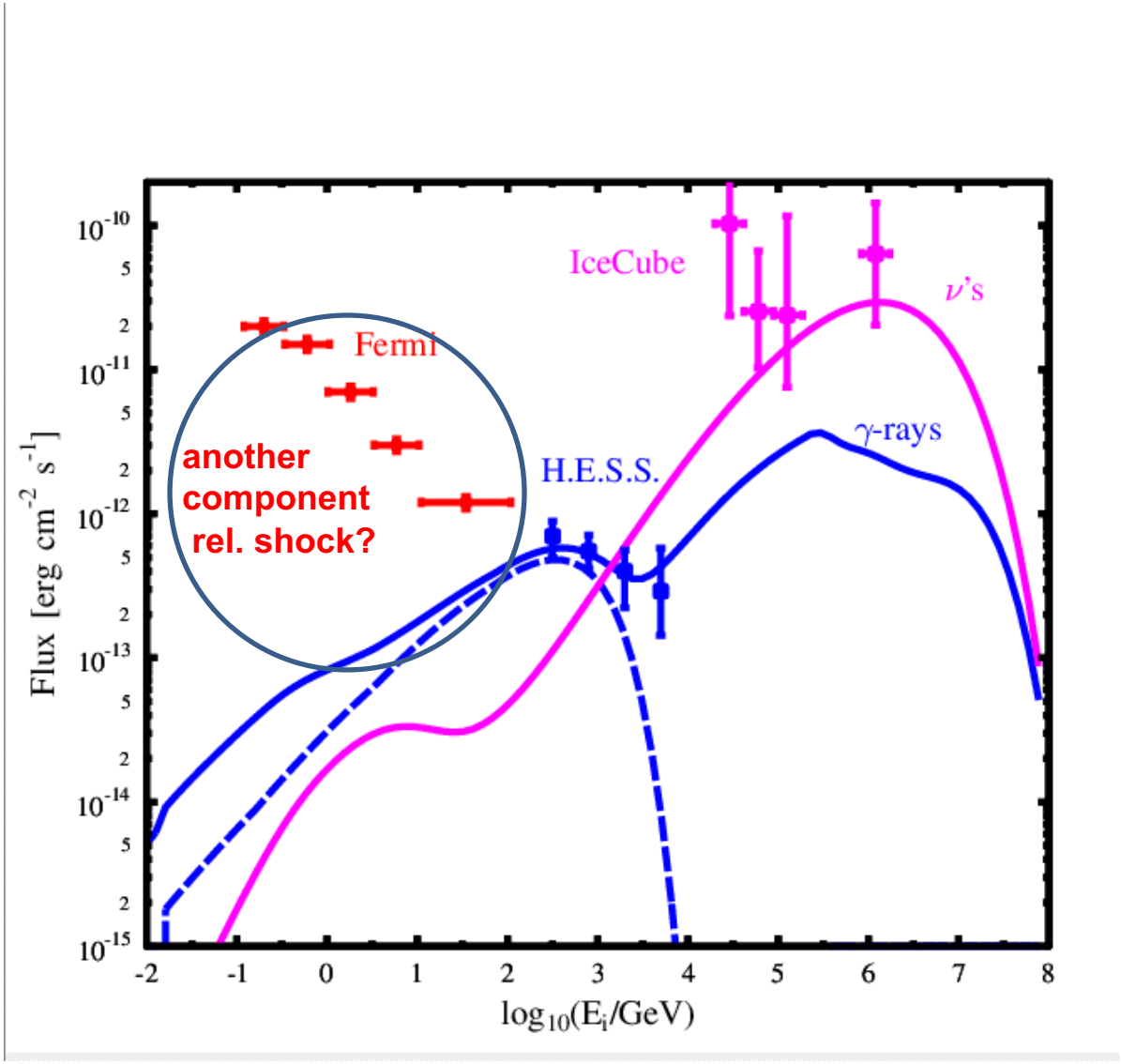

Note: IceCube flux is indicated here is for a few events "nearby" the cluster only

The two Galactic SN-clusters could contribute to a few neutrino likely Galactic events observed by Ice Cube

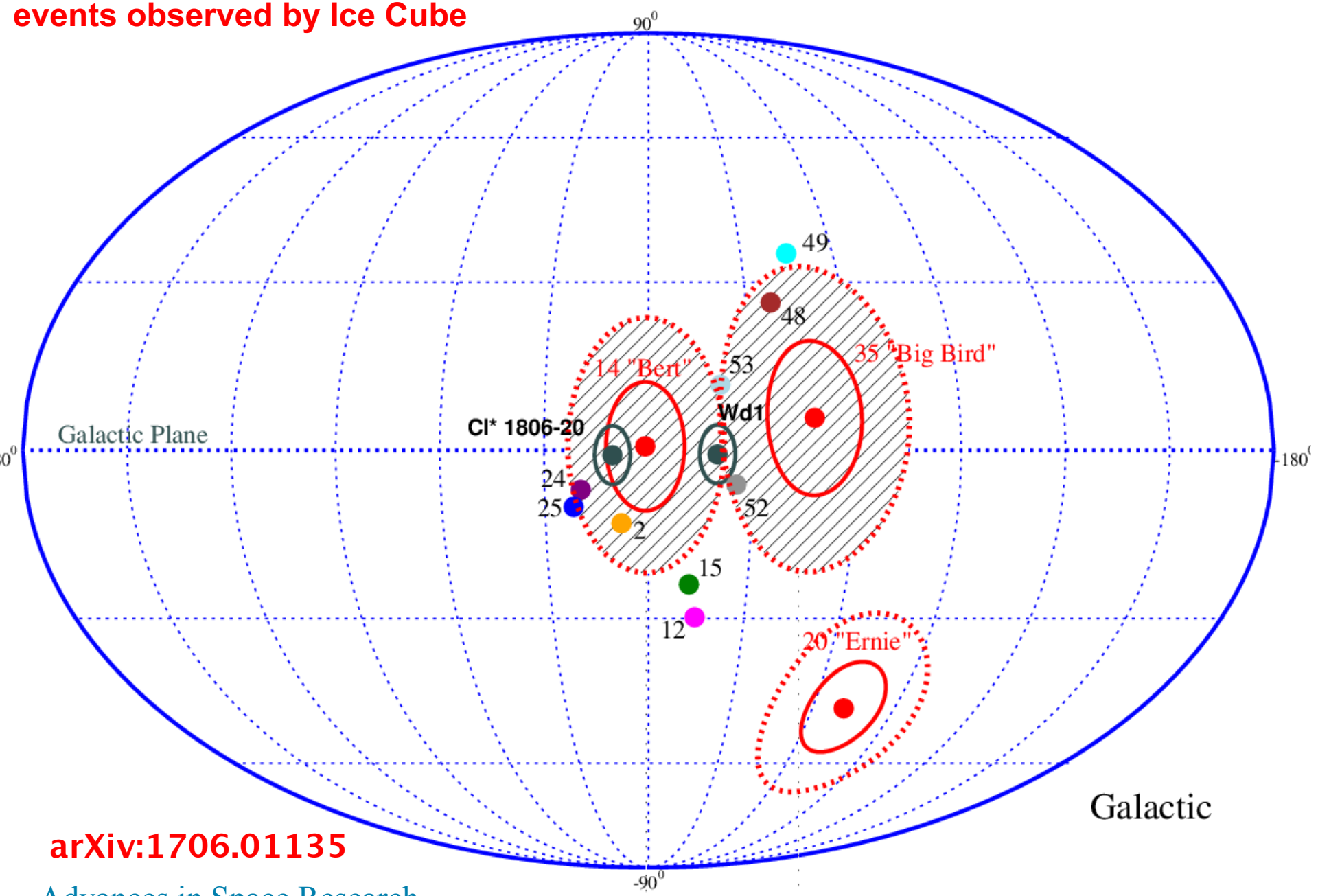

arXiv:1706.01135

Advances in Space Research

Currently the expected amount of PeV sources like SNe – cluster wind collision in the Milky Way is likely a few

They may be the sources of the light component indicated by LOFAR observations

LOFAR: evidence for light CR component at 0.1 EeV?

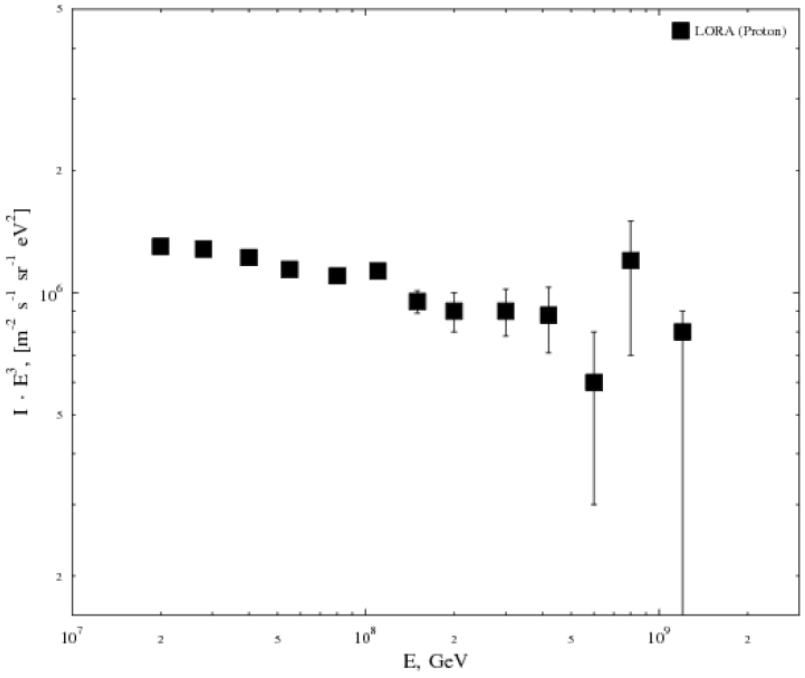

Bujtink + 2016

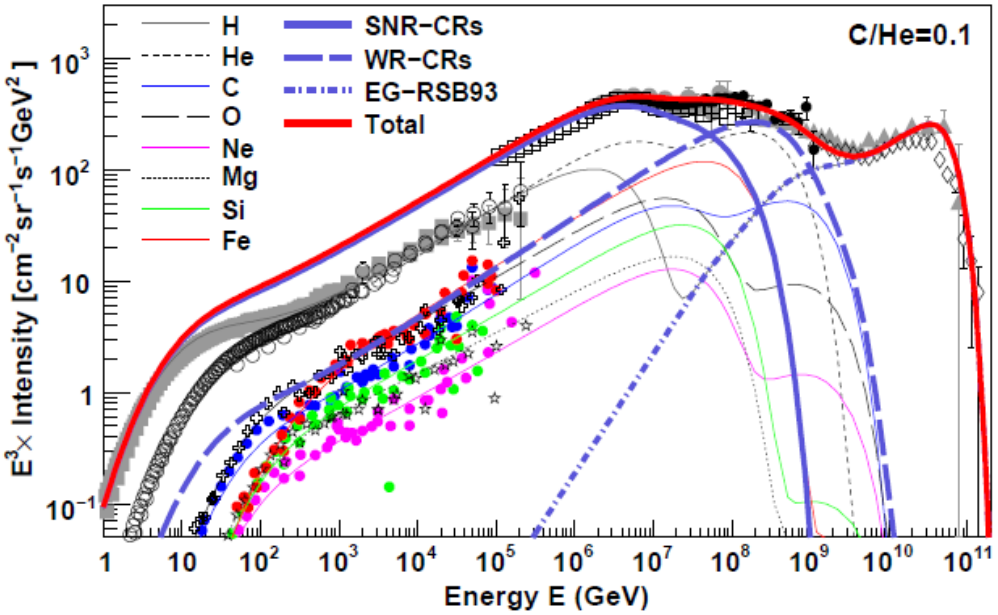

Thoudam + 2016

What are the possible sources of galactic CR above PeV?

Cosmic-ray energy spectrum and composition up to the ankle — the case for a second Galactic component

S. Thoudam[1,2,⋆], J.P. Rachen[1], A. van Vliet[1], A. Achterberg[1], S. Buitink[3], H. Falcke[1,4,5], J.R. Hörandel[1,4]

arXiv:1605.03111

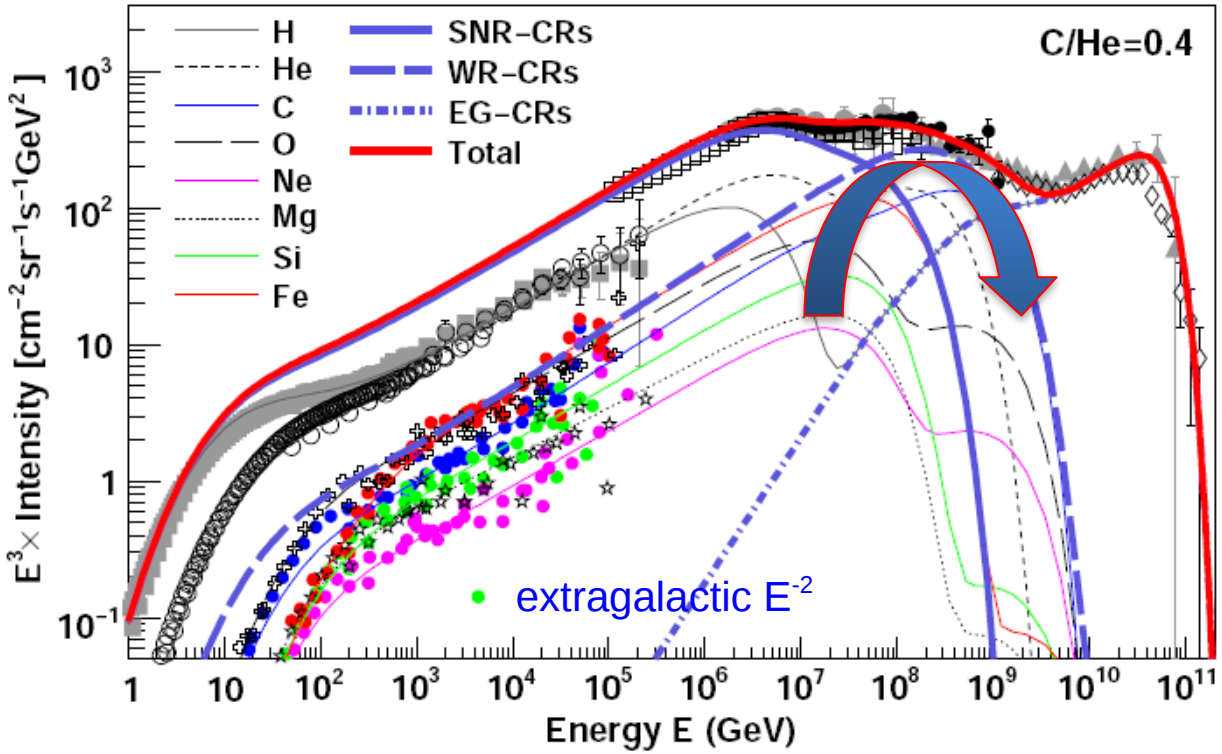

Fig. 6. Model prediction for the all-particle spectrum using the Wolf-Rayet stars model. *Top*: C/He = 0.1. *Bottom*: C/He = 0.4. The thick solid blue line represents the total SNR-CRs, the thick dashed line represents WR-CRs, the thick dotted-dashed line represents EG-CRs, and the thick solid red line represents the total all-particle spectrum. The thin lines represent total spectra for the individual elements. For the SNR-CRs, an exponential energy cut-off for protons at $E_c = 4.1 \times 10^6$ GeV is assumed. See

Currently the expected amount of PeV sources like SNe – cluster wind collision in the Milky Way is likely a few

However, the sources are likely dominated in the starburst galaxies (hundreds of clusters) with the high ISM pressure due to mergers etc.

They may be the CR sources for the Waxman-Bahcall starburst calorimeter hypothesis

SFR from FUV+IR

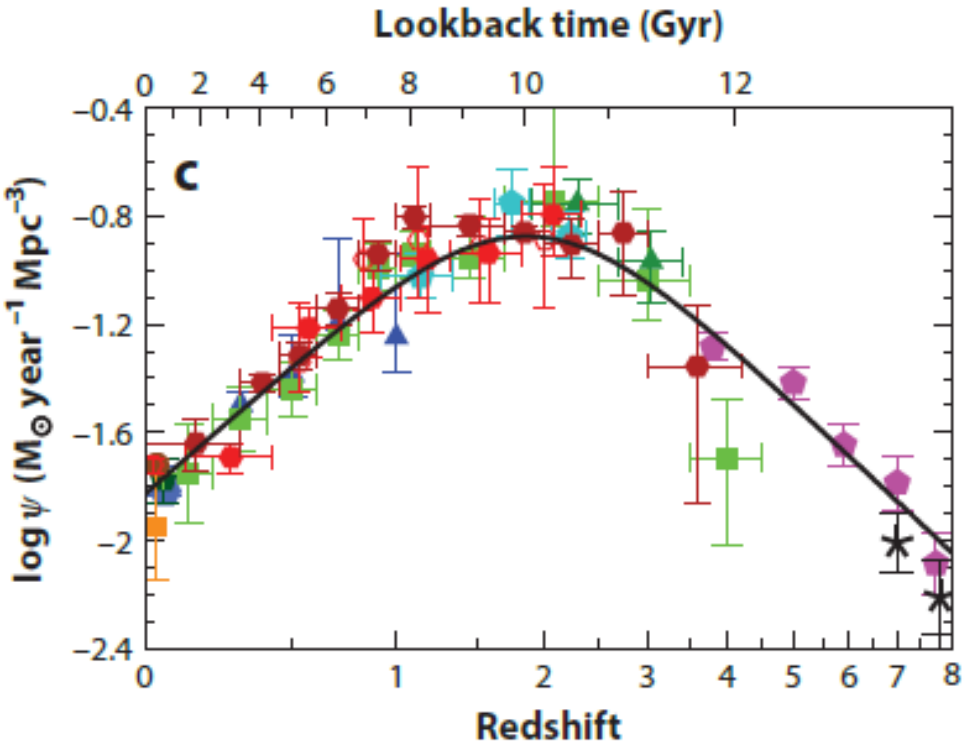

$$\psi(z) = 0.015 \frac{(1+z)^{2.7}}{1+[(1+z)/2.9]^{5.6}} \, \mathrm{M}_\odot \, \mathrm{year}^{-1} \, \mathrm{Mpc}^{-3}.$$

Madau & Dickinson, ARAA 2014

Cluster formation efficiency

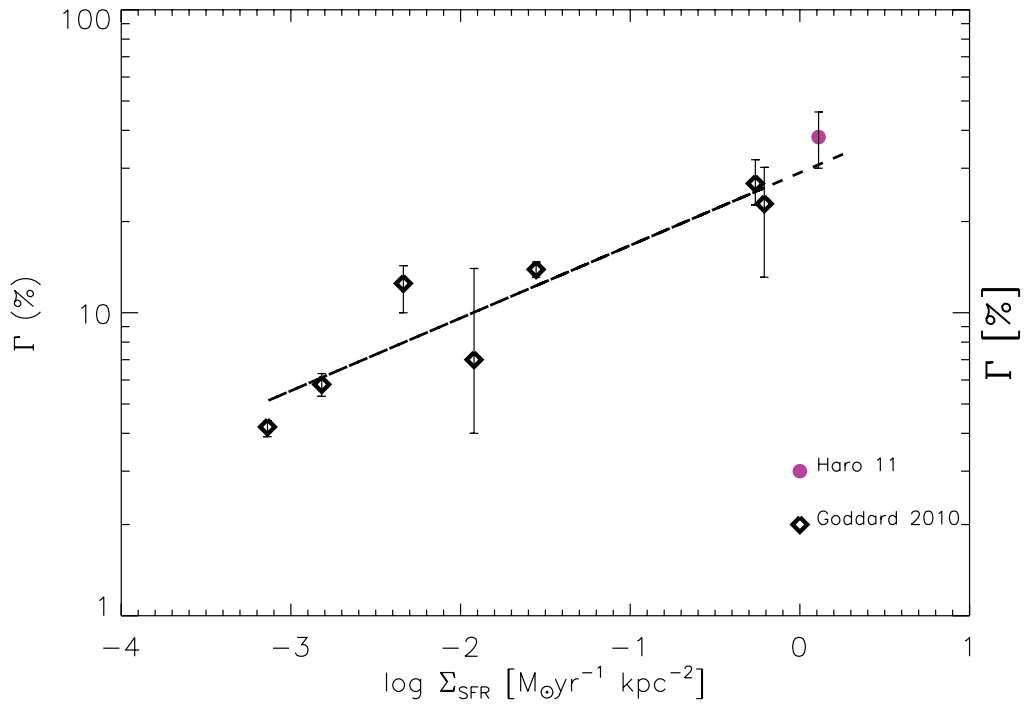

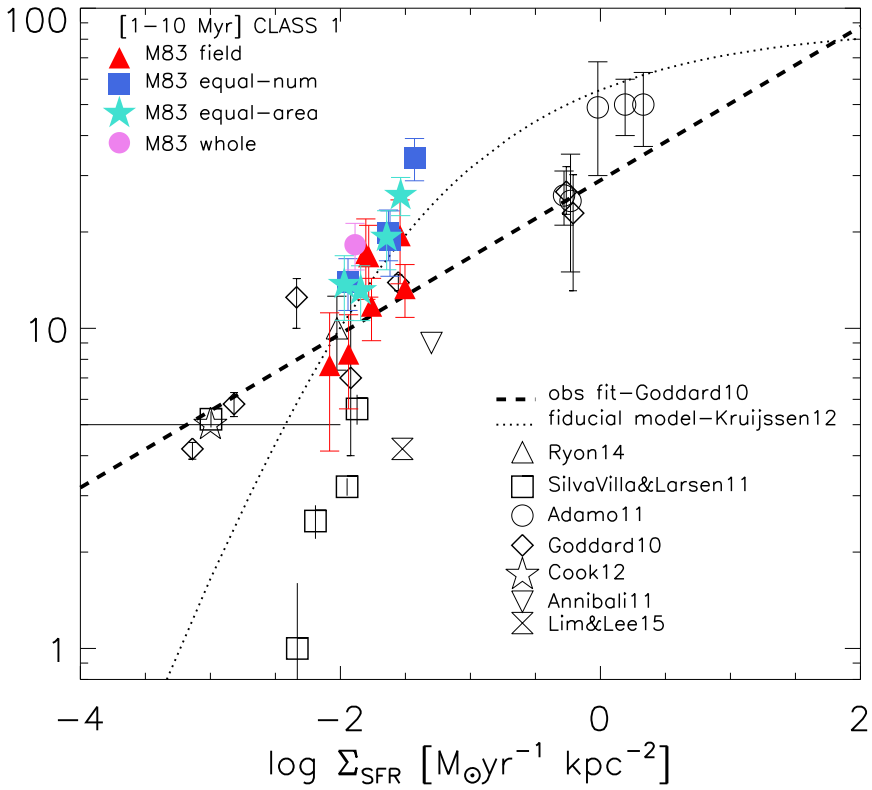

Figure 23. Cluster formation efficiency, Γ, as a function of the galactic SFR density, Σ_{SFR}. The black diamonds are the galaxy sample of Goddard et al. (2010) which were used to obtain the best-fitting power-low relation shown by the dashed line (Goddard et al. 2010, their equation 3). At the right-hand end we show the position of Haro 11 (filled dots) which fits the relation nicely despite its extreme Γ and SFR values.

SFR in Haro 11 galaxy is about 22 Msun/yr

Adamo + 2010

Adamo & Bastian 2016

Relativistic MHD flows in pulsar wind nebulae

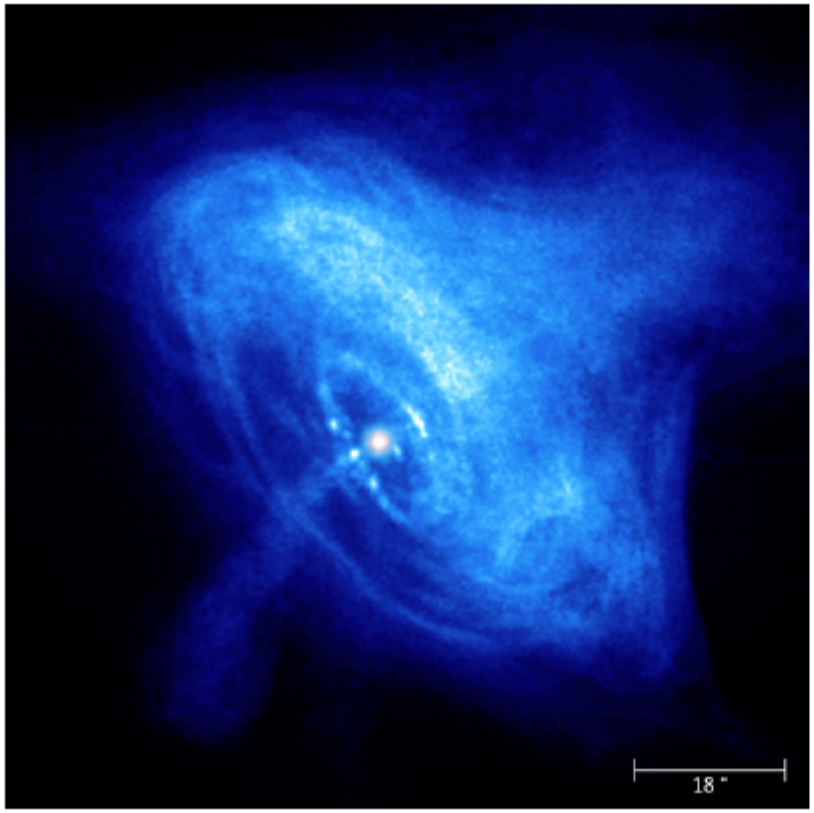

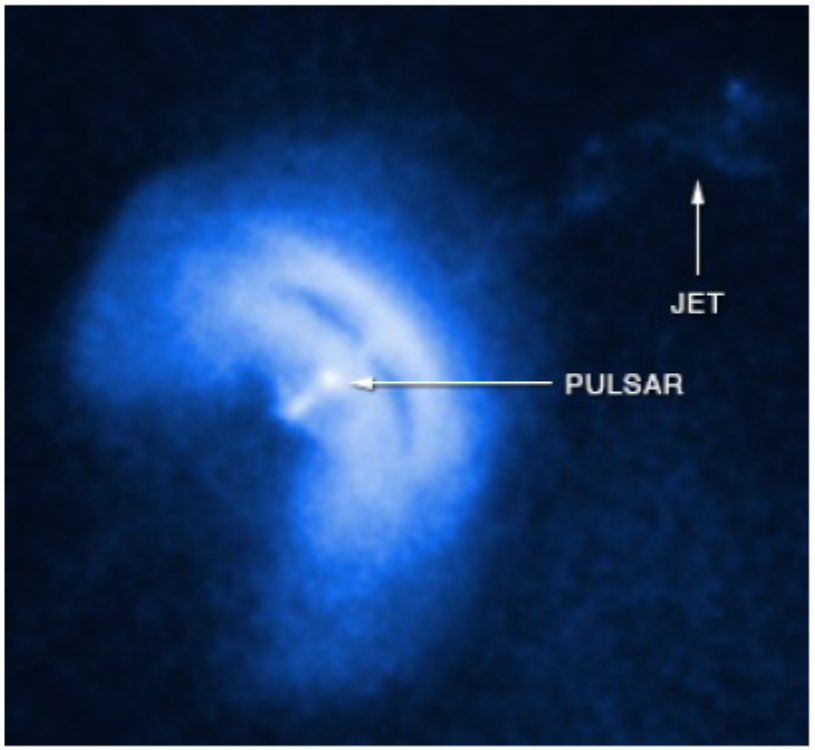

Chandra and HST images

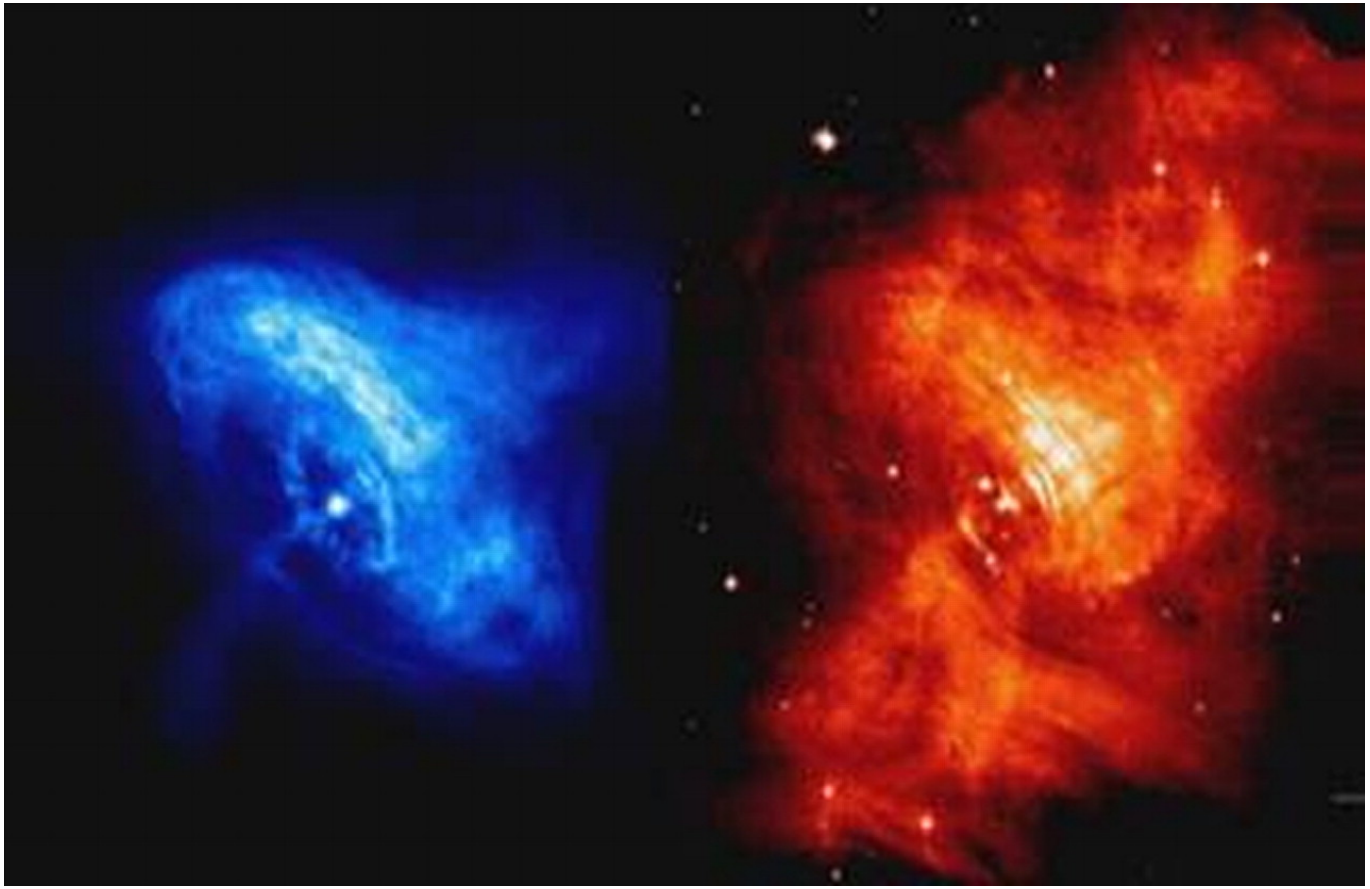

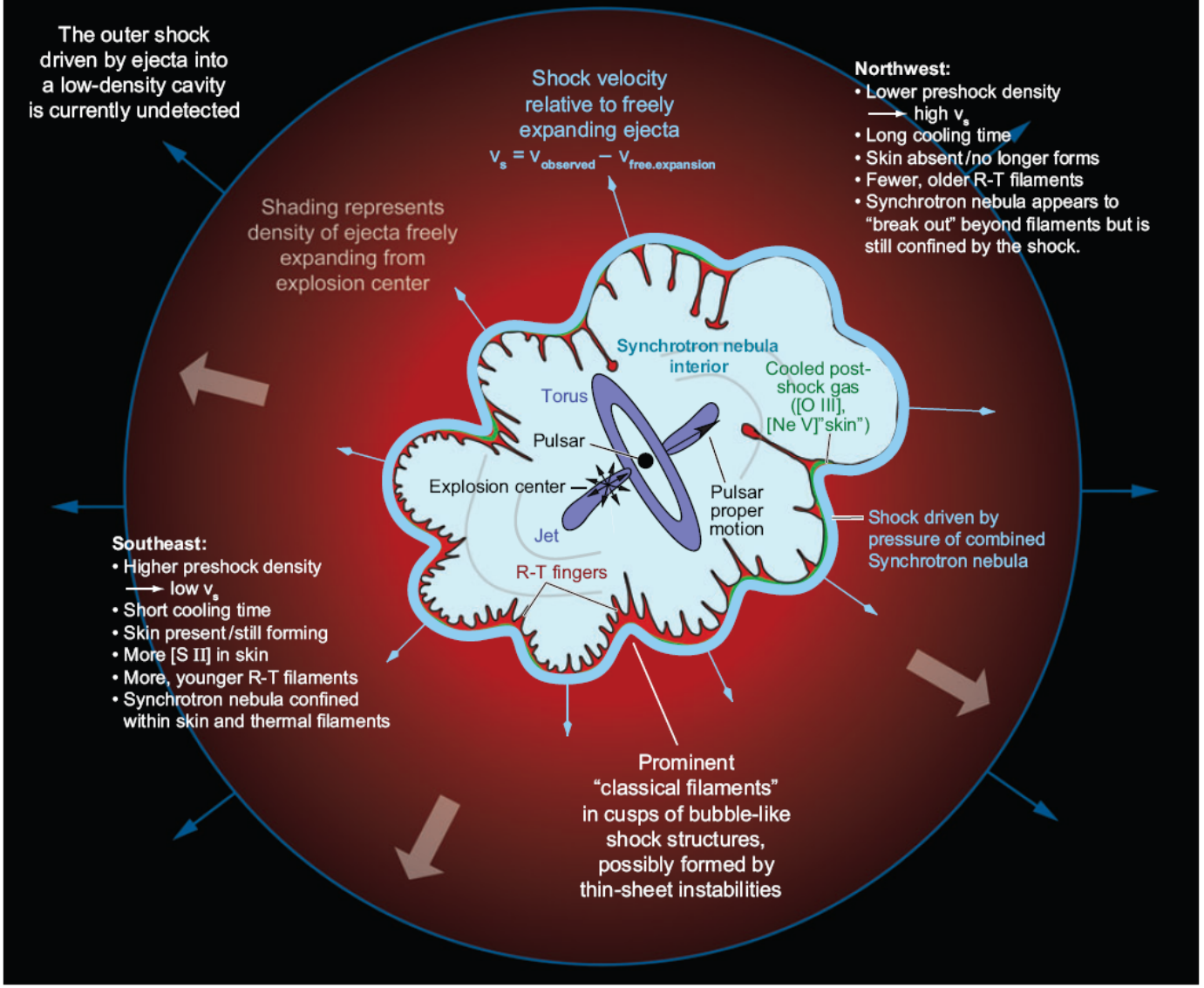

Figure 7

A summary of the structure of the Crab Nebula. The visible Crab consists of the synchrotron nebula, which is confined by thermal ejecta from the explosion. The pressure of the synchrotron nebula drives a shock into the surrounding freely expanding ejecta. This shock is radiative around most of the SE portion of the Crab and can be seen as a thin skin of [O III] and especially [Ne V] emission. The shock is nonradiative in the NW, where the synchrotron nebula extends beyond the boundary of the filaments. The SE-NW asymmetry can be understood as a consequence of the off-center location of the pulsar due to the velocity kick received by the pulsar at the time of the explosion. Rayleigh-Taylor (R-T) instabilities at the interface between the synchrotron nebula and the swept-up ejecta concentrate ejecta into small finger-like structures. The overall scalloped structure of the nebula may result from a thin-shell instability. The shock at the outer edge of the freely expanding ejecta has not been detected. (Features are not shown to scale.)

Hester 2008

Multi-wavelength Crab spectrum

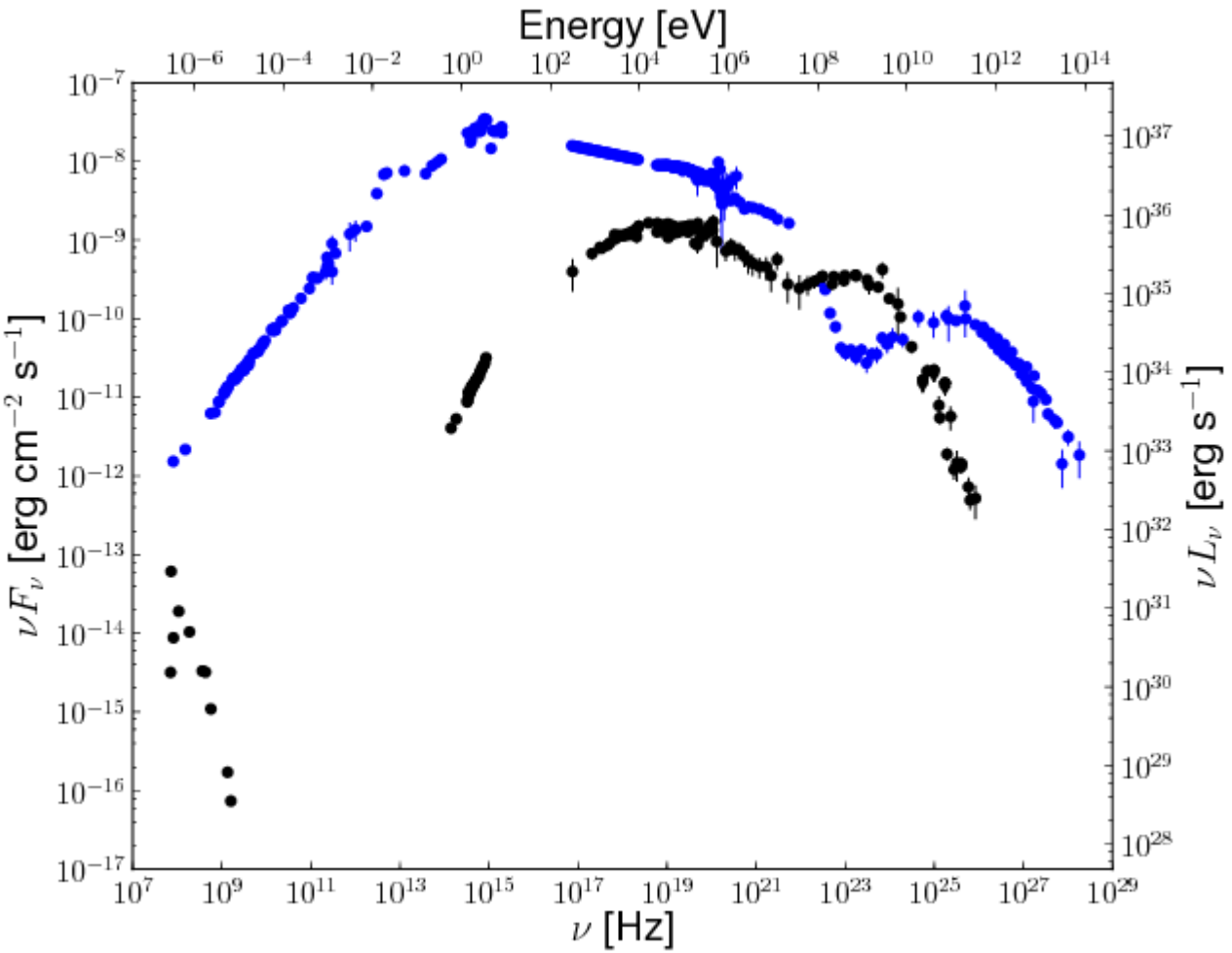

Buehler & Blandford 2014

AGILE DETECTION of Crab FLARE

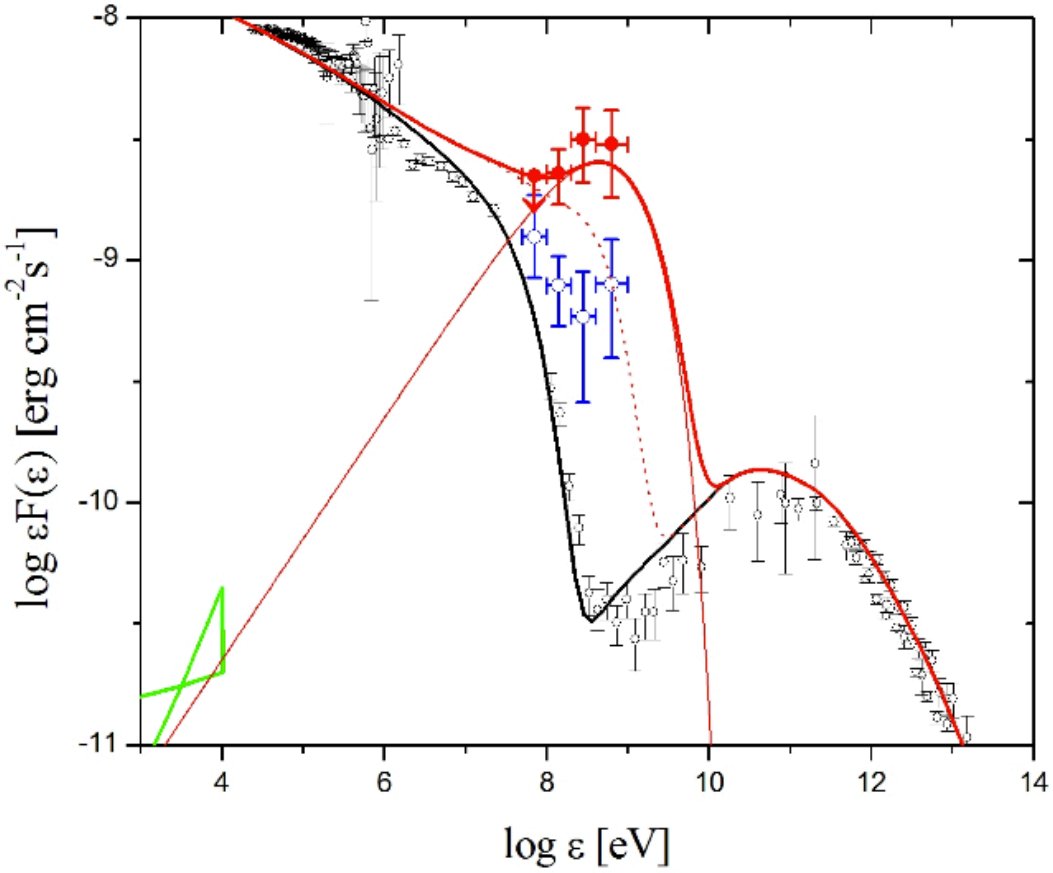

Tavani+ 2011

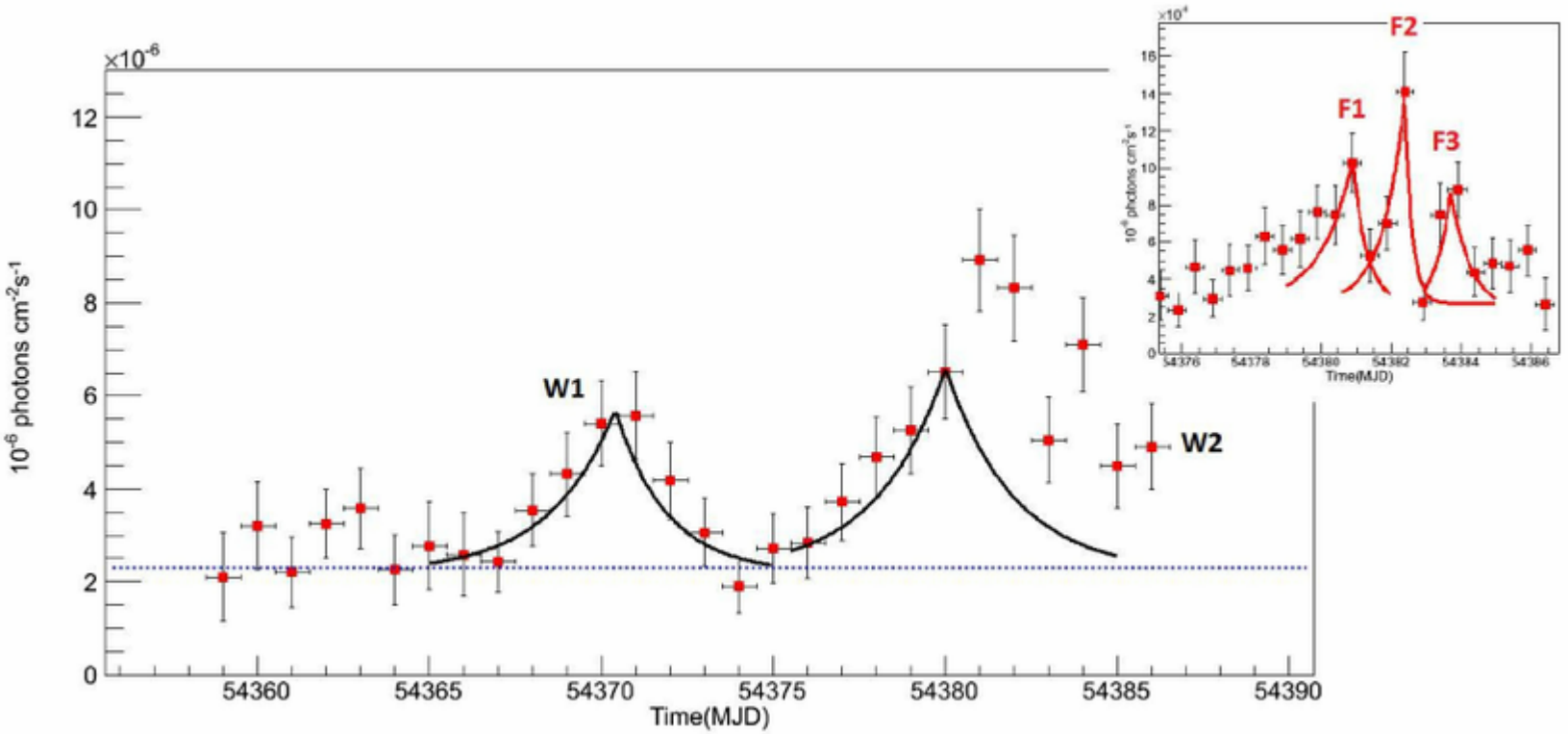

Striani Tavani Vittorini ea 2013

Fermi light curve of the April 2011 flare

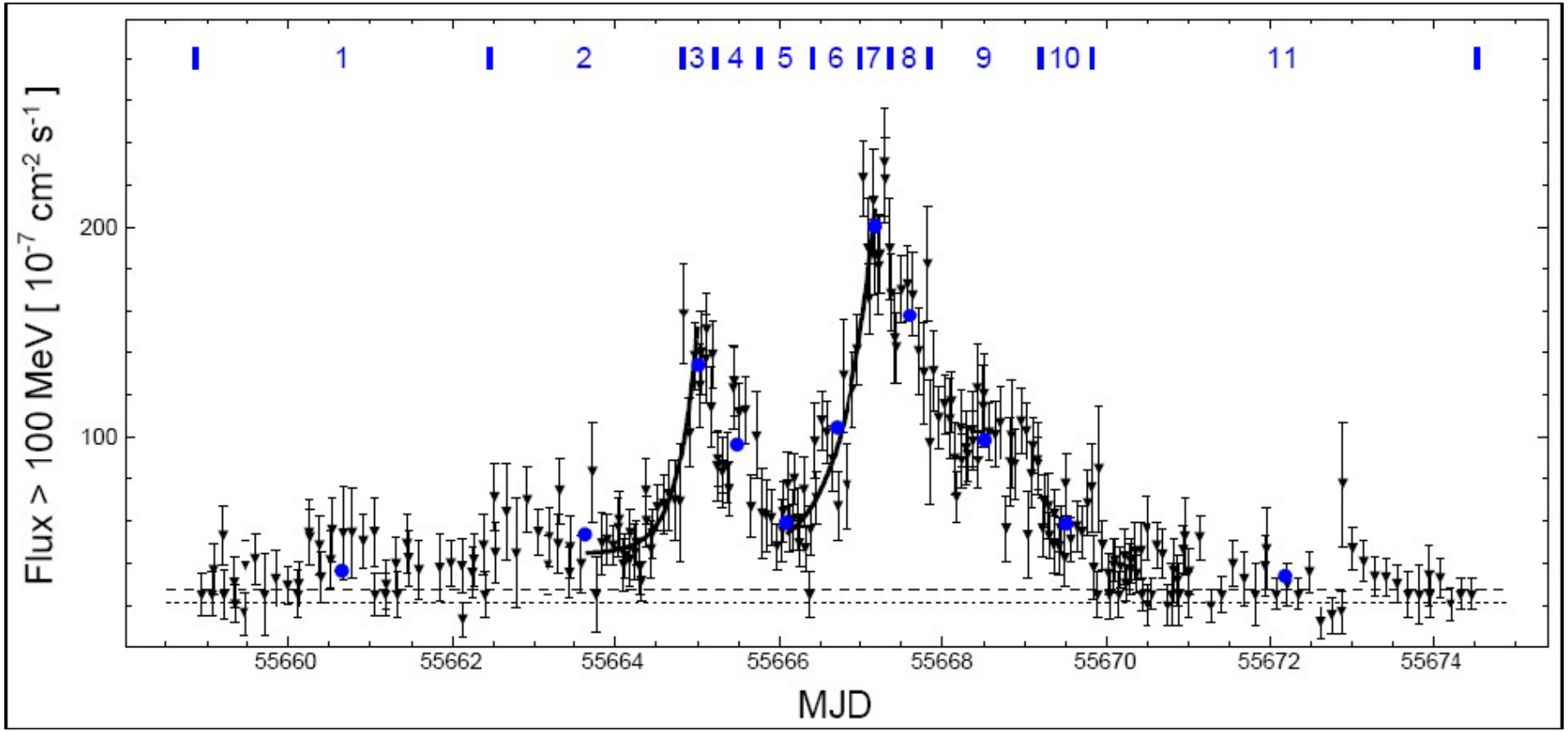

Buehler, Scargle, Blandford, ea 2012

Temporal evolution of the Fermi LAT spectra
April 2011 flare

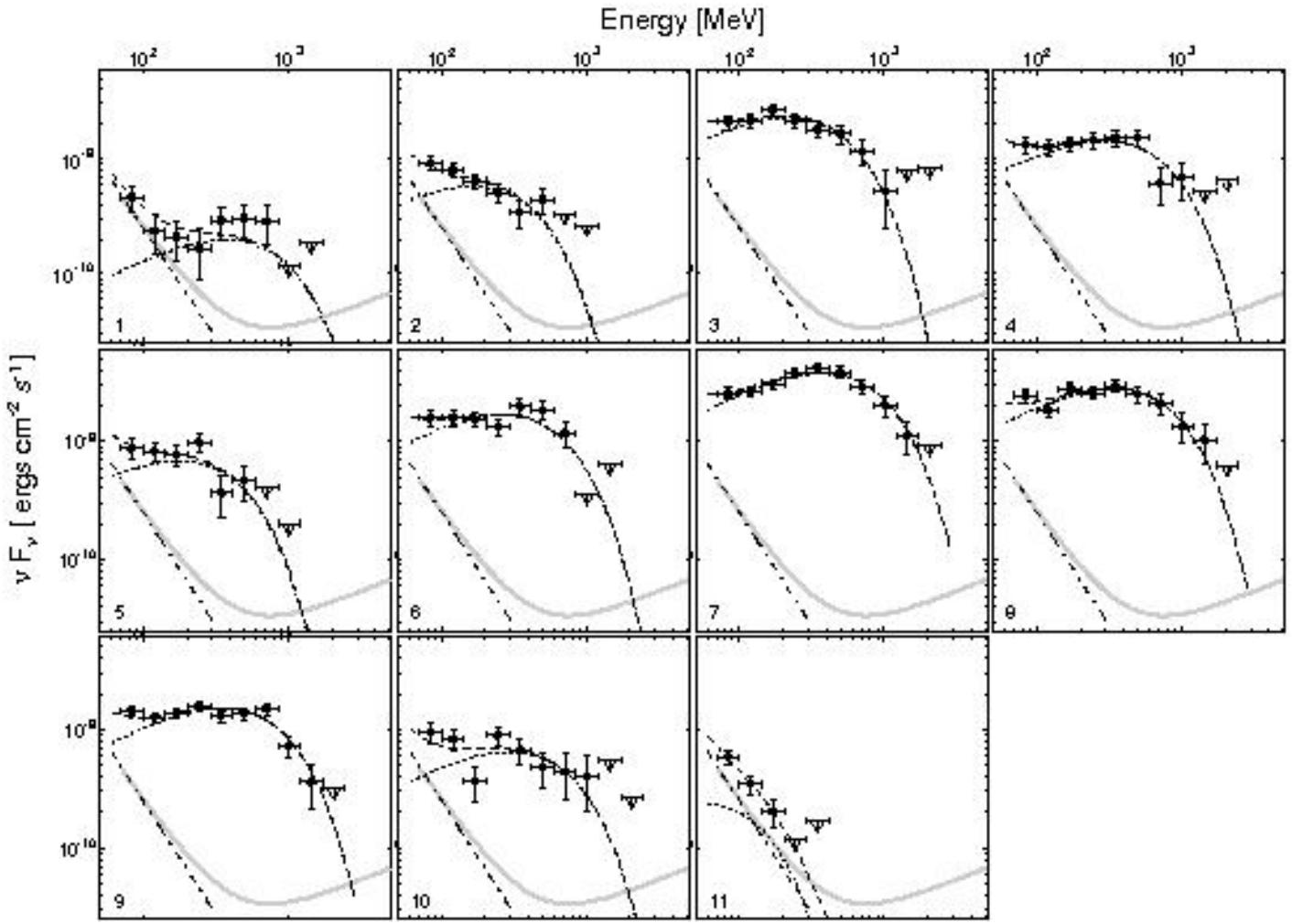

Buehler, Scargle, Blandford, ea 2012

Crab Nebula Giant Flares

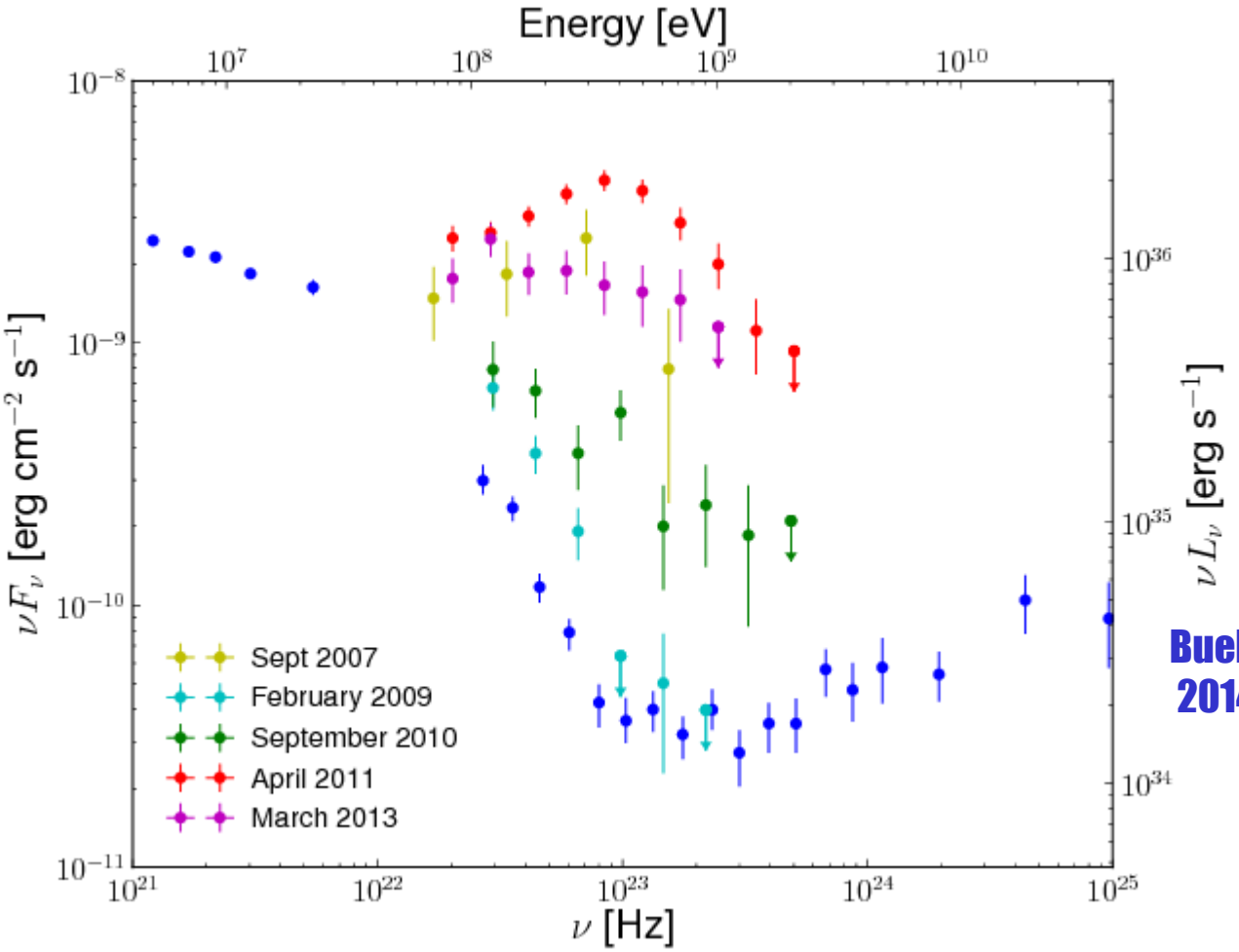

Buehler & Blandford 2014

Extremely high energetic efficiency a few percent of pulsar spin down
Short time variability scale
Energies of accelerated particles well above PeV
No simultaneous flare type variations in other spectral bands sofar...

Particle acceleration in magnetized PWN winds

Simulation setup

- Relativistic 3D e.m. PIC code TRISTAN-MP (Buneman 1993, Spitkovsky 2005)
- Incoming flow is reflected by a wall, which mimics a contact discontinuity
- Simulations are in the downstream fluid frame

Pre-shock parameters:

- composition (e^-- e^+ plasma)
- bulk Lorentz factor γ_0
- magnetization

$$\sigma = \frac{B_0^2}{4\pi\gamma_0 n_0 m c^2} \gg 1$$

- stripe wavelength λ
- stripe-averaged field $\langle B_y \rangle_\lambda$

or

$$\alpha = \frac{2\langle B_y \rangle_\lambda}{1 + |\langle B_y \rangle_\lambda|}$$

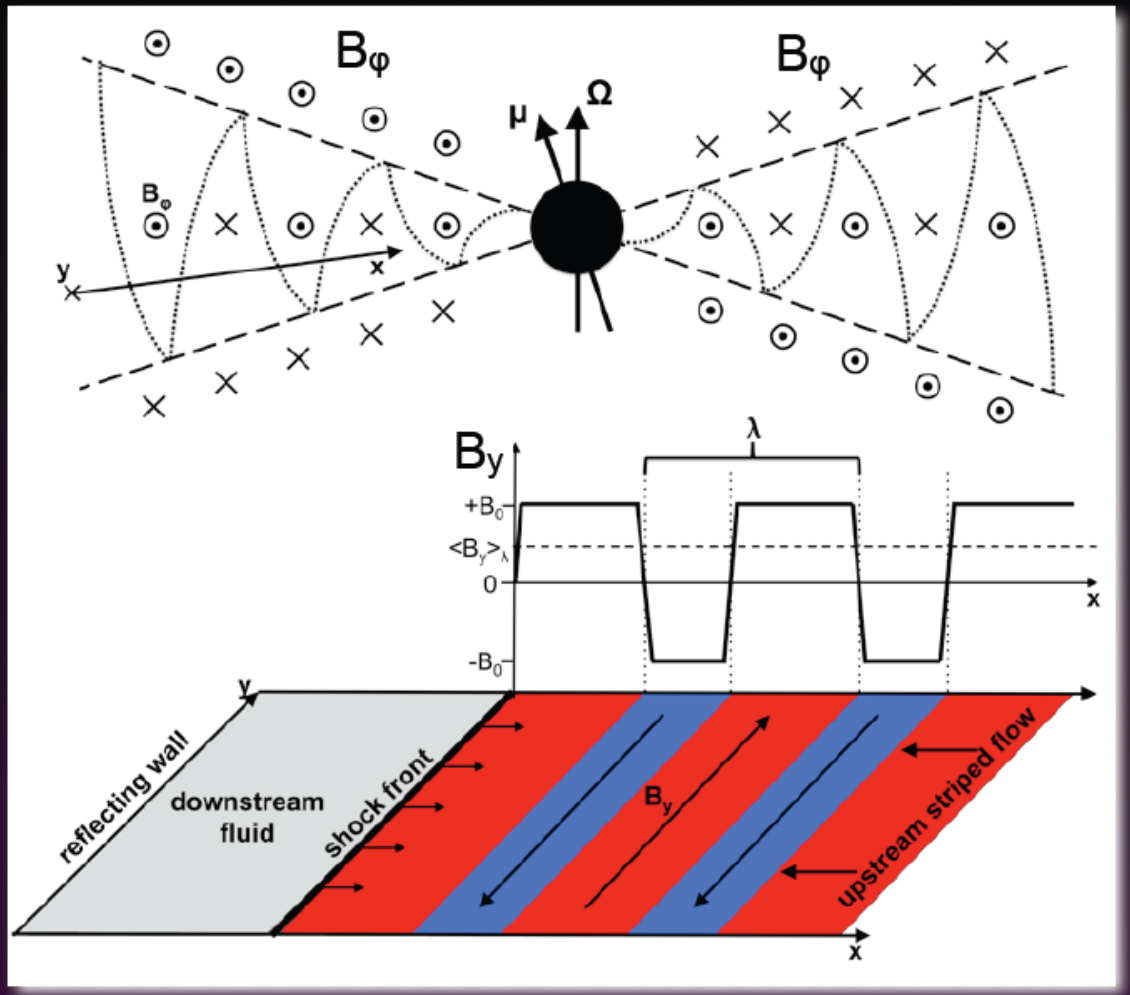

Sironi & Spitkovsky ApJ 2011

Shock-driven reconnection

σ=10 λ=640 c/ω_p α=0.1

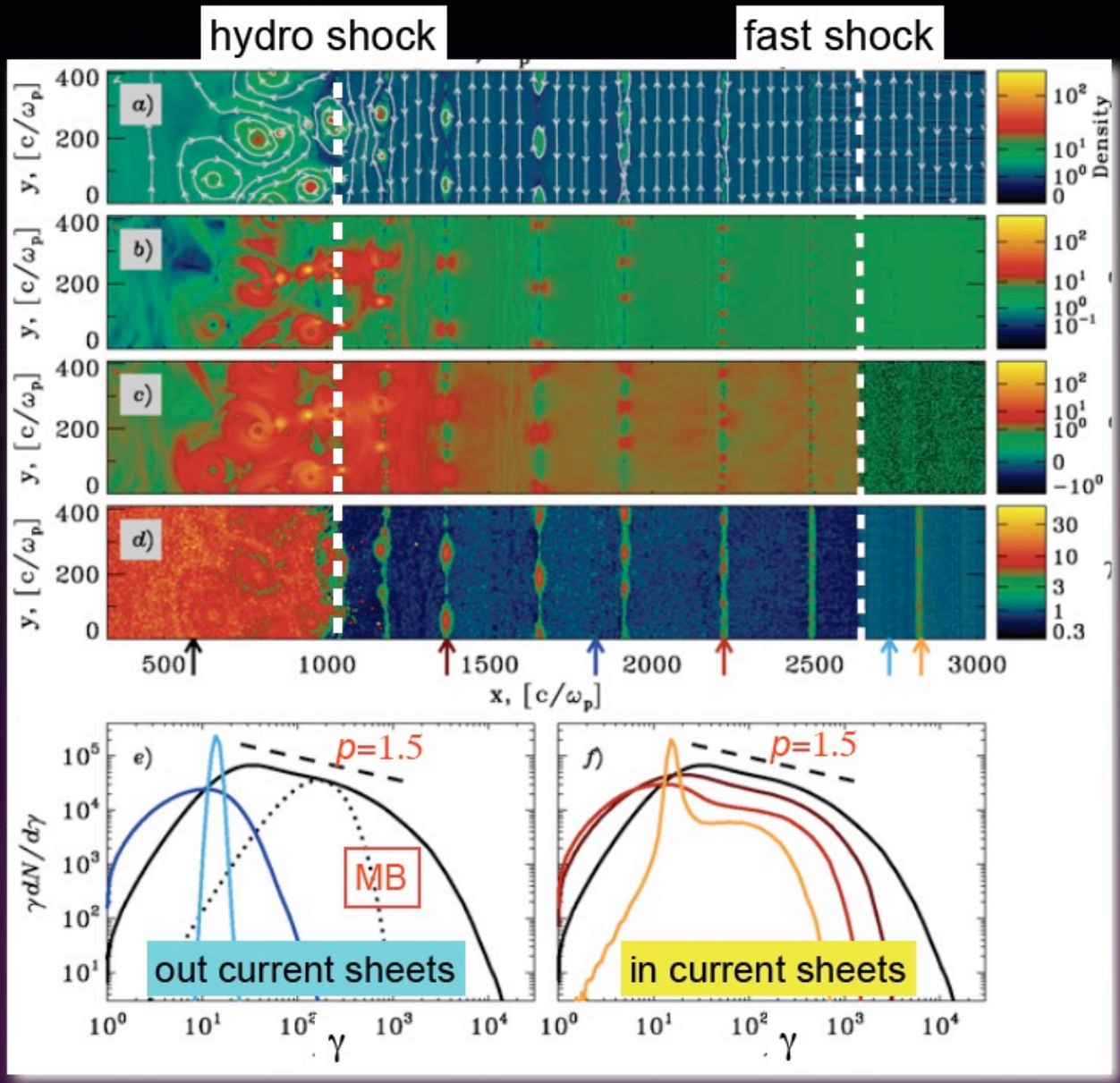

- The fast shock compresses the flow and drives magnetic reconnection
- The flow downstream from the hydro shock is almost unmagnetized
- The particle spectrum within current sheets gets broader from the fast to the hydro shock
- Behind the hydro shock, broad spectrum with flat tail of slope p~1.5

Sironi & Spitkovsky ApJ 2011

But what about the flares (PeV pairs)?

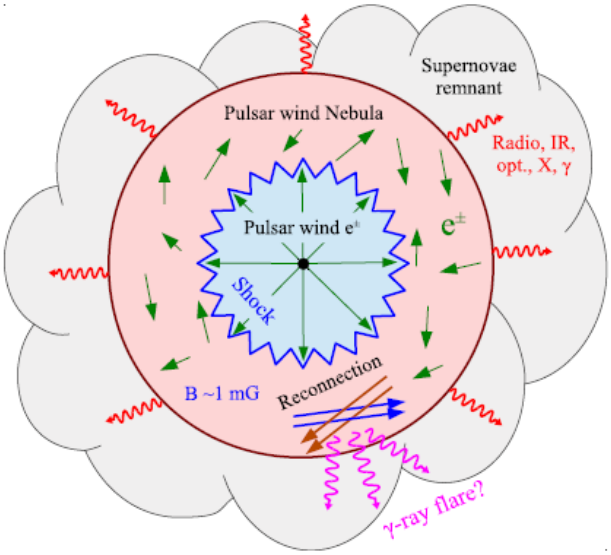

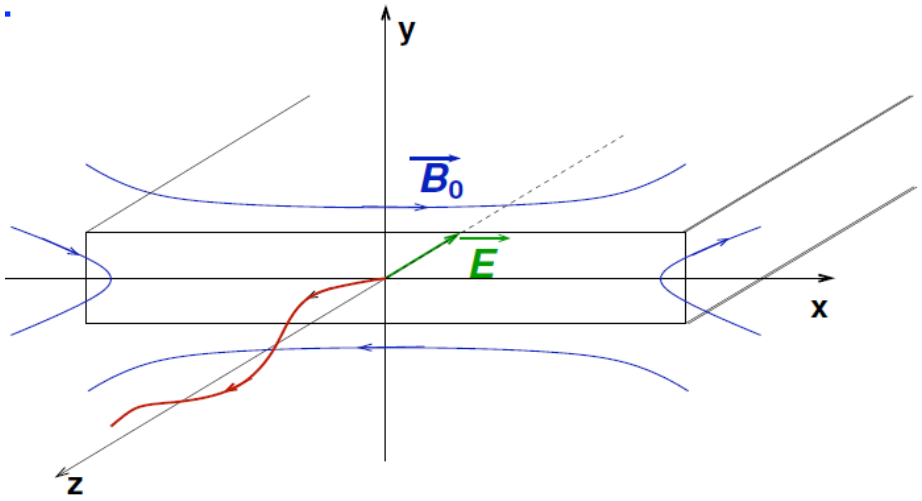

Electric fields produced by magnetic reconnection
Radiation-reaction limited acceleration above PeV
was discussed by Cerutti, Werner, Uzdensky, Begelman

Trans-relativistic MHD flows in pulsar wind nebulae with bow shocks

AB+ Space Sci. Rev v.207 p.235, 2017

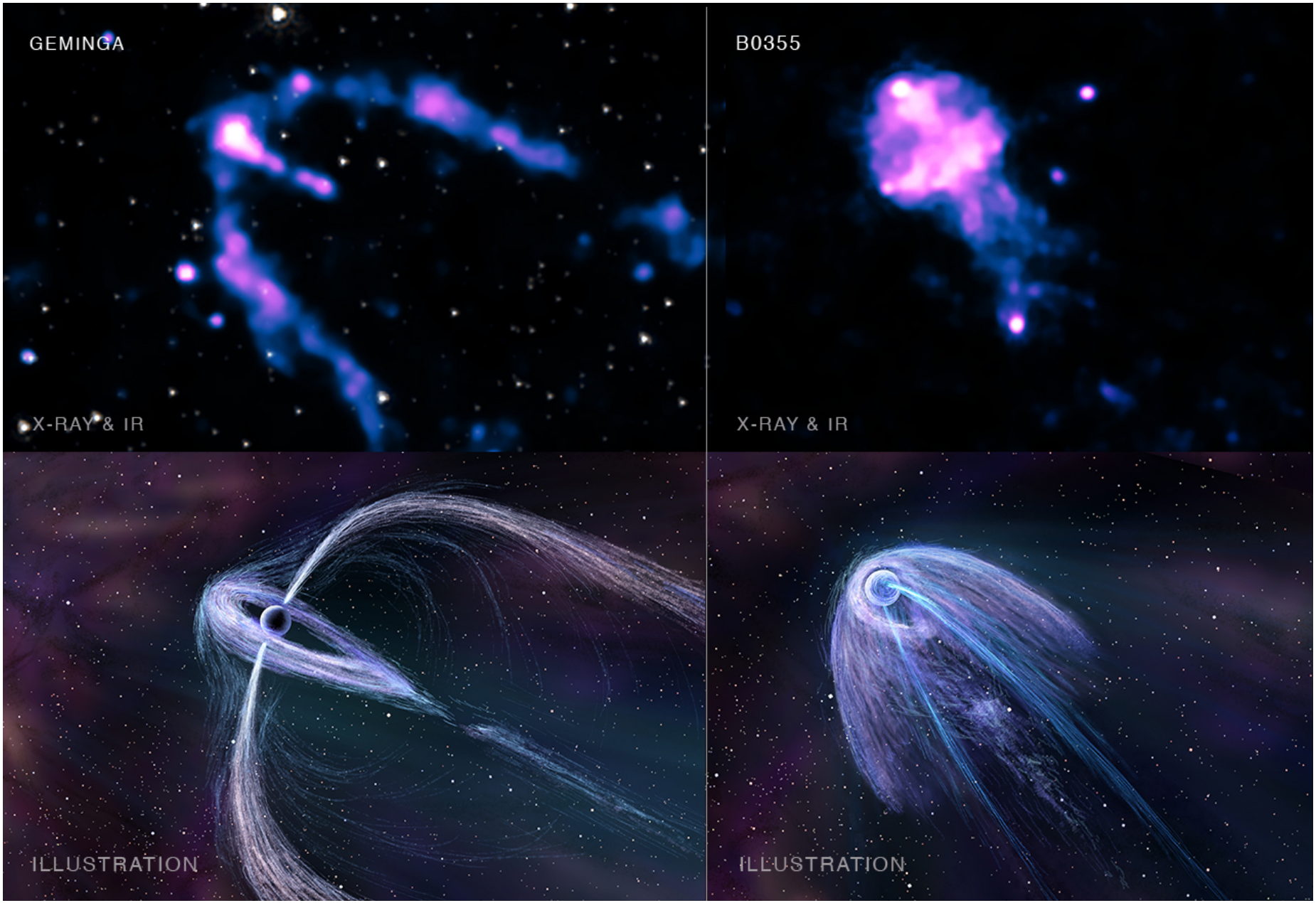

NASA Chanda CXO

Geminga PWN: Chandra 0.7- 8 keV
Synchrotron X-ray radiation of TeV regime pairs

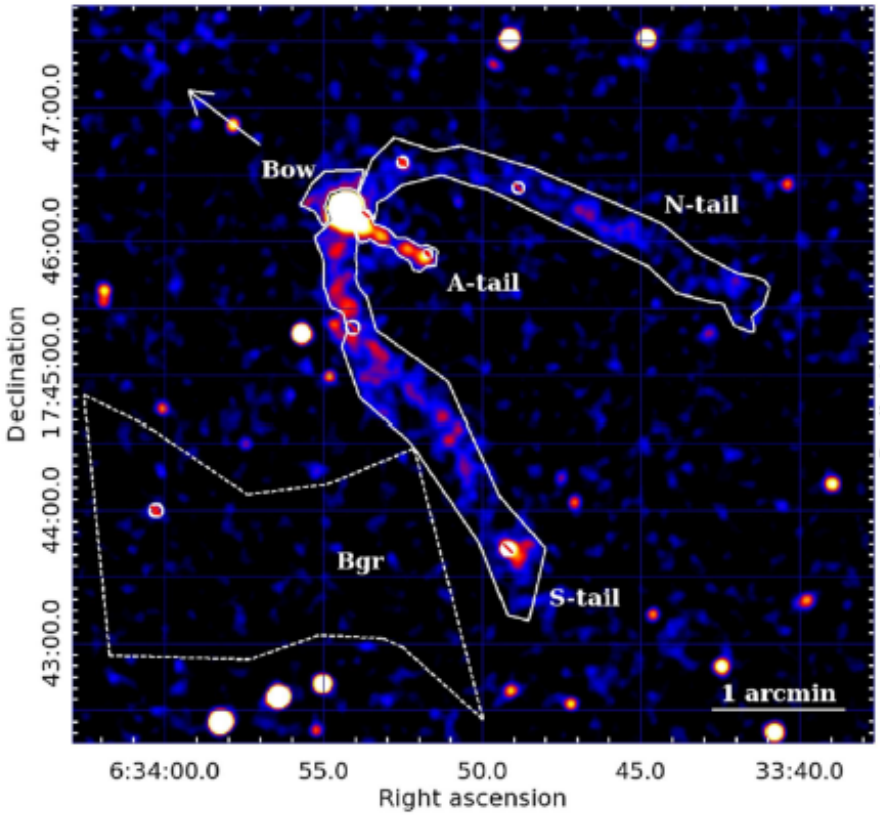

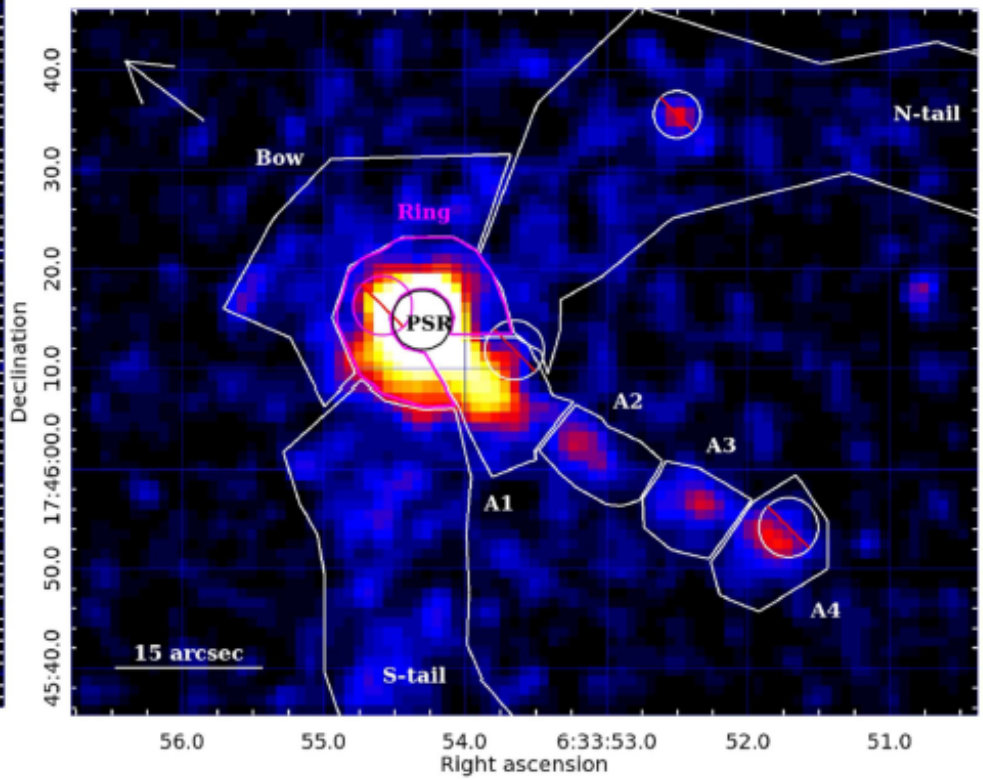

Photon indexes of the synchrotron emission at the bow and in S & N- tails are about 1!

Posselt + Ap J, v.835:66, 2017

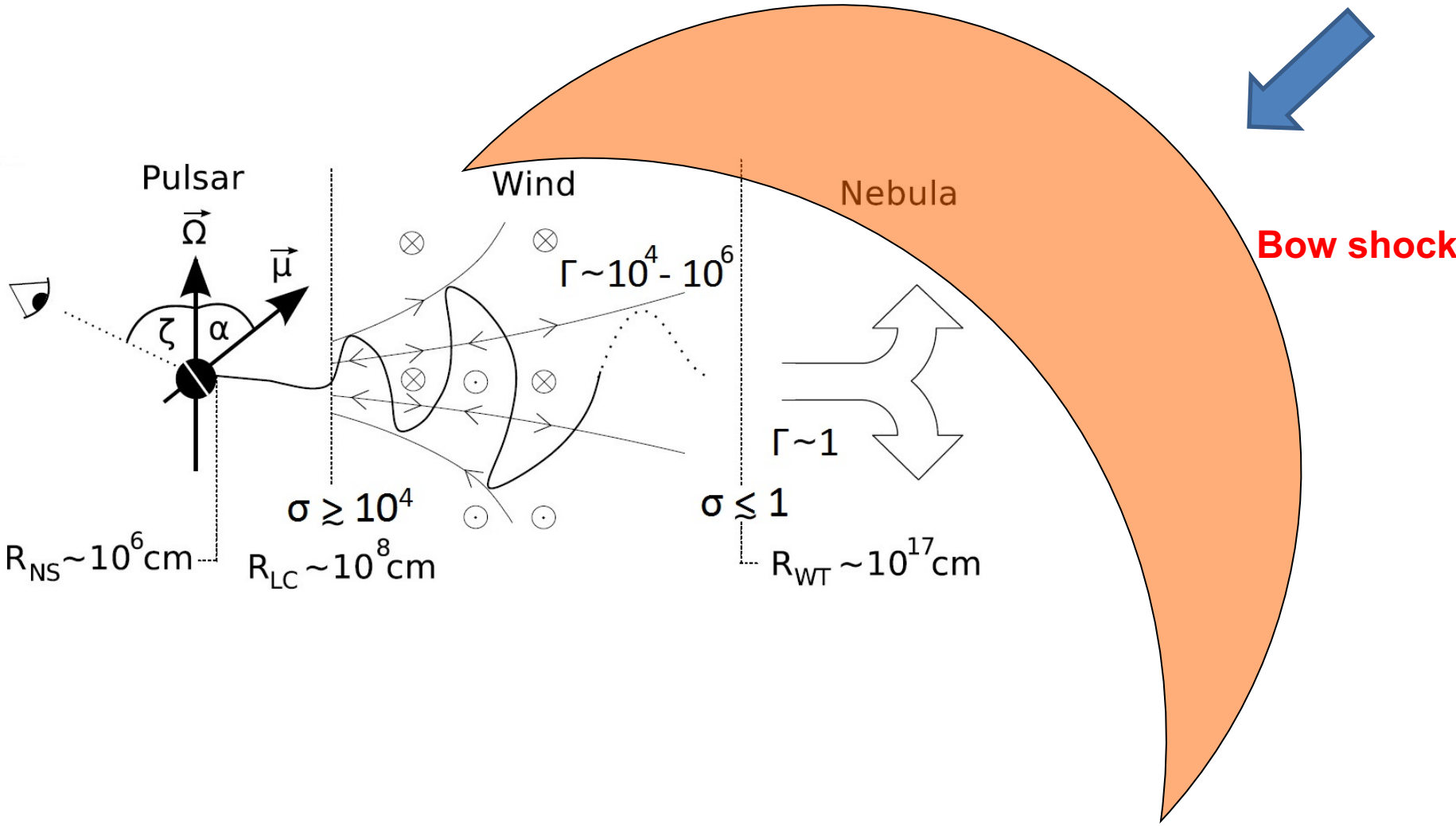
Pulsar
Wind
Nebula
Bow shock
$\vec{\Omega}$
$\vec{\mu}$
ζ
α
Γ~10^4- 10^6
Γ~1
σ ≳ 10^4
σ ≲ 1
R_NS~10^6cm
R_LC ~10^8cm
R_WT ~10^17cm

Bow shock PWN geometry for Monte Carlo simulations

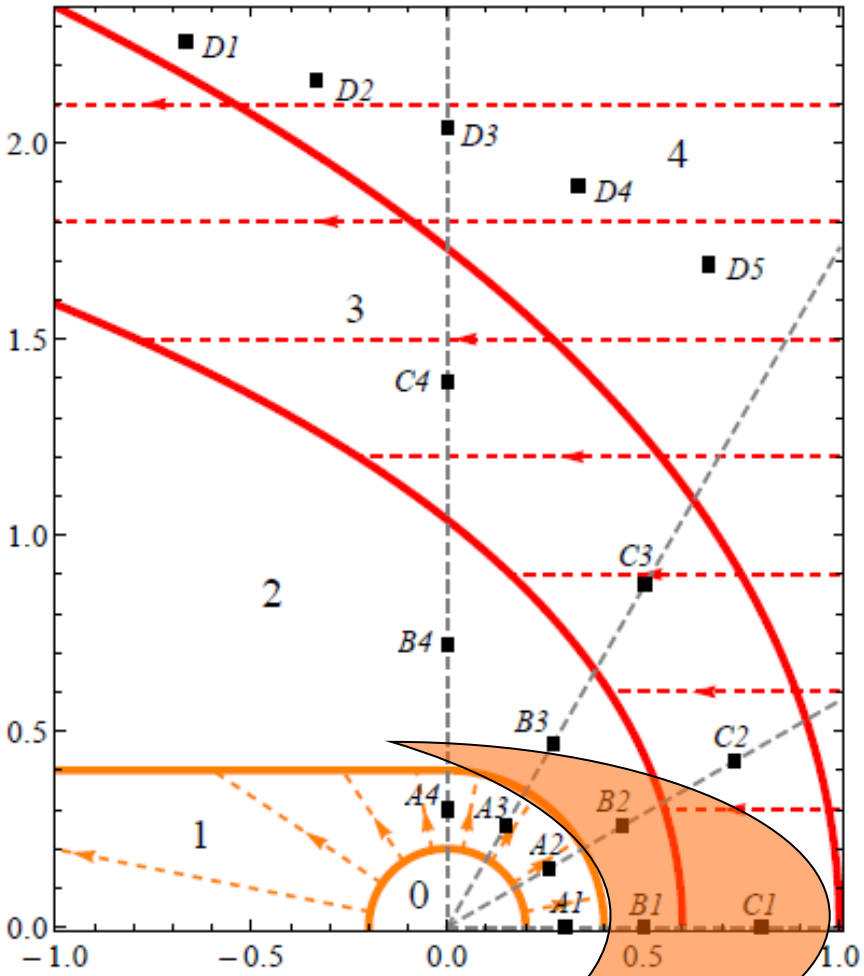

The numbers 0 - 4 label the regions with different transport regimes: 0 is the cold PW, 1 (between the orange curves) is the shocked PW, 2 is the zone near the contact discontinuity, 3 (between the red curves) is the postshock flow of the ISM matter, 4 is the unperturbed ISM. (A.Petrov, AB)

AB+ Space Sci. Rev v.207 p.235, 2017

Observations of PSR J0437-4715 with bow shock vs modeling

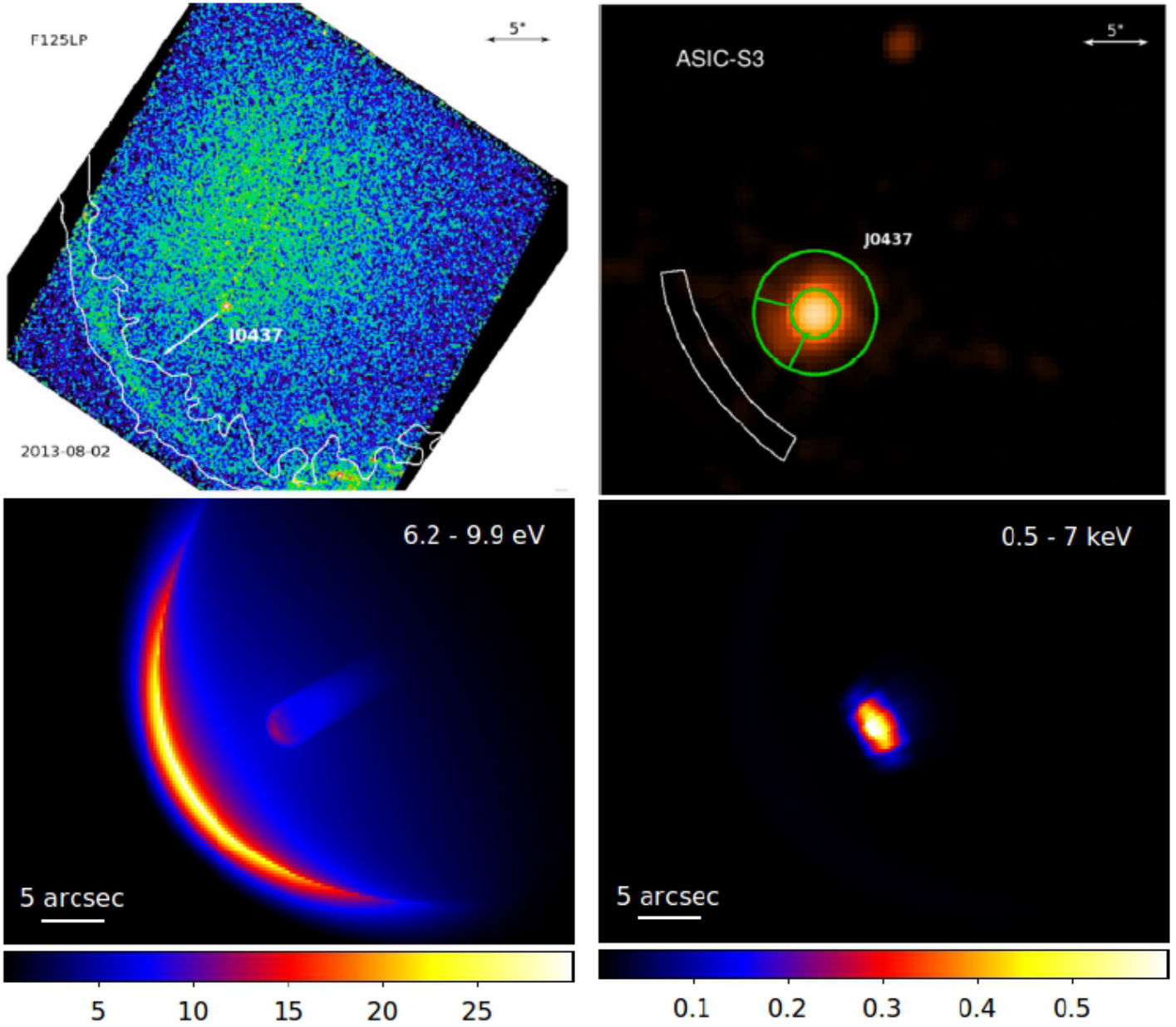

Observations: Rangelov+ 2016 **Modeling: Space Sci. Rev v.207 p.235, 2017**

Modeling PSR J0437-4715 with bow shock

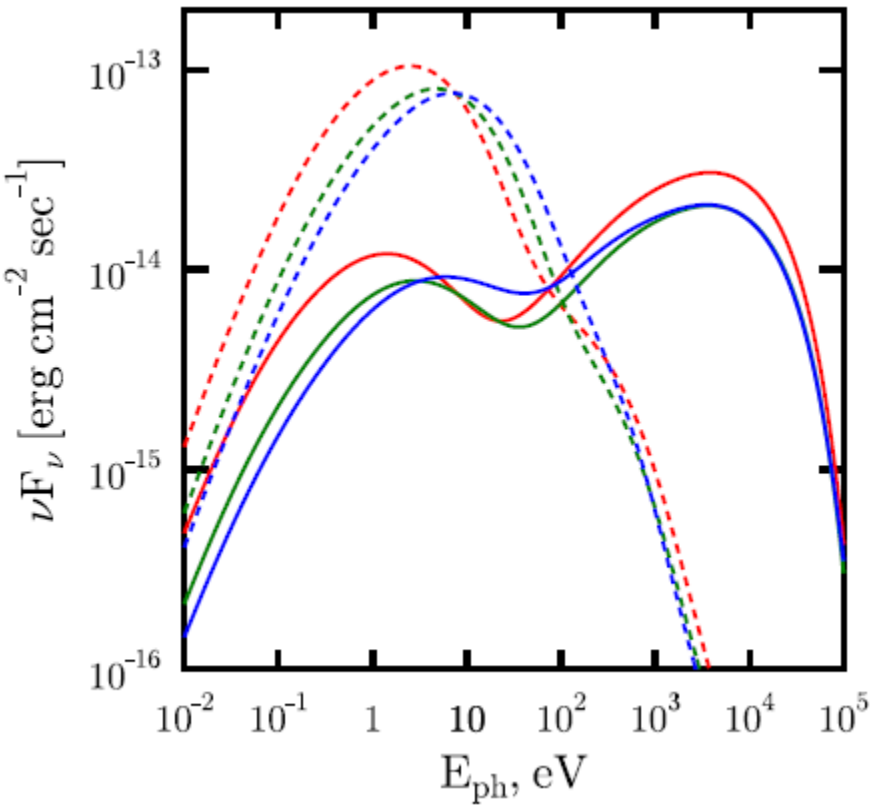

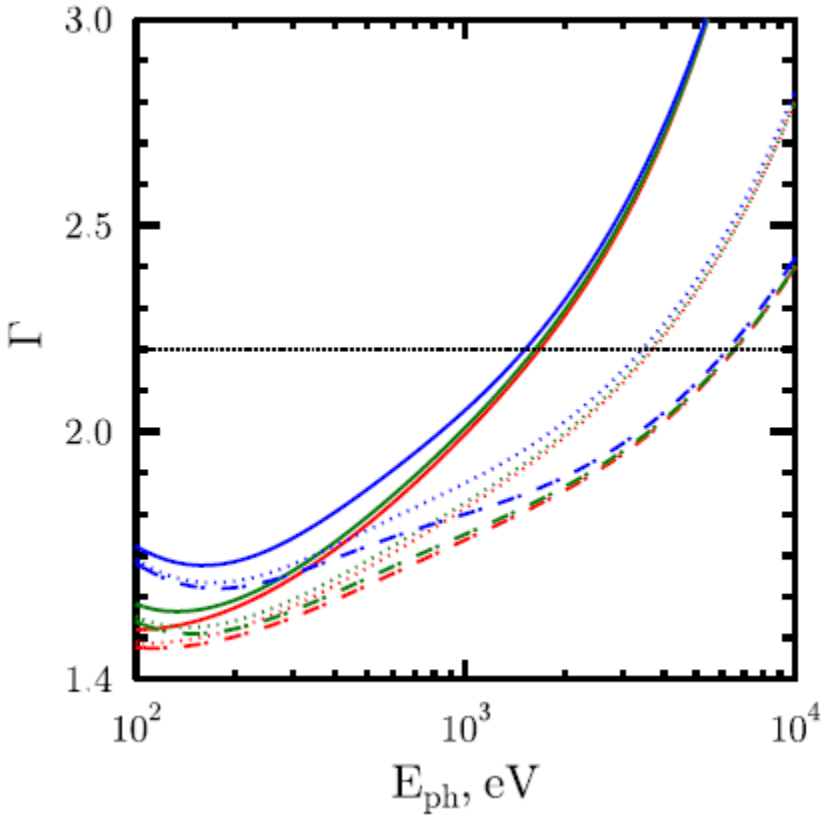

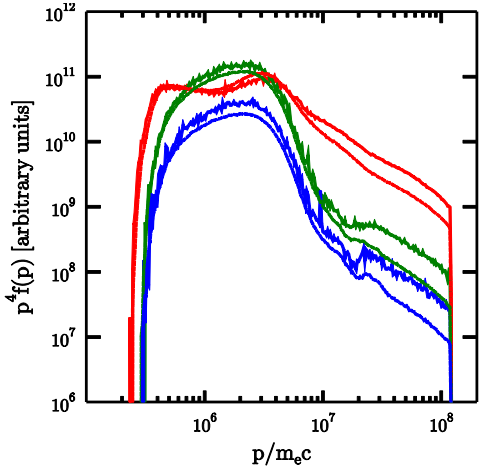

Chandra image of Vela PWN

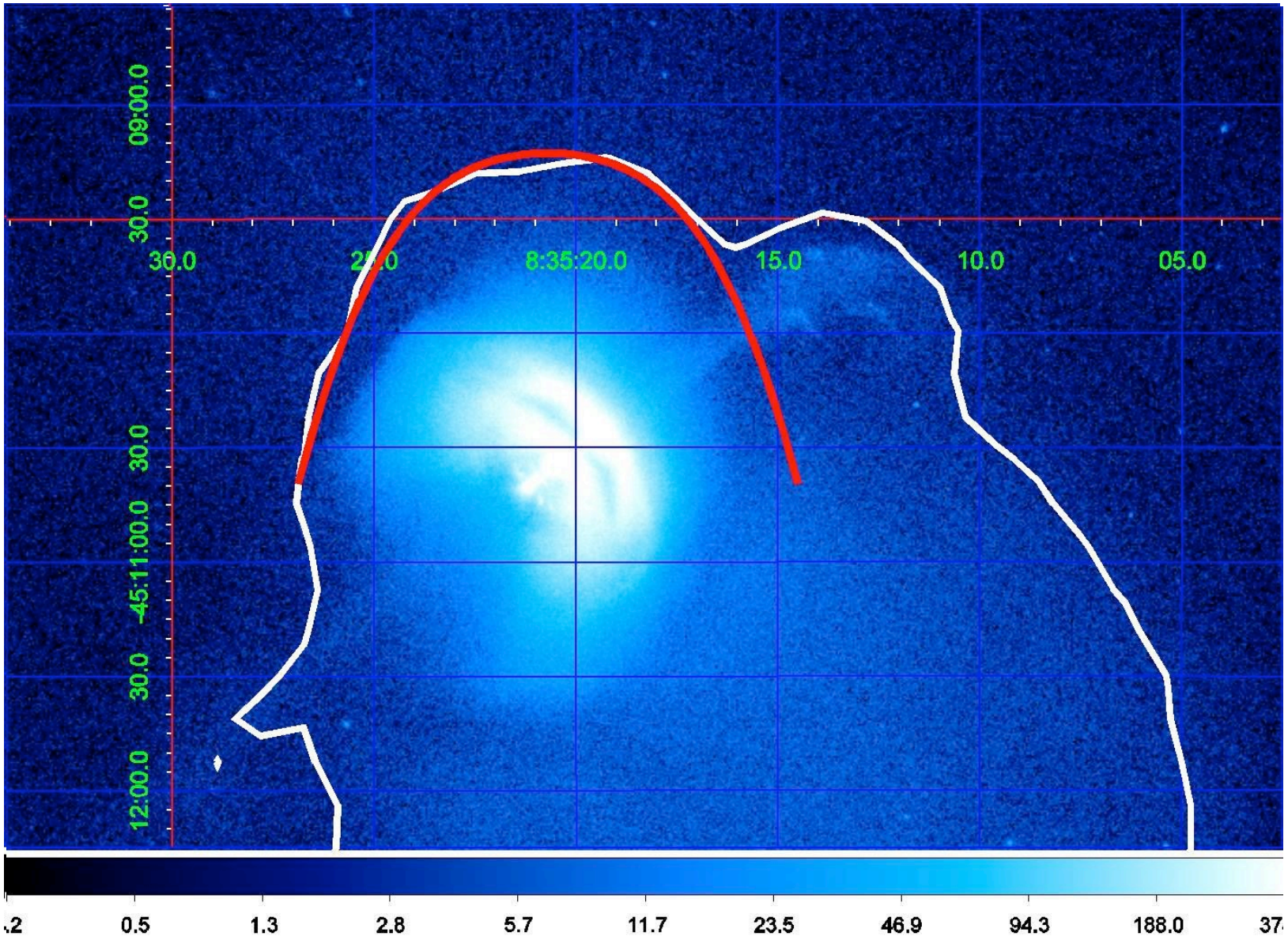

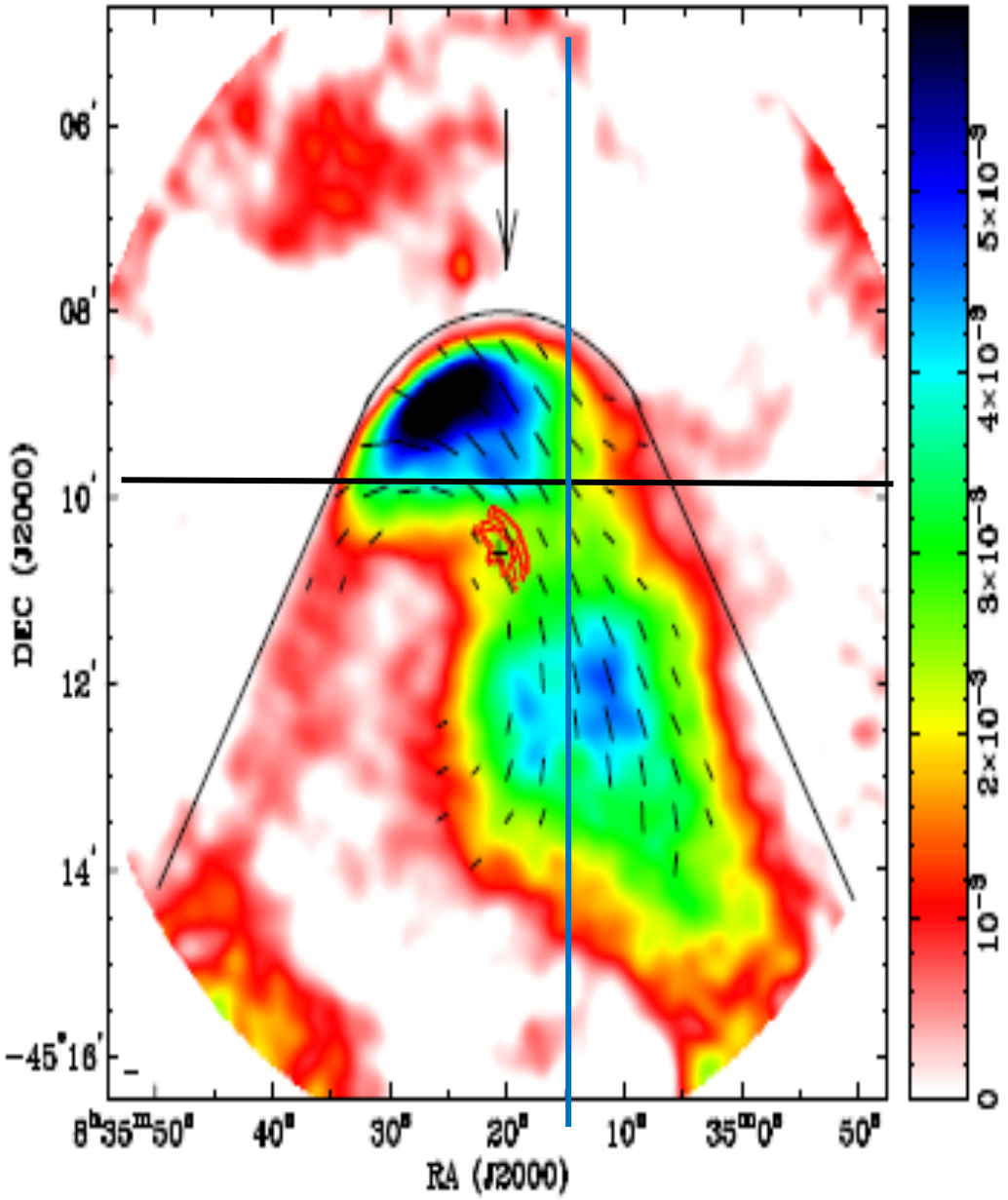

Vela PWN at 5 GHz from Dodson ea (2003) with the bow shock by Chevalier & Reynolds (2011)

Vela PWN spatially resolved pair spectra modeling

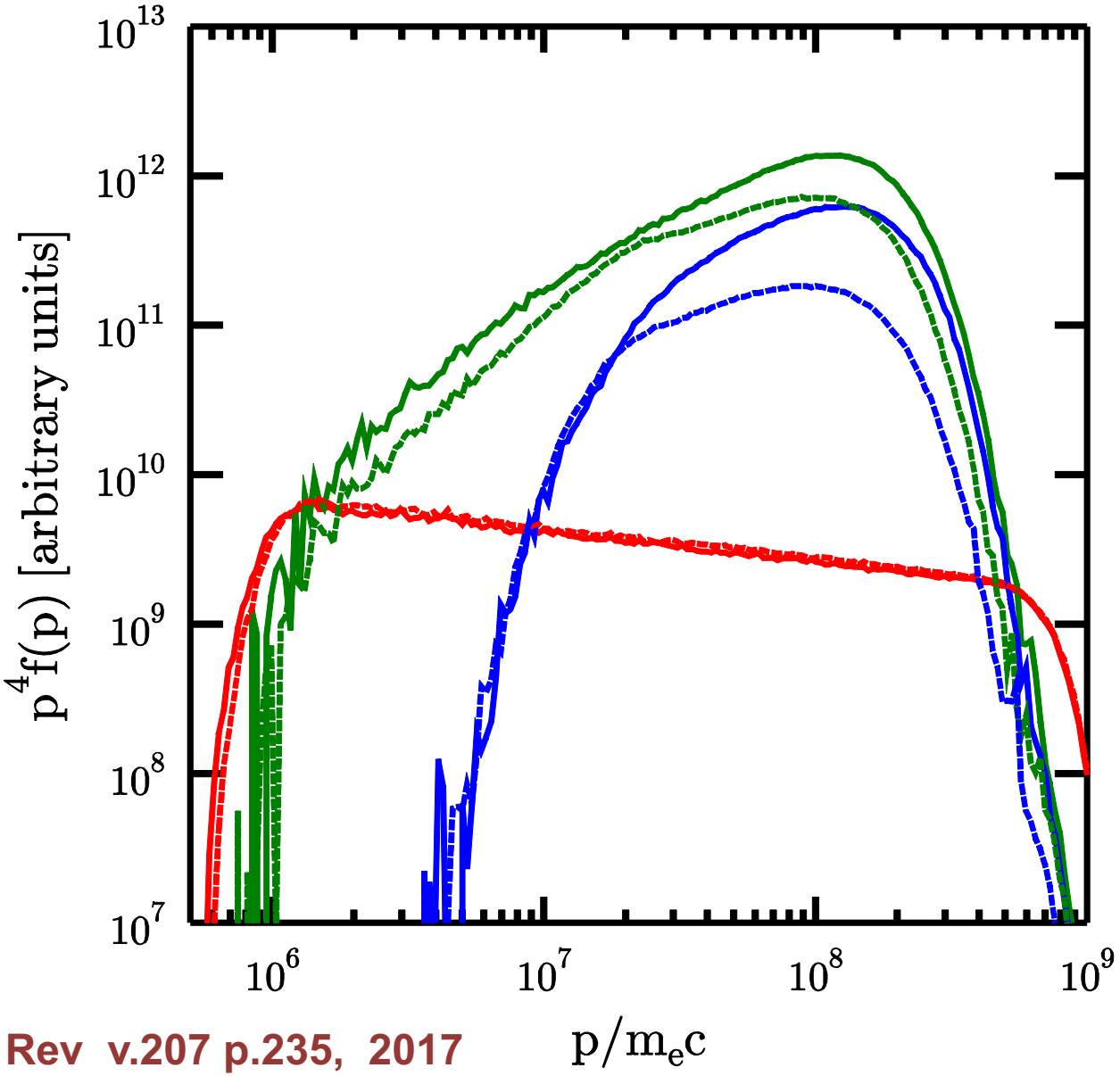

Space Sci. Rev v.207 p.235, 2017

Vela PWN spatially resolved radiation spectra modeling

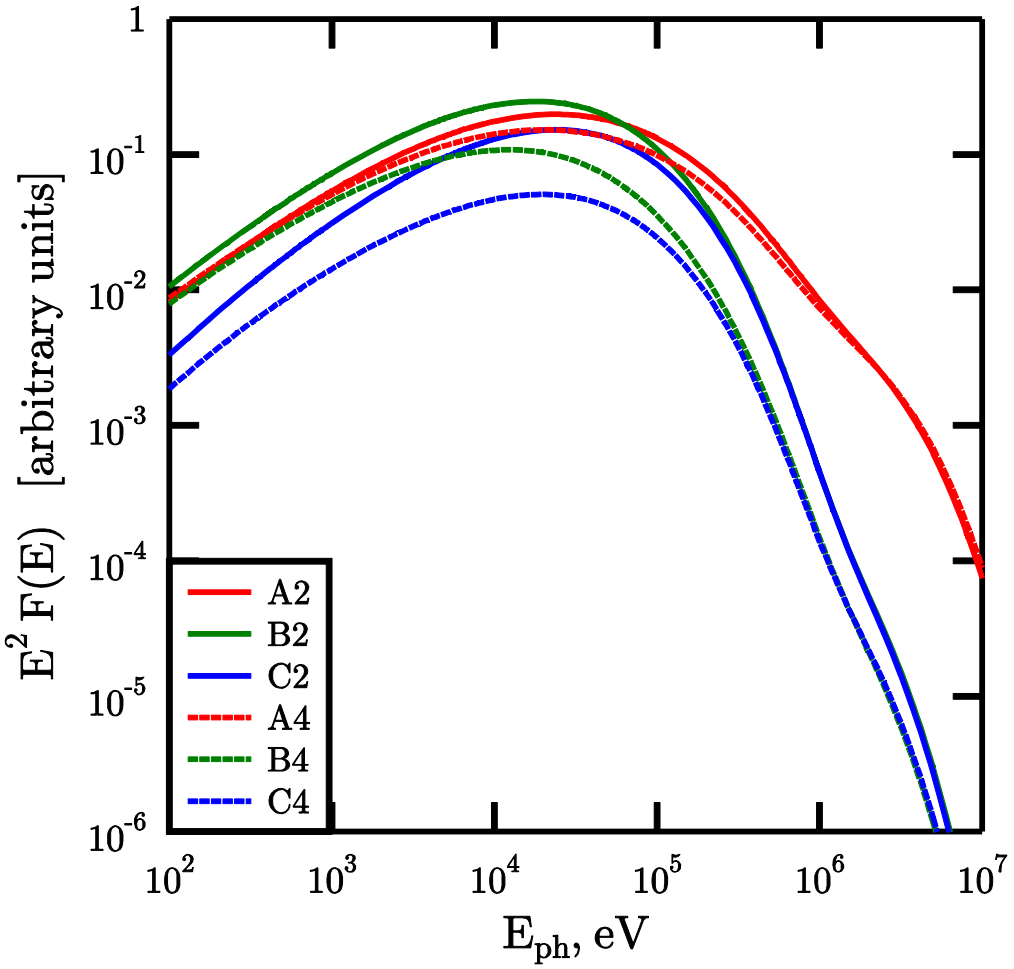

Vela PWN spatially resolved spectral photon index modeling

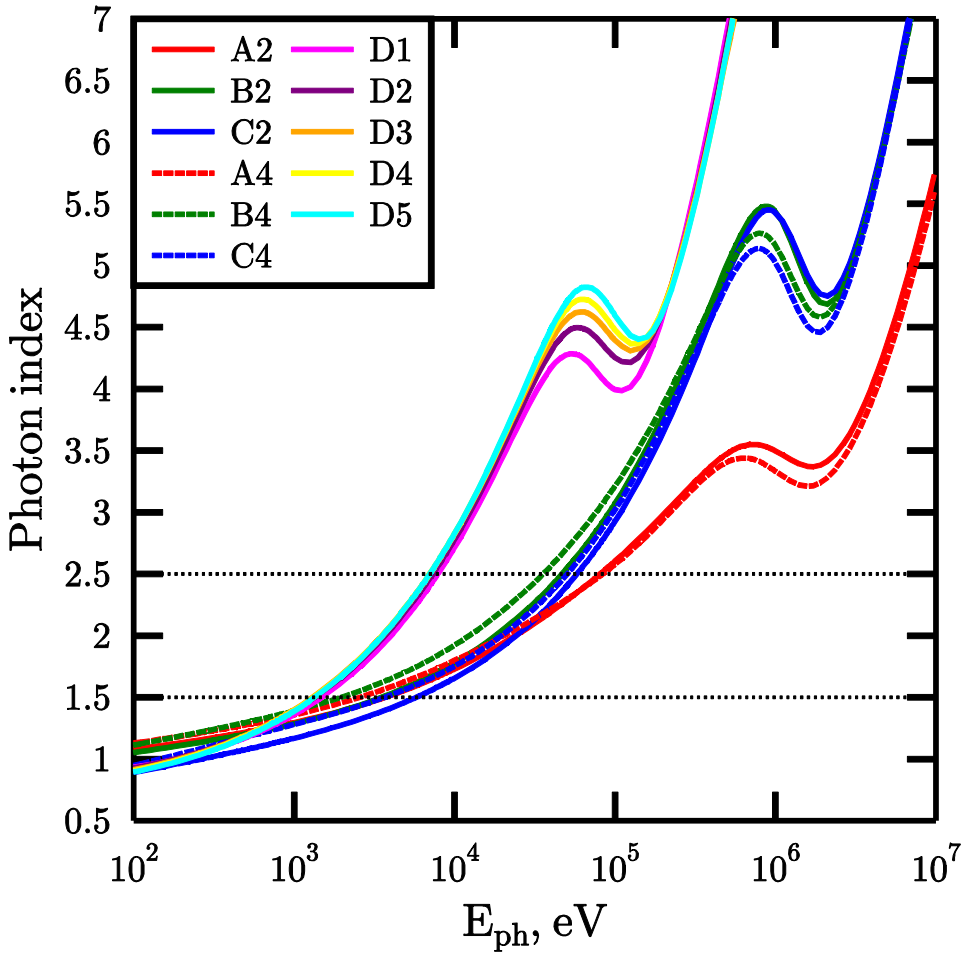

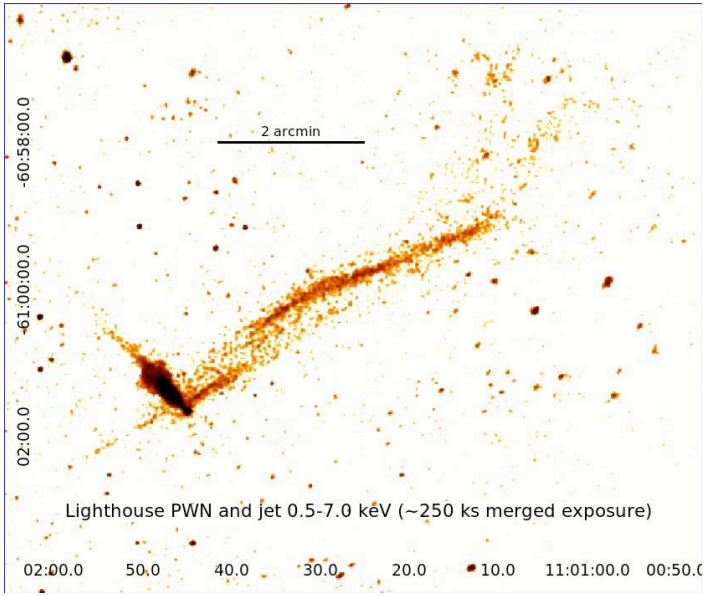

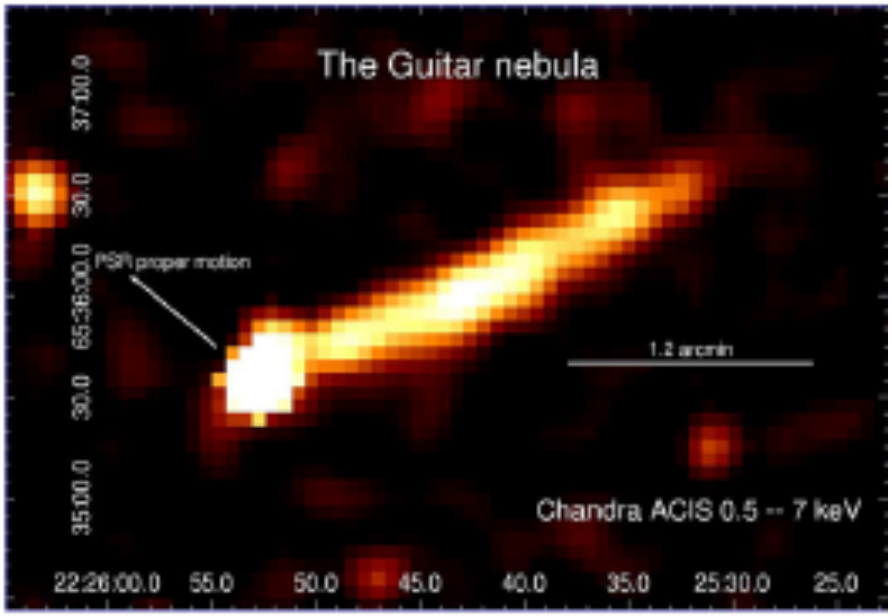

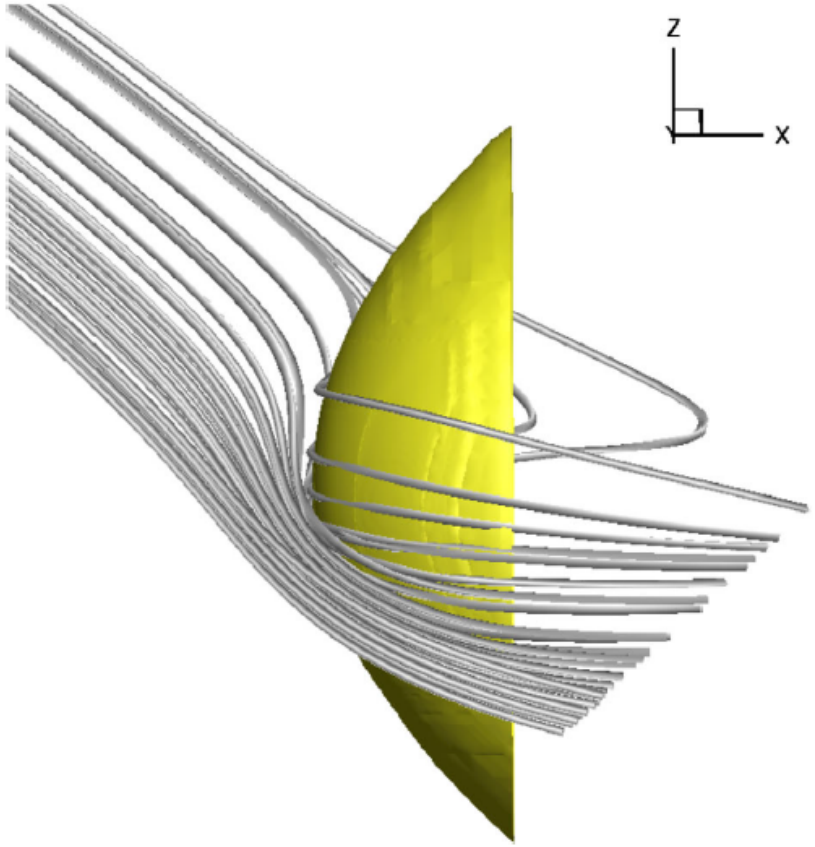

For details see
Space Sci. Rev. v.207 p.235, 2017

PSR B1259-63 at the binary orbit.

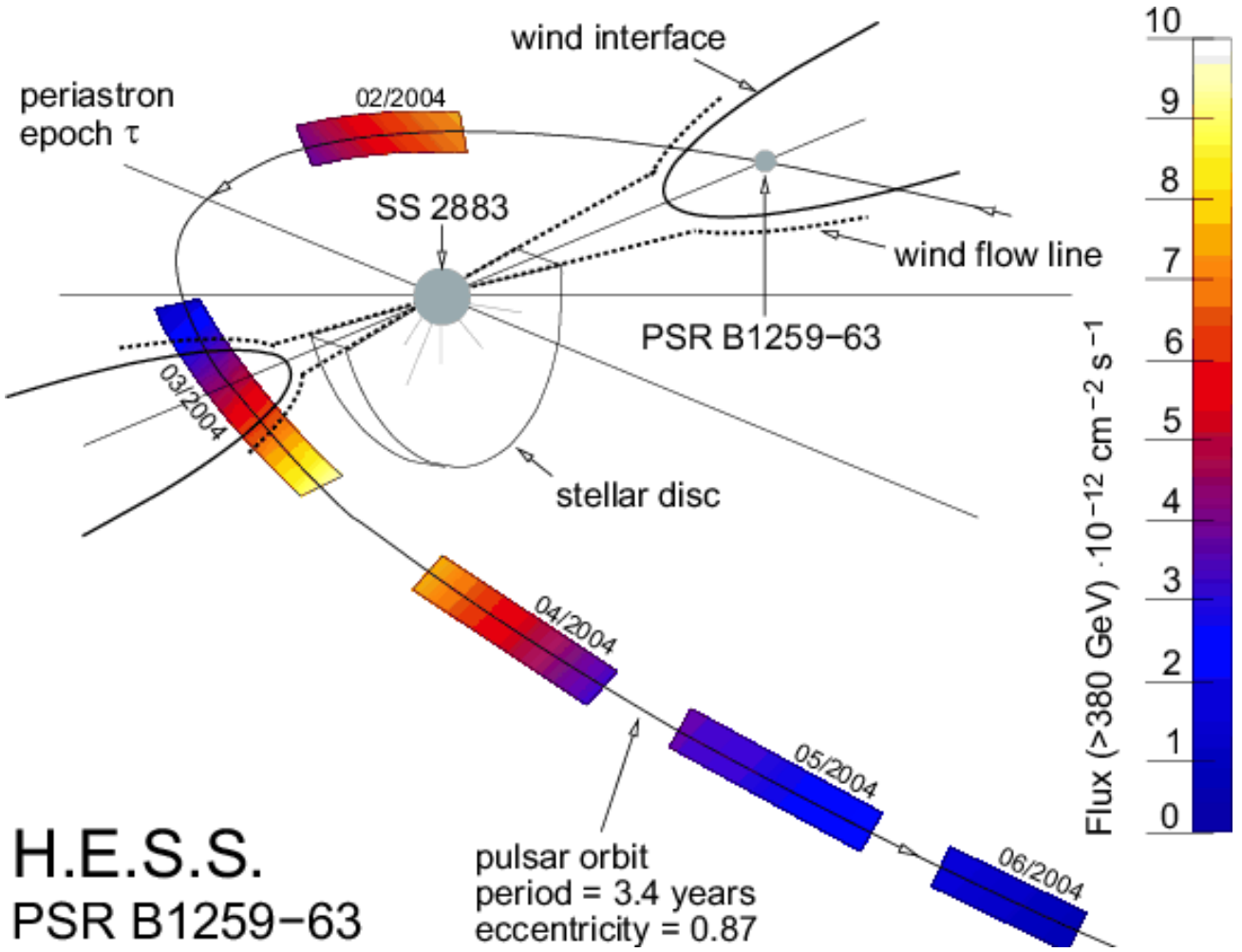

Aharonian et al. A&A 2005

RadioASTRON + VLBA observation
of the central pc indicated cilindric shape
Jet from Disk? (Blandford Payne model)

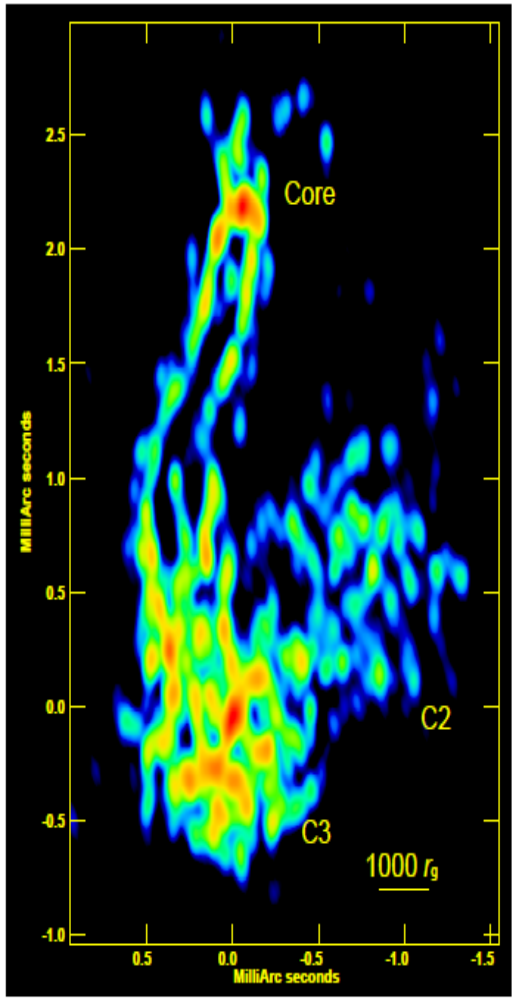

Figure 1: Radio image of the central parsec in 3C 84 obtained with the space-VLBI array. The half-power beam width (HPBW) is 0.10 × 0.05 mas at PA=0°. The noise level is 1.4 mJy/beam and the peak intensity is 0.75 Jy/beam. The radio core and emission features C2 and C3 (see text) are indicated in the image.

A wide and collimated radio jet in 3C 84 on the scale of a few hundred gravitational radii

G.Giovannini + 2018

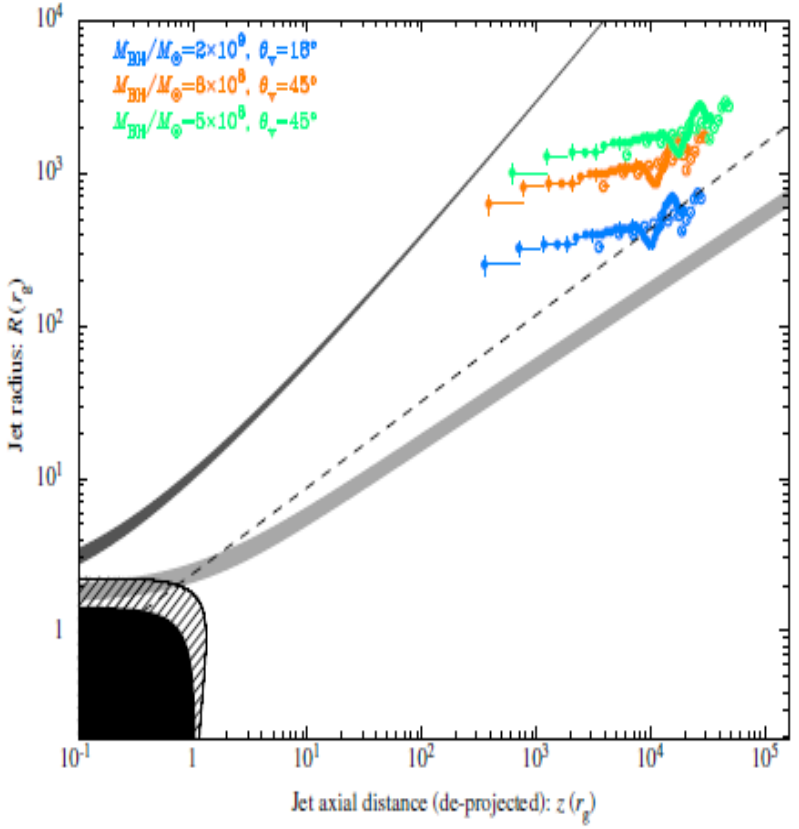

Figure 3: Jet width as a function of de-projected distance from the central engine in units of gravitational radii. Filled points are 22 GHz *RadioAstron* data, empty circles are previously published VLBA data at 43 GHz[5]. The data are plotted for three different assumptions of jet inclination angle and black hole mass (see Methods). Right-side horizontal error bars correspond to the uncertainty about a possible core-shift. The dashed line is the power-law fit to the collimation profile of M 87 (Nakamura et al., submitted). The filled black region on the lower left corner denotes the black hole event horizon, while the hatched area represents the ergosphere for the black hole spin parameter $a = 0.998$. The light gray area denotes the genuine parabolic streamline ($r \propto z^{0.5}$ at $r \gg r_g$) of the force-free steady-state jet solution[16], while the dark gray area denotes a quasi-conical outermost streamline ($r \propto z^{0.98}$ at $r \gg r_g$) of the force-free steady-state jet solution[35]. In both streamlines a variation from $a = 0.1$ (upper boundary) to $a = 0.998$ (lower boundary) is considered. Note that all the streamlines are anchored at the event horizon, $r_H = r_g(1 + \sqrt{1 - a^2})$, with the maximum angle of $\theta = \pi/2$ in polar coordinates.

Multi-wavelngth studies Mrk 501

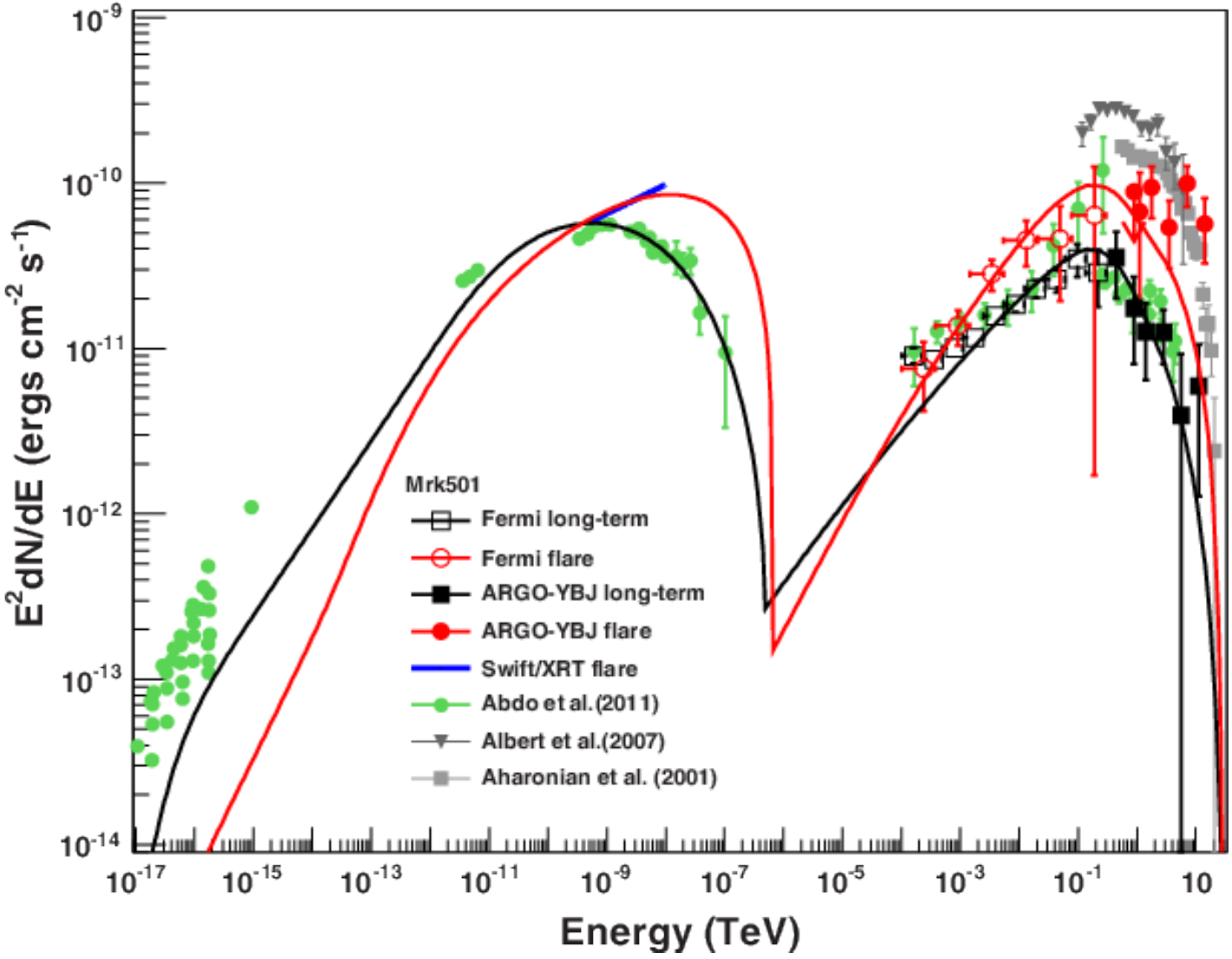

Bartoli +

PKS 2155-304

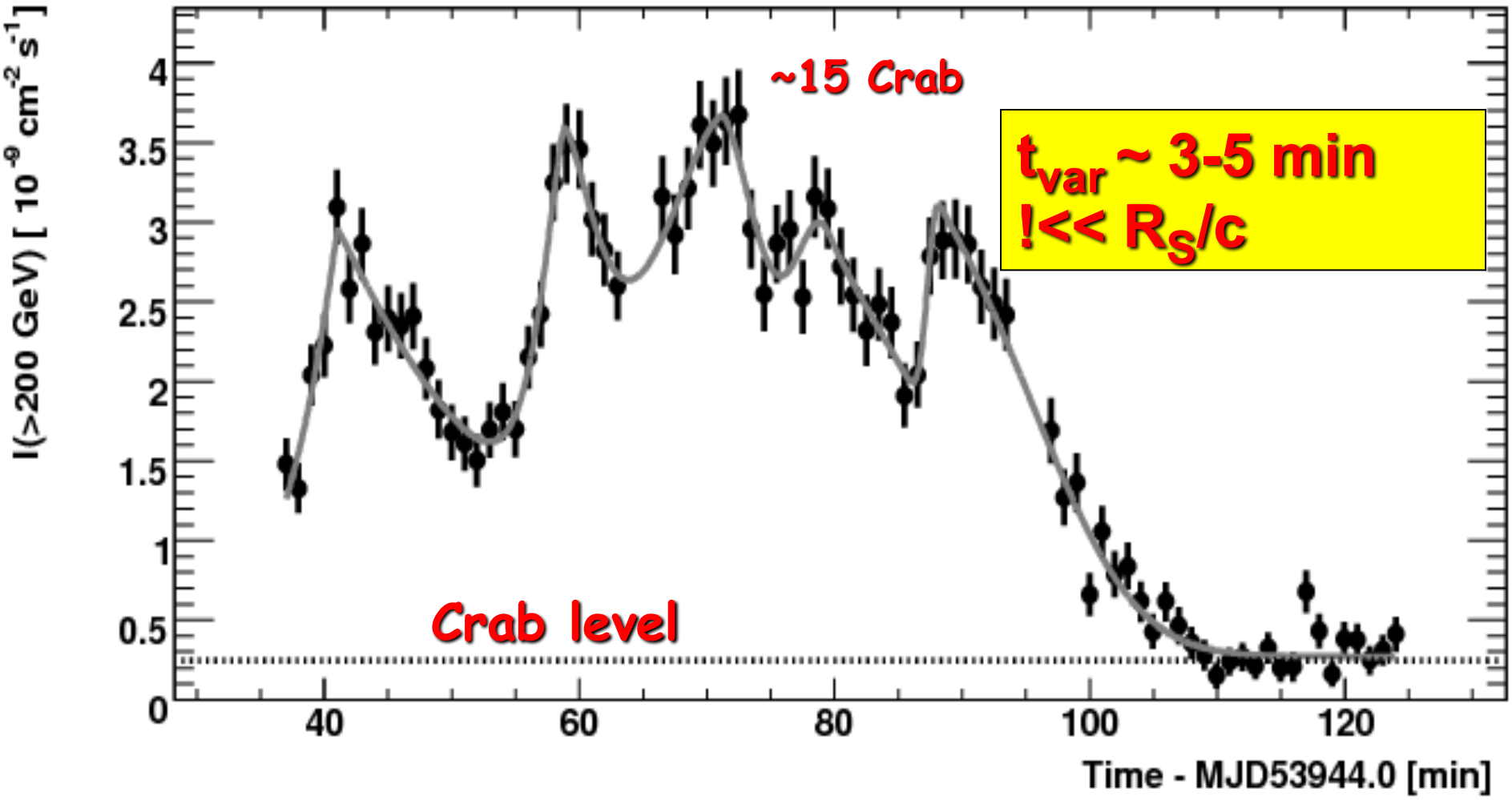

Aharonian et al. 2007

Thanks for your attention!

Work supported by RSF grant 16-12-10225